NUREG-1746

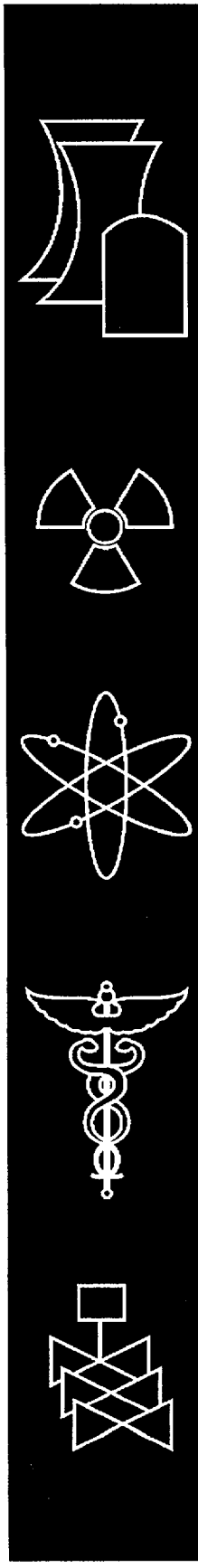

System-Level Repository Sensitivity Analyses, Using TPA Version 3.2 Code

Center for Nuclear Waste Regulatory Analyses

Swedish Nuclear Power Inspectorate

U.S. Nuclear Regulatory Commission
Office of Nuclear Material Safety and Safeguards
Washington, DC 20555-0001

AVAILABILITY OF REFERENCE MATERIALS IN NRC PUBLICATIONS

NRC Reference Material

As of November 1999, you may electronically access NUREG-series publications and other NRC records at NRC's Public Electronic Reading Room at www.nrc.gov/NRC/ADAMS/index.html. Publicly released records include, to name a few, NUREG-series publications; *Federal Register* notices; applicant, licensee, and vendor documents and correspondence; NRC correspondence and internal memoranda; bulletins and information notices; inspection and investigative reports; licensee event reports; and Commission papers and their attachments.

NRC publications in the NUREG series, NRC regulations, and *Title 10, Energy*, in the Code of *Federal Regulations* may also be purchased from one of these two sources.

1. The Superintendent of Documents
   U.S. Government Printing Office
   Mail Stop SSOP
   Washington, DC 20402–0001
   Internet: bookstore.gpo.gov
   Telephone: 202-512-1800
   Fax: 202-512-2250
2. The National Technical Information Service
   Springfield, VA 22161–0002
   www.ntis.gov
   1–800–553–6847 or, locally, 703–605–6000

A single copy of each NRC draft report for comment is available free, to the extent of supply, upon written request as follows:

Address: Office of the Chief Information Officer,
Reproduction and Distribution
Services Section
U.S. Nuclear Regulatory Commission
Washington, DC 20555-0001
E-mail: DISTRIBUTION@nrc.gov
Facsimile: 301–415–2289

Some publications in the NUREG series that are posted at NRC's Web site address www.nrc.gov/NRC/NUREGS/indexnum.html are updated periodically and may differ from the last printed version. Although references to material found on a Web site bear the date the material was accessed, the material available on the date cited may subsequently be removed from the site.

Non-NRC Reference Material

Documents available from public and special technical libraries include all open literature items, such as books, journal articles, and transactions, *Federal Register* notices, Federal and State legislation, and congressional reports. Such documents as theses, dissertations, foreign reports and translations, and non-NRC conference proceedings may be purchased from their sponsoring organization.

Copies of industry codes and standards used in a substantive manner in the NRC regulatory process are maintained at—

The NRC Technical Library
Two White Flint North
11545 Rockville Pike
Rockville, MD 20852–2738

These standards are available in the library for reference use by the public. Codes and standards are usually copyrighted and may be purchased from the originating organization or, if they are American National Standards, from—

American National Standards Institute
11 West 42nd Street
New York, NY 10036–8002
www.ansi.org
212–642–4900

Legally binding regulatory requirements are stated only in laws; NRC regulations; licenses, including technical specifications; or orders, not in NUREG-series publications. The views expressed in contractor-prepared publications in this series are not necessarily those of the NRC.

The NUREG series comprises (1) technical and administrative reports and books prepared by the staff (NUREG–XXXX) or agency contractors (NUREG/CR–XXXX), (2) proceedings of conferences (NUREG/CP–XXXX), (3) reports resulting from international agreements (NUREG/IA–XXXX), (4) brochures (NUREG/BR–XXXX), and (5) compilations of legal decisions and orders of the Commission and Atomic and Safety Licensing Boards and of Directors' decisions under Section 2.206 of NRC's regulations (NUREG–0750).

NUREG-1746

System-Level Repository Sensitivity Analyses, Using TPA Version 3.2 Code

Manuscript Completed: June 2001
Date Published: August 2001

Prepared by
R. B. Codell, M. R. Byrne, T. J. McCartin[a]
S. Mohanty, J. Weldy, M. Jarzemba, G. W. Wittmeyer[b]
Y. Lu[c]
R. W. Rice[d]

[a]Division of Waste Management
Office of Nuclear Material Safety and Safeguards
U.S. Nuclear Regulatory Commission
Washington, DC 20555-0001

[b]Center for Nuclear Waste Regulatory Analyses
6220 Culebra Road
San Antonio, TX 78238-5166

[c]Office of Nuclear Waste Safety
Swedish Nuclear Power Inspectorate
(Statens Kärnkraftinspektion)
S-106 58 Stockholm, Sweden

[d]Independent Consultant
307 Quincy
El Paso, TX 79922

For sale by the Superintendent of Documents, U.S.Government Printing Office
Internet: bookstore.gpo.gov Phone: (202) 512-1800 Fax: (202) 512-2250
Mail: Stop SSOP, Washington, DC 20402-0001

ISBN 0-16-050907-6

ABSTRACT

To review and quantitatively evaluate the safety case in a potential license application by the U.S. Department of Energy (DOE) for the proposed Yucca Mountain (YM) repository, the U.S. Nuclear Regulatory Commission (NRC), with technical assistance from the Center for Nuclear Waste Regulatory Analyses (CNWRA), developed a Total-system Performance Assessment (TPA) code. The most recent versions of the TPA code used in evaluation and calculation of YM performance are 3.2 and 3.2.3. This report describes a series of computations performed using these codes for determining the confidence in the estimation of future repository performance in light of the uncertainty in conceptual models and parameters of those models. This report primarily presents: (i) the system-level and process-level results (e.g., intermediate results) to demonstrate trends and variabilities in outputs; (ii) the results of system-level sensitivity and uncertainty analyses using a variety of analysis techniques to determine the parameters that have the most influence on repository performance; and (iii) the relative importance of the integrated subissues in reviewing the DOE total-system performance assessment. An influential parameter is one that either drives uncertainty in performance, or one to which performance is sensitive. The sensitivity and uncertainty analyses were conducted using numerous TPA code runs (several thousand realizations) for each sensitivity analysis technique. Results of system-level analyses are based on peak dose and peak expected dose to a receptor group 20 km (12.4 mi) from the repository at two time periods of interest (TPIs): 10,000 yr (the likely compliance period in the draft regulation) and either 50,000 or 100,000 yr [a longer period for investigating any significant effects that may not be evident because of the calculated long waste package (WP) life].

Using the basecase, which included the seismic disruptive event scenario, peak expected doses of 0.003 mrem/yr and 4 mrem/yr were obtained for the 10,000- and 100,000-yr TPIs, respectively. The faulting scenario changed the peak expected dose negligibly. The igneous activity scenario increased the peak expected dose to 0.6 mrem/yr. For both TPIs, it was found that the most influential parameters were: (i) the fraction of the repository wetted by infiltrating water; (ii) the fraction of water entering the WP; (iii) the well pumping rate at the 20-km receptor group location; (iv) alluvium retardation factors for radionuclides (specifically, ^{99}Tc and ^{129}I), and (v) the present-day infiltration. The most influential parameters for the 10,000-yr TPI, but not for the 50,000-yr TPI, were the initially defective fraction of WPs and the factor that focuses flow onto the WP. The most influential parameters for the 50,000-yr TPI, but not for the 10,000-yr TPI, were the alluvium retardation factors for radionuclides (specifically, ^{234}U and ^{237}Np). The influential parameters were then compared to the current integrated subissues, which are used by the NRC to focus work on items important to repository performance. Nine out of 14 of the integrated subissues reflected at least one influential parameter.

The analyses and results are limited by the use of simplifying assumptions, models, and sparse data in certain areas. As a consequence, these results are preliminary. However, the estimates resulting from this study allowed the staff to focus attention on what are likely to be the most important phenomena relative to repository performance and point out deficiencies in the current state of knowledge. The manner in which these analyses were conducted or the assumptions and approaches used should not be construed to express the views, preferences, or positions of the NRC staff regarding the nature of site-specific regulations for YM.

CONTENTS

Section *Page*

ABSTRACT iii
TABLE OF CONTENTS v
FIGURES ix
TABLES xiii
EXECUTIVE SUMMARY xv
ACKNOWLEDGMENTS xviii

1 INTRODUCTION 1-1
1.1 BACKGROUND 1-2
1.1.1 Previous IPA Analyses 1-2
1.1.2 IPA Phase 1 Sensitivity and Uncertainty Analyses 1-4
1.1.3 IPA Phase 2 Sensitivity and Uncertainty Analyses 1-4
1.1.4 TPA Version 3.1 Sensitivity and Uncertainty Analyses 1-5
1.2 PURPOSE OF CURRENT ANALYSIS 1-5
1.3 REPORT ORGANIZATION 1-7
1.4 CAVEATS 1-7

2 OVERVIEW OF THE TOTAL-SYSTEM PERFORMANCE ASSESSMENT CONCEPTUAL MODELS IN THE TPA VERSION 3.2 CODE 2-1
2.1 CONCEPTUALIZATIONS OF REPOSITORY AND GEOLOGIC SETTING 2-1
2.2 CONCEPTUAL MODELS IMPLEMENTED IN THE TOTAL-SYSTEM PERFORMANCE ASSESSMENT COMPUTER CODE 2-5
2.2.1 Infiltration and Deep Percolation 2-5
2.2.2 Near-Field Environment 2-6
2.2.3 Radionuclide Releases from the EBS 2-7
2.2.4 Treatment of Aqueous-Phase Transport in the Unsaturated and Saturated Zones 2-9
2.2.5 Airborne Transport from Direct Releases 2-9
2.2.6 Exposure Pathways and Reference Biosphere 2-10
2.3 BASECASE DEFINITION AND ALTERNATIVE CONCEPTUAL MODELS 2-11
2.3.1 Basecase 2-11
2.3.2 Alternative Conceptual Models 2-11
2.3.2.1 Fuel-Dissolution Models 2-11
2.3.2.2 Fuel-Wetting Assumptions 2-12
2.3.2.3 Transport Alternatives 2-13

3 ANALYSIS OF TOTAL-SYSTEM BEHAVIOR 3-1
3.1 SINGLE-REALIZATION DETERMINISTIC ANALYSES 3-1
3.1.1 Unsaturated Zone Flow 3-1
3.1.2 Near-Field Environment 3-2
3.1.2.1 Repository-Scale Thermohydrology 3-2
3.1.2.2 Drift-Scale Thermohydrology 3-5
3.1.2.3 Near-Field Geochemical Environment 3-5

CONTENTS

Section		*Page*
	3.1.3 WP Degradation	3-9
	3.1.4 Releases from WP	3-11
	3.1.4.1 Cladding Degradation	3-11
	3.1.4.2 SF Dissolution and Mobilization	3-11
	3.1.4.3 Transport in the EBS	3-14
	3.1.5 UZ Transport	3-14
	3.1.6 SZ Flow and Transport	3-19
	3.1.7 Dose to the Receptor Group	3-19
3.2	RESULTS FROM THE MEAN VALUE DATA SET	3-20
	3.2.1 10,000-Year Releases and Dose	3-23
	3.2.2 100,000-Year Releases and Dose	3-28
3.3	MULTIPLE–REALIZATION ANALYSIS	3-35
	3.3.1 UZ Flow	3-36
	3.3.2 Near-Field Environment	3-41
	3.3.3 WP Degradation	3-41
	3.3.4 WP Release	3-41
	3.3.5 UZ Transport	3-48
	3.3.6 SZ Flow and Transport	3-48
3.4	COMPARISON OF DOSES FROM MEAN VALUE DATA SET AND MULTIPLE-REALIZATION CASES	3-53
3.5	ALTERNATIVE CONCEPTUAL MODELS	3-55
	3.5.1 Fuel-Dissolution Models	3-60
	3.5.1.1 Fuel-Dissolution Model 1	3-60
	3.5.1.2 Fuel-Dissolution Model 3 (Natural Analog)	3-60
	3.5.1.3 Fuel-Dissolution Model 4 (Schoepite Dissolution)	3-61
	3.5.2 Fuel-Wetting Assumptions	3-61
	3.5.2.1 Flowthrough Model with Fuel-Dissolution Model 2	3-61
	3.5.2.2 Flowthrough Model with Fuel-Dissolution Model 1	3-61
	3.5.2.3 Focused Flow	3-61
	3.5.2.4 Cladding Credit with Model 1	3-62
	3.5.2.5 Grain-Size Model with Fuel Dissolution Model 1	3-62
	3.5.3 Transport Alternatives	3-62
	3.5.3.1 No Retardation of Pu, Am, and Th	3-62
	3.5.3.2 No-Invert Model	3-62
	3.5.3.3 Matrix Diffusion	3-62
3.6	DISRUPTIVE EVENTS	3-63
	3.6.1 Single-Realization Analysis of Disruptive Events	3-63
	3.6.2 Multiple-Realization Analysis of Disruptive Events	3-72
3.7	CALCULATION OF RISK	3-72
	3.7.1 Scenarios Other Than Extrusive Igneous Activity	3-72
	3.7.2 Extrusive Igneous-Activity Scenario	3-76
	3.7.3 Combining Conditional Risks into an Overall Risk	3-78

CONTENTS

Section *Page*

4 SYSTEM-LEVEL SENSITIVITY STUDIES 4-1
4.1 SENSITIVITY ANALYSIS TECHNIQUES 4-1
4.1.1 Regression Analyses Methods 4-3
4.1.1.1 Scatter Plot/Single Linear Regression on One Variable 4-3
4.1.1.2 Variable Transformations and Their Attributes 4-5
4.1.1.3 Stepwise Multiple Linear Regression 4-8
4.1.1.4 Application of the Kolmogorov-Smirnov and Sign Tests for Determining Important Parameters 4-10
4.1.2 Differential Analysis Technique 4-10
4.1.3 Morris Method Technique 4-12
4.1.4 The Fourier Amplitude Sensitivity Test Method 4-13
4.1.5 Parameter Tree Method 4-14
4.2 ANALYSIS OF SENSITIVITY FROM MONTE CARLO RUNS 4-16
4.2.1 Procedure for Screening Monte Carlo Sensitivity Results 4-16
4.2.1.1 Sensitivity Results from Monte Carlo Analysis 4-17
4.2.1.2 Parameter Sensitivity at High End of Peak Doses 4-22
4.3 ANALYSIS OF SENSITIVITY FROM NONSTATISTICAL METHODS 4-26
4.3.1 Results from Differential Analyses 4-26
4.3.2 Results from the Morris Method 4-28
4.3.3 Results from the FAST Method 4-31
4.4 RESULTS FROM THE PARAMETER TREE METHOD 4-31
4.4.1 Parameter Trees Using Different Branching 4-36
4.4.2 Stepwise Implementation of the Technique 4-39
4.5 ALTERNATIVE CONCEPTUAL MODELS AND SCENARIO CASES STUDIED AT THE SYSTEM LEVEL 4-41

5 SYNTHESIS OF SENSITIVITY RESULTS AND LINKAGE OF SENSITIVE PARAMETERS TO INTEGRATED SUBISSUES 5-1
5.1 SELECTION OF INFLUENTIAL PARAMETERS 5-1
5.2 COMPARING INFLUENTIAL PARAMETERS WITH INTEGRATED SUBISSUES 5-3
5.2.1 Key Integrated Subissues for 10,000-yr TPI 5-5
5.2.2 Key Integrated Subissues for 50,000-yr TPI 5-7

6 CONCLUSIONS 6-1
6.1 BASECASE RESULTS 6-1
6.2 ALTERNATIVE CONCEPTUAL MODELS 6-1
6.3 SENSITIVITY ANALYSES 6-2
6.4 IMPORTANCE OF RADIONUCLIDES 6-3
6.5 INTEGRATED SUBISSUES REQUIRING FURTHER STUDIES 6-4

7 REFERENCES 7-1

CONTENTS

Section *Page*

APPENDIX A DESIGN MATRIX FOR THE MORRIS METHOD A-1

APPENDIX B FORMALISM OF FOURIER AMPLITUDE SENSITIVITY TEST TECHNIQUE B-1

APPENDIX C FORMALIZATION OF PARAMETER TREE SENSITIVITY ANALYSIS APPROACH C-1

APPENDIX D DESCRIPTION OF ABBREVIATIONS USED FOR TPA VERSION 3.2 CODE INPUT PARAMETERS D-1

APPENDIX E DETAILED RESULTS FROM DIFFERENTIAL ANALYSES E-1

FIGURES

Figure		*Page*
1-1	Flowdown diagram showing the subsystems and the integrated subissues	1-3
2-1	Flow diagram for TPA Version 3.2 code	2-2
2-2	Conceptualization of the repository system	2-4
3-1	Mean annual precipitation and infiltration at the repository horizon averaged over all subareas and encompassing both the current and pluvial periods for the mean value data set	3-3
3-2	Effect of the thermal perturbation on the near-field seepage rate in each subarea for the mean value data set	3-3
3-3	Subarea average infiltration rate, flow into the drift, and amount of water entering the WP for the mean value data set	3-6
3-4	WP surface temperature in each subarea for the mean value data set	3-6
3-5	WP surface relative humidity in each subarea for the mean value data set	3-7
3-6	Time history of chloride concentration computed by MULTIFLO	3-7
3-7	WP wall thickness as a function of time for the mean value data set	3-10
3-8	Cumulative number of failed WP for the mean value data set	3-10
3-9	Thickness of subarea stratigraphic units	3-15
3-10	^{36}Cl normalized release rates from the EBS, UZ and SZ for the mean value data set	3-20
3-11	SZ streamtubes assigned to each subarea	3-21
3-12	Groundwater dose to an average individual as a function of time at the receptor location 20 km (12.4 MI)downgradient of the repository, for the mean value data set in the: (a) 10,000-yr, and (b) 100,000-yr, time periods of interest	3-24
3-13	Release rates in the 10,000-yr time period of interest from the: (a) EBS; (b) UZ; and (c) SZ for the mean value data set	3-25
3-14	Groundwater dose in 10,000-yr time period of interest with and without: (a) faulting; and (b) igneous-activity disruptive events, for the mean value data set, without probability weighting.	3-27
3-15	Release rates in 100,000 yr from the: (a) EBS, (b) UZ, and (c) SZ for the mean value data set	3-29
3-16	^{237}Np and ^{99}Tc total release and releases by subarea in 100,000 yr from the: (a) EBS; (b) UZ; and (c) SZ for the mean value data set	3-31
3-17	^{99}Tc groundwater doses, total and by subarea, in 100,000 yr, for the mean value data set	3-32
3-18	Groundwater dose, total and by subarea, in: (a) 10,000 and (b) 100,000 yr, for the mean value data set	3-33
3-19	Groundwater dose in 100,000 yr with and without: (a) faulting, and (b) igneous activity disruptive events for the mean value data set, without probability weighting	3-34
3-20	Groundwater dose in: (a) 10,000, and (b) 100,000 yr, including the average dose, for 250 realizations	3-37
3-21	Mean, maximum, and minimum infiltration rates in the UZ for each subarea.	3-38
3-22	Cumulative release rates of ^{99}Tc and ^{237}Np from the EBS plotted with the maximum flow rate of water into the repository, for 250 realizations	3-39

FIGURES (cont'd)

Figure *Page*

3-23 Peak groundwater dose in: (a) 10,000, and (b) 100,000 yr, plotted with the maximum flow rate of water into the repository, for 250 realizations 3-40
3-24 WP surface temperature: (a) averaged over the repository and for each subarea; and (b) in subarea 1, the average, minimum, and maximum values, for 250 realizations 3-42
3-25 Fraction of WPs failed by corrosion for each of the 250 realizations, and the average fraction of failed WPs 3-43
3-26 Average WP failure time by corrosion plotted with: (a) peak groundwater dose; and (b) time of the peak groundwater dose, for 250 realizations 3-44
3-27 Peak groundwater dose, and the: (a) ^{99}Tc, and (b) ^{237}Np, peak release rates from subarea 1, for 250 realizations 3-45
3-28 Peak release rates from the EBS and time of the peak release for: (a) ^{99}Tc, and (b) ^{237}Np, in 250 realizations 3-46
3-29 ^{99}Tc release rates from the EBS over: (a) 10,000, and (b) 100,000 yr, including the average release rate, in subarea 1, for 250 realizations 3-47
3-30 Cumulative releases from the EBS, the UZ, and the SZ, together with the initial inventory in the repository 3-49
3-31 UZ average release rates of ^{99}Tc, ^{237}Np, and ^{239}Pu, for 250 realizations 3-49
3-32 UZ release rates of ^{99}Tc over: (a) 10,000, and (b) 100,000 yr, including the average release rate, in subarea 1, for 250 realizations 3-50
3-33 CCDF of UZ groundwater travel times, for 250 realizations 3-51
3-34 SZ average release rates of ^{99}Tc, ^{237}Np, and ^{239}Pu, for 250 realizations 3-51
3-35 SZ release rates of ^{99}Tc over: (a) 10,000; and (b) 100,000 yr, including the average release rate, in subarea 1, for 250 realizations 3-52
3-36 CCDF of UZ GWTTs, for 250 realizations 3-54
3-37 Peak groundwater dose of: (a) ^{99}Tc; and (b) ^{237}Np; and time of the peak dose, for 250 realizations 3-56
3-38 Percent each radionuclide contributes to the peak groundwater dose, for 250 realizations . . . 3-57
3-39 Average groundwater dose in (a) 10,000, and (b) 100,000 yr, for each nuclide, including the total dose, for 250 realizations 3-58
3-40 Peak groundwater dose and the volume of well water pumped, for 250 realizations. 3-59
3-41 Groundwater dose from the basecase and the fuel-dissolution alternative conceptual models, for: (a) 10,000, and (b) 100,000 yr, using the mean value data set 3-64
3-42 Groundwater dose from the basecase and the fuel-wetting alternative conceptual models, for: (a) 10,000; and (b) 100,000 yr, using the mean value data set 3-65
3-43 Groundwater dose from the basecase and the transport alternative conceptual models, for: (a) 10,000; and (b) 100,000 yr, using the mean value data set 3-66
3-44 Seismic hazard curve comprises ground accelerations and recurrence times used to determine the time of seismic events 3-67
3-45 Vertical extent of rockfall associated with the 5 rock types and 10 seismic events defined by the seismic hazard curve 3-67
3-46 Joint spacing of the 5 rock types and 10 seismic events 3-68
3-47 Fraction of the area with ground motion for each of the 10 seismic events defined by the seismic hazard curve 3-68

FIGURES (cont'd)

Figure *Page*

3-48 Groundwater dose in 10,000 and 100,000 yr with and without: (a) faulting, and (b) igneous activity, in 10,000 yr, for 250 realizations. . . . 3-73
3-49 Mean dose arising from extrusive igneous-activity shown with various times for the volcanic event in 400 realizations . . . 3-79
3-50 Contribution of extrusive igneous-activity to the total dose, weighted by an annual probability for the volcanic event of 10^{-7} . . . 3-79

4-1 A diagram illustrating the use of the Monte Carlo method in performance assessment . . . 4-2
4-2 Example of a scatter plot/single linear regression . . . 4-4
4-3 Normal probability plot of dose for 10,000 yr in the 1,000-vector basecase . . . 4-7
4-4 Figure showing a close fit to normal distribution after using p = 0.1 transforms . . . 4-7
4-5 General parameter tree . . . 4-15
4-6 Plot of the residual sum of squares versus number of parameters included in the fit for the basecase, with a time period of interest of 10,000 yr . . . 4-23
4-7 Plot of the residual sum of squares versus number of parameters included in the fit for the basecase with a time period of interest of 50,000 yr . . . 4-23
4-8 Results from the Morris method from the basecase with a time period of interest of 10,000 yr . . . 4-32
4-9 Results from the Morris method from the basecase with a time period of interest of 50,000 yr . . . 4-33
4-10 Median-based parameter tree describing the technique for examining system sensitivity to groups of parameters . . . 4-35
4-11 Mean-based parameter tree describing the technique for examining system sensitivity to groups of parameters . . . 4-37
4-12 Mean-percentile-based parameter tree describing the technique for examining system sensitivity to groups of parameters; input parameters divided based on their median values, and output variable divided based on its 90^{th} percentile value from all 4000 realizations . . . 4-38
4-13 Tree developed using a stepwise implementation of the technique, based on the importance factor . . . 4-40
4-14 Bar chart showing the effects of alternative conceptual models at 10,000 yr . . . 4-43
4-15 Bar chart showing the effects of alternative conceptual models at 50,000 yr . . . 4-43

TABLES

Table		*Page*
3-1	Mean values and sampled distributions of parameters for infiltration calculations	3-4
3-2	Mean values and sampled distributions of parameters for determining repository-scale and drift-scale thermo-hydrology	3-4
3-3	Parameters for determining the corrosion failure of WP	3-8
3-4	Parameters used in determining radionuclide releases from the engineered barrier system	3-12
3-5	Distributions of solubility limits	3-13
3-6	Radionuclide decay chains	3-13
3-7	Initial inventory, gap inventory, and half-life of radionuclides in spent nuclear fuel for groundwater release	3-14
3-8	Mean values and sampled distributions of sorption coefficient, K_d (m^3/kg), parameters	3-16
3-9	Parameter values used for SZ flow and radionuclide transport in TPA	3-22
3-10	Biosphere dose conversion factors for groundwater at the 20-km receptor location	3-23
3-11	Correlated parameters and correlation coefficients for the multiple realizations	3-38
3-12	Average, maximum, and minimum SZ groundwater travel times, by subarea and average, for all subareas, from 250 realizations	3-53
3-13	Primary radionuclides contributing to peak expected dose	3-54
3-14	Parameters used in determining seismic failure of WPs	3-69
3-15	Faulting disruptive event parameters.	3-69
3-16	Igneous activity parameters	3-70
3-17	Initial inventory and half-life of *additional* radionuclides considered for ground-surface release, but not for groundwater release	3-71
3-18	Parameters used in computing ash and radionuclide removal from the ground surface	3-74
3-19	Biosphere dose conversion factors of all 43 nuclides for ground surface at the 20-km receptor location.	3-75
4-1	Summary of regression and screening for basecase, 10,000-yr time period of interest	4-18
4-2	Summary of regression and screening for basecase, 50,000-yr time period of interest	4-20
4-3	Standardized sensitivities for basecase, 10,000-yr time period of interest	4-24
4-4	Standardized sensitivities for basecase, 50,000-yr time period of interest	4-24
4-5	t-test on means of high- and low-dose categories for 50,000-yr time period of interest	4-25
4-6	Top 10 influential parameters (standardized) from statistical and nonstatistical analyses, for 10,000-yr time period of interest	4-29
4-7	Top 10 influential parameters from statistical and nonstatistical analyses, for 50,000-yr time period of interest	4-30
4-8	Most influential parameters from differential analysis for disruptive event scenarios	4-31
4-9	Statistical information about the 4000 realizations	4-36
4-10	Sensitivity coefficients calculated for various parameter trees	4-39
5-1	Influential parameters for 10,000-yr time period of interest, from sensitivity analysis studies	5-2
5-2	Influential parameters for 50,000-yr time period of interest, from sensitivity analysis studies	5-2

TABLES (cont'd)

Table *Page*

5-3 A crosswalk between the integrated subissues, alternative conceptual models, and the influential parameters 5-4

EXECUTIVE SUMMARY

To review and quantitatively evaluate the safety case in a potential license application by the U.S. Department of Energy (DOE) for the proposed Yucca Mountain (YM) repository, the U.S. Nuclear Regulatory Commission (NRC), with technical assistance from the Center for Nuclear Waste Regulatory Analyses (CNWRA), developed a Total-system Performance Assessment (TPA) code. To date, the NRC staff has written three reports on performance assessment (PA) for the proposed YM repository. The first, referred to as iterative performance assessment (IPA) Phase 1 (Codell, *et al.*, 1992), assembled and demonstrated the NRC assessment methodology. The second NRC Total System Performance Assessment (TSPA), IPA Phase 2 (Wescott, *et al.*, 1995), used the TPA Version 2.0 code to investigate the features, events, and processes influencing isolation performance of the proposed YM repository. Information obtained in these IPA analyses was used in NRC reviews of early DOE TSPAs for YM. The third NRC TSPA (U.S. Nuclear Regulatory Commission, 1999) used the TPA Version 3.1 code (Mohanty and McCartin, 1998) to determine whether the NRC would be able to quantitatively evaluate the soundness of the conclusions reached by the DOE in its viability assessment (VA). Revisions were made to the TPA code, leading to the development of the most recent version of the code, TPA Version 3.2 code (Mohanty and McCartin, 1998), which was used in evaluating the TSPA-VA. This report documents the most recent system- and process-level sensitivity and uncertainty analyses performed by the NRC and the CNWRA in conjunction with the review of the TSPA-VA. This report presents:

- A brief description of the conceptual models implemented in the TPA code;
- An in-depth discussion of basecase results for a single realization, using the mean parameter values, as well as for a full Monte Carlo run; deterministic results from alternative conceptual models; deterministic results from disruptive scenarios; and a proposed method for combining basecase and disruptive scenario results;
- The results of system-level sensitivity and uncertainty analyses, using statistical and nonstatistical techniques to determine the parameters that have the most influence on repository performance;
- The results from the comparative studies of alternative conceptual models and combinations of models explicitly incorporated in the TPA Version 3.2 code or that can be mimicked, through adjustment of input parameters, to determine model and parameter uncertainties;
- An estimation of the relative importance of the integrated subissues, to focus staff effort; and
- A documentation of improvements in NRC staff capabilities in PA, based on the insights gained from process- and system-level results and sensitivity analyses.

Most calculations were made using the basecase data set in which 246 out of 838 parameters were sampled from specified ranges and distributions that represent data uncertainty and variability. To develop a better understanding of the trends of the outputs at a process level, results from a single realization (using the mean value data set) were also analyzed. Calculations to date, using the basecase data set (the basecase is defined as the undisturbed scenario along with the effects of rockfall, from seismicity with multiple realizations) indicate peak expected doses of 3×10^{-5} mSv/yr (0.003 mrem/yr) in 10,000 yr (the proposed compliance

period) and 4 mrem/yr in 100,000 yr[1]. For a time period of interest (TPI) of 10,000 yr, primarily six radionuclides (^{237}Np, ^{129}I, ^{99}Tc, ^{234}U, ^{36}Cl, and ^{79}Se) contributed to the peak expected dose. For a TPI of 100,000 yr, four radionuclides (^{237}Np, ^{234}U, ^{99}Tc, and ^{129}I) were the primary contributors to peak expected dose, with 92 percent of the contribution coming solely from ^{237}Np. Igneous activity is the primary contributor to the peak expected dose during the 10,000-yr TPI, estimated to be 0.006 mSv/yr (0.6 mrem/yr). The faulting disruptive event is a negligible contributor to the peak expected dose.

The sensitivity and uncertainty analyses were conducted using numerous (several thousands for each analysis method) TPA code runs. The sensitivity and uncertainty of repository performance to specific parameters were evaluated using a number of different statistical tests. The statistical tests examined the sensitivity of repository performance to individual parameters in an effort to identify, as comprehensively as possible, those parameters most important for understanding repository performance. This helped to focus the review of the VA and prepare for the forthcoming review of the TSPA-site recommendation (SR). Sensitivity analyses used peak dose, expressed as total effective dose equivalent, for each TPA run as the performance measure. The use of peak dose eliminated the time dependency of the performance measure, thus simplifying the analyses. Alternative conceptual model studies used case-by-case analyses, with peak expected dose from multiple realizations as the performance measure.

This report identifies and presents influential parameters for twoTPIs—10,000 and 50,000 yr. An influential parameter is one that either drives uncertainty in performance, or one to which the estimated performance is sensitive. For both TPIs, several parameters were found most influential for the basecase. The influential parameters include:

- Areal fraction of the repository wetted by water infiltrating into the repository;
- The fraction of water infiltrating into the repository from the unsaturated zone above the repository that will enter the waste package (WP) and contribute to the release of radionuclides;
- Well-pumping rate at the 20-km (12.3 mi) receptor group location;
- Alluvium sorption properties (i.e., R_ds) for ^{99}Tc and ^{129}I;
- Present-day areal average mean annual infiltration above the repository.

In addition, the parameters influential for the 10,000-yr TPI, but not influential for the 50,000 yr TPI, are:

- Initially defective fraction of WPs; and
- A flow-focusing factor that expresses the flow reaching a wetted WP.

The only parameters significant for the 50,000-yr TPI, but not influential for the 10,000 yr TPI, are the alluvium R_ds for ^{234}U and ^{237}Np.

---

[1]The time period of interest of 100,000 yr used in presenting the basecase results is different from that used in the sensitivity analyses (10,000 and 50,000 yr), primarily because the basecase results were also used in reviewing the DOE TSPA–VA results, which extended to 100,000 yr and beyond.

The influential parameters were used to focus the review of the VA and were also traced back to the integrated subissues used by the NRC to focus its high-level waste program on aspects important to repository performance (U.S. Nuclear Regulatory Commission, 1998). Nine out of 14 integrated subissues have at least one influential parameter (including the integrated subissues related to disruptive scenarios), based on the results of the TPA Version 3.2 code. It should be noted that the staff has not yet developed appropriate techniques for conducting sensitivity analyses of results from the disruptive scenarios with appropriate consideration of probability weighting. Therefore, the sensitivity analyses results from disruptive scenarios are used as such (i.e., without probability weighting) for crosswalking the influential parameters with the integrated subissues. The integrated subissues deserve careful examination because the current models delay any significant radionuclide releases past the 10,000-yr TPI. The delay is primarily attributable to: (i) corrosion-resistant material of the inner overpack pushing the WP failure time beyond 10,000 yr; (ii) thermal reflux delaying the onset of flow into the repositor; (iii) WP filling time delaying the radionuclide release time by hundreds to thousands of years; and (iv) radionuclide sorption in the alluvium causing significant delay in the arrival time of radionuclides.

This TSPA serves to aid the NRC staff in focusing its review of DOE TSPAs, especially those for the VA and SR, on those models and parameters that could significantly influence the estimated system performance. It should be noted that the results presented in the following chapters are based on numerous simplifying assumptions and use only limited site-specific data. Consequently, the numerical results should not be taken as representative of the performance of the proposed repository at Yucca Mountain, Nevada. Conclusions drawn from the analyses presented in this report may change as the models and assumptions are updated based on revised design, ongoing site characterization, recommendations from reviewers and experts, new regulatory requirements, and improved model conceptualization and data interpretation by staff. The analysis also contains uncertainties regarding conceptual models for consequences and scenarios. Finally, this report should be considered as an interim demonstration of some of the methods that the NRC staff has developed to review a PA submitted by the DOE as part of any potential license application. Thus, at the conclusion of some future TSPA effort, instructions to the NRC staff will be developed and documented regarding which specific compliance determination methods will be used to review a DOE PA. Neither the manner in which these analyses were conducted nor the assumptions and approaches used should be construed to express the views, preferences, or positions of the NRC staff regarding the nature of site-specific regulations for YM.

ACKNOWLEDGMENTS

This report was prepared to document work performed by the Center for Nuclear Waste Regulatory Analyses (CNWRA) for the Nuclear Regulatory Commission (NRC) under Contract No. NRC-02-97-009. The activities reported here were performed on behalf of the NRC Office of Nuclear Material Safety and Safeguards, Division of Waste Management. The report is an independent product of the CNWRA and does not necessarily reflect the views or regulatory position of the NRC.

The authors wish to thank B. Sagar (CNWRA) and C. Lui (NRC) for their technical reviews and W. Patrick (CNWRA) and K. McConnell (NRC) for their programmatic reviews. Technical support provided by R. Rice (consultant) at various stages of this report is gratefully acknowledged. The effort of J. Firth (NRC), program element manager for the Total System Performance Assessment and Integration (TSPA&I) key technical issue, and C. Lui (NRC) in coordinating the multidisciplinary discussions leading to the identification of important integrated subissues is also recognized. Thanks to R. Janetzke for code quality assurance (QA), and debugging the code when needed, to O. Pensado for observing during the analyses of Total System Performance Assessment-Viability Assessment (TSPA-VA) results and providing insights into Total-system Performance Assessment code outputs behavior, and to M. Smith for helping to regenerate several output tables. Thanks are also expressed to K. Poor of Portage Environmental, Inc. for an informal technical review of the document; J.M. Menchaca, Southwest Research Institute (SwRI), for assistance in debugging and testing the computation of several sensitivity analysis methods; M. Muller (SwRI) for help in generating some of the outputs and plotting results. Some staff also tested the initial version of the code. Their contributions are acknowledged and much appreciated. Thanks are also expressed to B. Long, A. Woods, C. Gray and C. Cudd for editorial reviews and C. Weaver, C. Garcia and A. Ramos for their secretarial support.

QUALITY OF DATA, ANALYSES, AND CODE DEVELOPMENT

DATA: CNWRA–generated data contained in this report meet QA requirements described in the CNWRA QA Manual. Data from other sources are freely used. The respective sources of non-CNWRA data should be consulted for determining levels of QA.

ANALYSES AND CODES: The TPA Version 3.2, 3.2.3, and 3.2MM codes have been developed following the procedures described in the CNWRA Technical Operating Procedure (TOP), TOP-018, which implements the QA requirements contained in the CNWRA QA Manual. The TPA Version 3.2MM code reflects a minor modification to the Version 3.2 code for use in conjunction with the Morris method. Codes used in conducting the Morris method and Fourier Amplitude Sensitivity Test have also been developed following procedures described in TOP-018.

1 INTRODUCTION

In accordance with the provisions of the Nuclear Waste Policy Act (NWPA) of 1982, as amended, and the Energy Policy Act (EnPA) of 1992, the U.S. Nuclear Regulatory Commission (NRC) is responsible for evaluating the license application for a proposed geologic repository constructed for emplacement of high-level nuclear waste (HLW) [i.e., commercial spent fuel (SF); several types of U.S. Department of Energy (DOE) and U.S. Navy SF; and vitrified HLW] at Yucca Mountain (YM), Nevada. In support and preparation of its regulatory review activities outlined in the NWPA and EnPA, the NRC staff is conducting detailed technical performance assessments (PAs) to understand and identify the potentially important isolation characteristics and capabilities of the proposed repository system at the YM site, based on the available information.

This PA activity, which is part of an ongoing process at the NRC to prepare for the review of a potential DOE license application for the proposed HLW disposal facility at YM, includes regular interactions between the NRC and the DOE on the topic of PA. For example, NRC staff comments on model abstraction related to the Total System Performance Assessment-Viability Assessment (TSPA-VA) were relayed to the DOE in a letter to Dr. S. Brocoum dated July 6, 1998 (Bell, 1998). Furthermore, the DOE, NRC, and various stakeholders regularly interact on the topic of PA through technical exchanges.

As part of these Iterative Performance Assessment (IPA) activities, the NRC and its support contractor, the Center for Nuclear Waste Regulatory Analyses (CNWRA), are using the enhanced Total-system Performance Assessment (TPA) computer code. The TPA code, which evolves with each IPA phase, is designed to simulate the behavior of the geologic repository, taking into account the essential characteristics of the natural and engineered barrier systems (EBS), and changes in knowledge about the geologic setting and design. This document presents system-level sensitivity and uncertainty analyses using the latest version of the TPA code, Version 3.2.

The NRC previously conducted analyses of repository performance (Codell, *et al.*, 1992; Wescott, *et al.*, 1995). For the latest iteration, Version 3.2 of the TPA code was developed as a more general and versatile computer code that more readily can accommodate changes to the design of the proposed YM repository. This version: (i) accommodates the repository design outlined in the TSPA-VA (U.S. Department of Energy, 1998) [e.g., repository layout and waste package (WP) emplacement and design]; (ii) quantifies total system performance related to the proposed compliance performance measure [the peak expected dose, expressed as total effective dose equivalent (TEDE), in the time period of interest (TPI)] expected in the forthcoming U.S. Environmental Protection Agency (EPA) standard and as proposed in the draft NRC site-specific regulations (Nuclear Regulatory Commission, 1999a); and (iii) includes recent site data and improved conceptual models. In addition, because approaches to estimate the performance of geologic repositories and site and repository design data continue to evolve, the TPA Version 3.2 code was developed with the flexibility to perform alternative calculations. Some of the examples include:

- Evaluate alternative repository and design features;
- Analyze the effect of different areal mass loadings;
- Assess the significance of various disruptive scenario classes;
- Evaluate radionuclide dilution in the saturated zone (SZ);
- Compute the dose as a function of time for a 10,000-yr or longer TPI; and
- Evaluate alternative SF dissolution models.

1.1 BACKGROUND

The PAs for geologic repositories are based on conceptual models of physical processes (embodied in computer codes) and parameters derived from field and laboratory data or expert elicitation. Because of the variability and sparsity of measured data and the underlying uncertainty involved with modeling physical processes for many thousands of years, the results of any PA are uncertain. Therefore, an important aspect of conducting a PA is quantifying the sensitivity of the results to, and the uncertainty associated with, the input parameters. An analysis of PA code output sensitivity and uncertainty will provide information delineating which input parameters most affect the model results. A better understanding of the parameters that have the most influence on model results can be used to improve the code and build confidence in the numerical results produced by the code. Likewise, identification of the most influential parameters and those parameters that drive uncertainty provides a means of comparing and evaluating different PA models and indicates where future design, site characterization, and analysis activities should be focused.

The staff developed a systematic approach to reviewing the DOE TSPAs. As currently envisioned, the approach is hierarchical, as illustrated in Figure 1-1. The focal point is the overall repository system where the performance measure is anticipated to be the expected annual dose to the average member of the critical group during the performance TPI. To facilitate review of the DOE TSPAs, staff will examine the contribution to performance from each of three repository subsystems—engineered, geosphere, and biosphere—as shown in the second tier of Figure 1-1. Each of these subsystems is further subdivided into discrete components of the respective subsystems—engineered barriers that make up the engineered system; unsaturated zone (UZ) flow and transport, SZ flow and transport, and direct release to the biosphere; and the dose calculation for the biosphere. This characterization of components is not strictly based on the physical aspects of the system but stems from the perspective of dose or risk calculations for total system performance evaluation. Recognizing there are many different ways of dividing the overall system into smaller and analyzable components, this particular division is primarily based on the natural progress of radionuclide release and transport to a receptor group at the YM site and takes advantage of the results of past NRC IPA and reviews of the DOE TSPAs. At the base of the hierarchy are the key elements of the repository system that need to be appropriately abstracted into a TSPA. These key elements of subsystem abstraction (KESAs), in general, are the integrated processes, features, and events that could affect system performance. In conformance with recently proposed changes to the structure of the NRC program for resolving issues related to the HLW repository program, the KESAs are now known as the integrated subissues.

1.1.1 Previous IPA Analyses

To date, the NRC staff has written three reports on PA for the proposed YM repository. The first, referred to as IPA Phase 1 (Codell, *et al.*, 1992), assembled and demonstrated the NRC assessment methodology. IPA Phase 1 examined the sensitivity and uncertainty in radionuclide releases to the accessible environment for a geologic repository in unsaturated tuff. The second NRC TSPA, IPA Phase 2 (Wescott, *et al.*, 1995), was performed using the TPA Version 2.0 code to investigate the features, events, and processes influencing isolation performance of the proposed YM repository. Information obtained in these IPA analyses was used in NRC reviews of early DOE TSPAs for YM. The overall performance measures for the geologic repository used in IPA Phase 2 were cumulative total releases of radionuclides (normalized release) to the accessible environment and radiation dose (effective dose equivalent) to the exposed population. The third NRC TSPA (U.S. Nuclear Regulatory Commission, 1999b) was performed using the

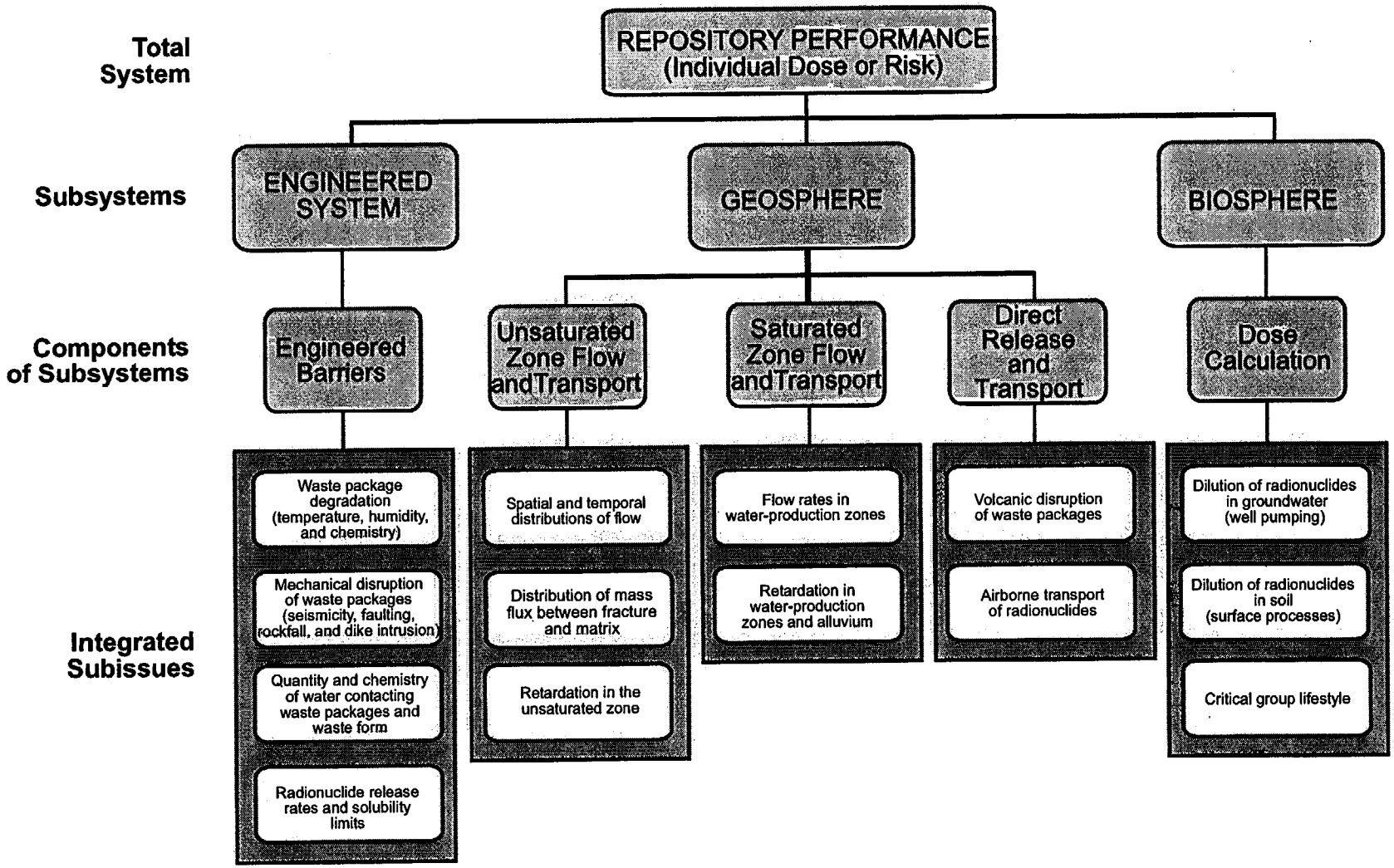

Figure 1-1. Flowdown diagram showing the subsystems and the integrated subissues.

TPA Version 3.1 code, to determine whether the NRC would be able to quantitatively evaluate the conclusions reached by the DOE in its VA. Subsequent to developing and testing the TPA Version 3.1 code, detailed sensitivity and uncertainty analyses were undertaken (U.S. Nuclear Regulatory Commission, 1999b) that indicated the need for further refinement of the TPA code before its use to evaluate the DOE TSPA-VA (U.S.Department of Energy, 1998). Revisions were made to the TPA code leading to the development of the current TPA Version 3.2 code, which was used in the evaluation of the TSPA-VA.

In addition, the TSPA analyses are used to better focus NRC activities on those factors of greatest importance to repository performance. The draft site-specific rule developed by the NRC for the proposed YM repository is a risk-informed, performance-based rule. Therefore, the NRC review of a potential license application to build and operate a deep geologic repository at YM necessarily will focus on those physical aspects of the repository system of greatest importance to radiological safety. The results from this study, in part, will be used to focus and direct the review strategy outlined by the NRC in its Yucca Mountain Review Plan (YMRP).

1.1.2 IPA Phase 1 Sensitivity and Uncertainty Analyses

Four sensitivity or uncertainty analyses were performed for IPA Phase 1 (Codell, *et al.*, 1992): (i) demonstration of the effect of individual parameters on the resultant complementary cumulative distribution function (CCDF) for cumulative release to the accessible environment; (ii) use of stepwise linear regression to estimate sensitivity of key parameters in the consequence models; (iii) determination of relative importance of individual radionuclides in the waste; and (iv) sensitivity of CCDFs to performance of the natural and engineered barriers. The sensitivity and uncertainty analyses considered only groundwater pathway releases, not those from human intrusion or airborne release through igneous activity. Gaseous release of radionuclides was not part of the IPA Phase 1 TSPA results, but was included as an auxiliary analysis.

Although IPA Phase 1 conducted full sensitivity and uncertainty analyses for the groundwater pathway, only CCDFs for cumulative release were generated for the scenario cases (basecase, basecase with human intrusion, and basecase with pluvial conditions with and without human intrusion). Cumulative release refers to the sum of releases of all radionuclides during the TPI. The CCDFs reflected the uncertainty in the sampled parameters propagated through the analysis. Peak dose was not calculated as a performance measure for the IPA Phase 1 study.

1.1.3 IPA Phase 2 Sensitivity and Uncertainty Analyses

In IPA Phase 2 (Wescott, *et al.*, 1995), model results were evaluated to develop regression equations describing TSPA model output and to analyze input parameter sensitivity. Techniques used to develop a regression equation that emulated the TPA model included transformation of data (Iman and Conover, 1979; Seitz, *et al.*, 1991); test for heteroscedasity (residual variation—Draper and Smith, 1981; Bowen and Bennett, 1988; Sen and Srivastava, 1990); and Mallows' C_p statistic (Sen and Srivastava, 1990). In addition to techniques used in previous PA work (e.g., the stepwise linear regression), several techniques were evaluated to determine parameter importance and sensitivity, including Kolmogorov-Smirnov (K-S) and Signs tests (Bowen and Bennett, 1988) and differential analysis (Helton, *et al.*, 1991).

Phase 2 IPA included a number of disruptive scenarios. These scenarios included igneous activity, seismicity, faulting, climate change, and exploratory drilling. Sensitivity and uncertainty analyses were

conducted on the undisturbed case as well as on the other scenario cases. These analyses were conducted with radionuclide release to the accessible environment and integrated population dose as the output variables, in contrast to peak expected dose described in this report.

1.1.4 TPA Version 3.1 Code Sensitivity and Uncertainty Analyses

For the TPA Version 3.1 code (U.S. Nuclear Regulatory Commission, 1999b), a variety of analytical procedures was implemented to assess the sensitivity of the estimated peak dose caused by variations in the values of model parameters as well as by changes resulting from use of alternative conceptual models. Scaled sensitivity coefficients were obtained by univariate and stepwise, multiple linear regression, and by standard differential analysis. To make linear regression models as accurate as possible, the dependent (peak dose) and independent (sample parameter values) variables were transformed using four methods: (i) normalization, in which the variable is divided by its mean; (ii) standardization, in which the difference between the variable and its mean is divided by the standard deviation of the variable; (iii) rank transformation, in which the value of the variable is replaced by its numerical rank; and (iv) logarithmic transformation, in which a multiplicative model is converted to an additive model. The statistical significance of the scaled sensitivity coefficients obtained by stepwise regression was determined using Student's t-statistic. The importance or influence of each parameter was ranked by the order in which the stepwise procedure selected the parameter for inclusion as an explanatory variable in the regression equation and by the use of K-S and Sign tests.

Sensitivity coefficients were calculated for both 10,000- and 50,000-yr TPIs and for waste canisters constructed with an inner corrosion-resistant layer of either Alloy 625 or Alloy C-22, leading to the identification of four distinct sets of important parameters. The effects of employing alternative conceptual models were also investigated for a number of the repository subsystems. Alternative conceptual models that were considered include: (i) backfilling of the repository; (ii) matrix diffusion in the rock matrix; (iii) credit for protection of the fuel provided by zircaloy cladding, (iv) focusing the flow of water to a smaller number of WPs; (v) use of the flowthrough model for SF dissolution and transport; (vi) radionuclide release rates based on natural analogs for SF; (vii) no credit for sorption of radionuclides; and (viii) instantaneous failure of all WPs.

Based on the results of the sensitivity and uncertainty analyses, preliminary conclusions were drawn about the relative importance of the integrated subissues or KESAs. For the 10,000-yr TPI, the most important integrated subissues are those for WP corrosion and the quantity and chemistry of water contacting the WPs. When Alloy C-22 is used, corrosion of the WPs is minimal during the 10,000-yr TPI, and mechanical disruption of the WPs is the most important integrated subissue. For the 50,000-yr TPI, the integrated subissues related to dilution of radionuclides in groundwater through well pumping and retardation in water production zones and alluvium are of increased importance.

1.2 PURPOSE OF CURRENT ANALYSIS

Similar to the sensitivity and uncertainty analyses conducted for previous IPA phases and the TPA Version 3.1 code, multiple sensitivity and uncertainty analyses have been conducted using the TPA Version 3.2 code. Sensitivity is defined as the relative change in output for a unit change of input, and uncertainty is the comparative change in overall output range because of input value uncertainty. Sensitivity and uncertainty analyses described in this report have been used to:

- Focus staff reviews of the DOE TSPA-VA on those factors most significant to total-system performance.

- Determine the input parameters in the TPA Version 3.2 code that are most influential to the estimated peak dose for the TPI at the receptor location by using a number of techniques. Although process-level sensitivity and uncertainty analyses have been conducted with the TPA code to determine the parameters most important in a given key technical issue (KTI) (e.g., unsaturated and saturated flow under isothermal conditions, igneous activity), this report summarizes analyses conducted to determine the most influential parameters at the total system level.

- Estimate the relative importance of the integrated subissues or KESAs.

- Continue improving staff capabilities, including improving the TPA code, for conducting independent evaluation of future DOE TSPAs for the site recommendation and license application for the proposed YM repository.

Since the release of the TPA Version 3.1.4 code, which was used in the TPA Version 3.1 code sensitivity analyses (U.S. Nuclear Regulatory Commission, 1999b), several major improvements were incorporated into the TPA code and associated input data sets that may have a significant effect on the sensitivity analysis results. Most of these changes were based on new information provided by the DOE after the completion of the TPA Version 3.1.4 code. For example, the DOE decision to replace Alloy 625 with Alloy C-22 as the material for the inner overpack in WP required substantial changes to the TPA model abstraction and its associated model parameters. The second basis for improvements resulted from experience gained from the process- and system-level sensitivity analyses using TPA Versions 3.1.1–3.1.4. Specific changes that were made to the TPA Version 3.1.4 code to obtain the new TPA Version 3.2 code include:

- Accounting for the effect of secondary mineral formation on SF dissolution;

- Considering the effects of a concrete tunnel invert on the transport of radionuclides;

- Introducing correlation between sampled radionuclide sorption parameters for chemically similar species to reflect realization-to-realization homogeneity of water chemistry;

- Assessing the significance of the radionuclide inventory between the fuel pellet and the cladding (gap inventory);

- Refining the model used to estimate mechanical failure of the WP from seismically induced rockfall;

- Allowing the user to specify the volume of SF wetted (i.e., bathtub height) so that alternate WP failure modes can be better modeled; and

- Revising the code to implement parameter value distributions that reflect the most current data.

1.3 REPORT ORGANIZATION

This report documents the most recent system-level sensitivity and uncertainty analyses performed by the NRC and the CNWRA that were conducted using the TPA Version 3.2 code. Chapter 2 provides a brief description of the TPA Version 3.2 code. Chapter 3 presents an in-depth discussion of basecase results for a single realization using the mean parameter values, as well as for a full Monte Carlo run, deterministic results from alternative conceptual models, deterministic results from disruptive scenarios, and a proposed method for combining basecase and disruptive scenario results.

Chapter 4 describes the system-level sensitivity studies, which were conducted in two parts. A set of alternative conceptual models and disruptive scenario cases were compared to evaluate the relative importance of specific components and assumptions used in the model. Evaluating the influence of individual components of the model in this way, where the full set of parameter values is used and a more comprehensive range of repository behavior is modeled, allows the relative importance of the components to be investigated. The sensitivity and uncertainty of repository performance to specific parameters were evaluated using a number of different statistical tests because no single test is completely comprehensive. The use of numerous statistical tests (described in this chapter and Appendices A–C and E) to examine the sensitivity of repository performance to individual parameters is intended to identify, as comprehensively as possible, those parameters most important for understanding repository performance.

Evaluation of important parameters based on the system-level sensitivity studies is provided in Chapter 5. Here, the important parameters and the alternative conceptual model investigations are related to the NRC integrated subissues or KESAs. Conclusions resulting from this study are described in detail in Chapter 6. Appendix D describes the abbreviated parameter names used throughout the report.

1.4 CAVEATS

Because it is not possible to model a system as complex as a geologic repository in a complete and exhaustive manner, a number of assumptions and limitations are used directly, or are implicit, in the analyses conducted in this report. These assumptions and limitations are listed next.

- Any underlying assumptions, limitations, and bases used to construct the models in the TPA Version 3.2 code also apply to these analyses. These models are described in Chapter 2 and discussed in greater detail in the TPA Version 3.2 code "User's Guide" (Mohanty and McCartin, 1998).

- The results are limited by the use of simplifying assumptions, models, and sparse data in certain areas. As a consequence, these results are preliminary. Moreover, the manner in which these analyses were conducted or the assumptions and approaches used should not be construed to express the views, preferences, or positions of the NRC staff regarding the ongoing efforts to develop site-specific regulations for YM.

2 OVERVIEW OF THE TOTAL-SYSTEM PERFORMANCE ASSESSMENT CONCEPTUAL MODELS IN THE TPA VERSION 3.2 CODE

Analysis of repository performance is anticipated to be complex with substantial uncertainties because of the first-of-a-kind nature of the repository, extended period of performance, and reliance on engineered and natural barriers. The TPA analysis focuses on the postclosure performance of the proposed HLW repository at YM over long time periods (e.g., 10,000 yr). To attempt to quantify the uncertainty in estimating repository performance over long time periods, the TPA analysis is conducted in a probabilistic manner in which many realizations are calculated using input parameter sets sampled from probability distributions. Therefore, detailed simulation models that include all the process couplings, heterogeneities, and complexities are not incorporated into PA models to maintain reasonable computer execution times with modest hardware resources. Though a probabilistic code, the TPA analysis can also be performed in a deterministic mode.

The TPA Version 3.2 code is used in this analysis to obtain deterministic and probabilistic estimates of dose for specified time periods (e.g., regulatory compliance TPI and beyond) at designated receptor locations [e.g., 20 km (12.4 mi) down gradient of YM]. The TPA Version 3.2 code, which is specifically tailored for evaluation of performance of the proposed repository at YM, is an update of the code used in the NRC IPA Phase 2 study. Conceptual models used in the previous version of the TPA code have been documented in Mohanty and McCartin (2001) and for the 3.2 version in Mohanty and McCartin (1998).

A key part in developing the model used in the TPA Version 3.2 code is determining the level of detail in the processes, design, and attributes of the site necessary to produce a credible analysis that provides meaningful insights into performance without an unreasonable computational burden. A discussion of the repository system and the basecase conceptual models is presented in this section to provide a general overview of the TPA Version 3.2 code. This chapter also includes descriptions of the alternative conceptual models analyzed in Chapters 3 and 4.

The TPA Version 3.2 code "User's Guide" contains more detailed information on the conceptual and mathematical models and the code structure (Mohanty and McCartin, 1998). A simplified flow chart illustrating the structure of the TPA Version 3.2 code is presented in Figure 2-1. The TPA input parameter values and the bases for their selection are presented in Appendix A of the same "User's Guide."

2.1 CONCEPTUALIZATIONS OF REPOSITORY AND GEOLOGIC SETTING

For ease of use and computational efficiency, the TPA Version 3.2 code replaces the intricate repository layout and the complex geologic setting with relatively simple conceptual representations. The repository layout, for example, is represented by an idealized planar feature discretized into a set of subareas, while the geology is replaced by a sequence of homogeneous layers. Properties and environmental conditions for each subarea are assumed uniform. Except for the influence of the thermal load, flow and transport processes in and below a given subarea are independent of processes in other subareas. Thus, flow is entirely vertical with no lateral diversion in the UZ.

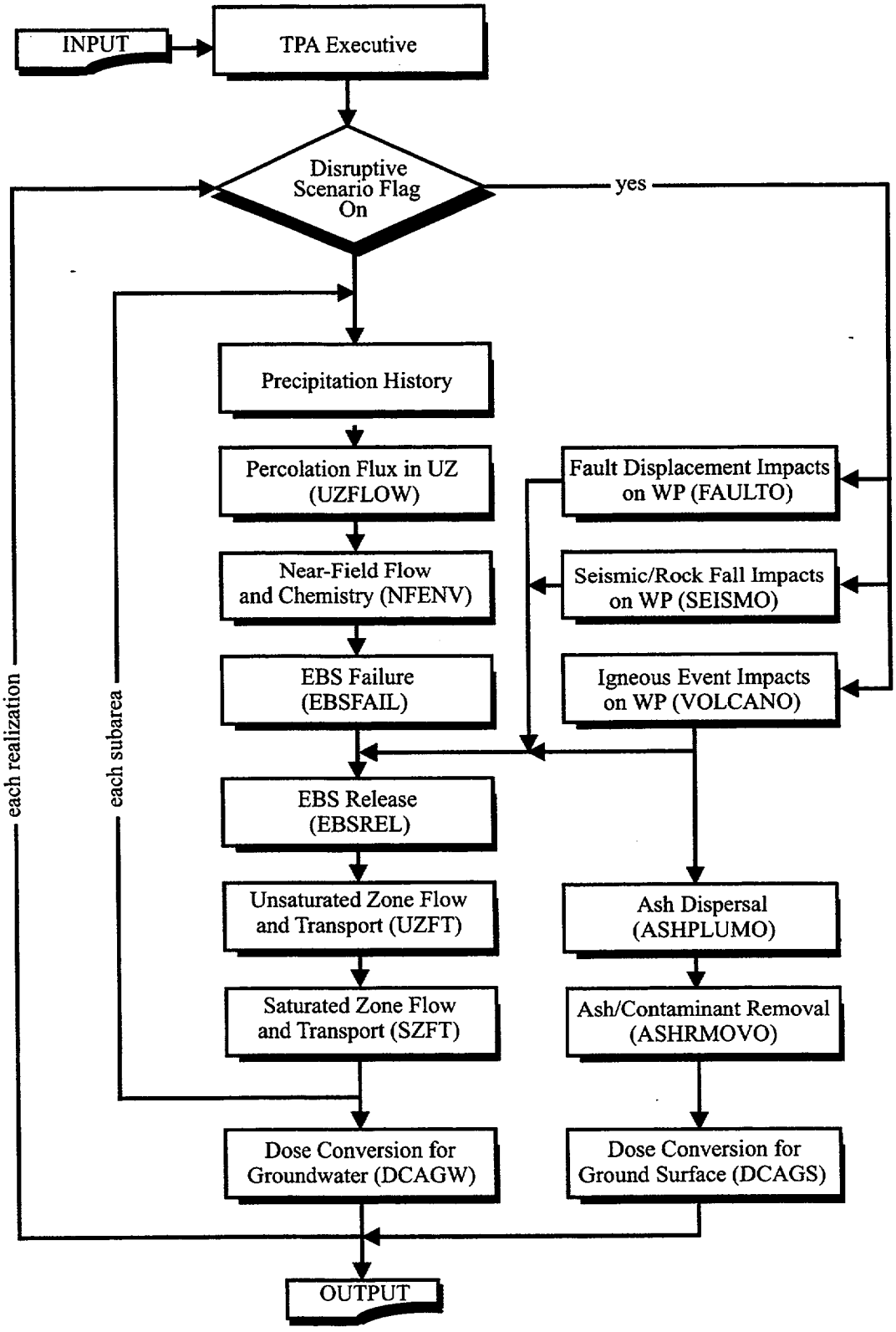

Figure 2-1. Flow diagram for TPA Version 3.2 code.

As illustrated in Figure 2-2, quadrilateral subareas of uniform thickness are used to represent individual subregions of the repository. In the current application, the repository is divided into seven subareas; however, the TPA Version 3.2 code has the capability to use much finer discretizations of both the repository and the geologic setting beneath it. The number of WPs in each subarea is assumed proportional to the fraction of the total repository area represented. Radionuclide releases from the EBS are calculated by modeling a single prototypical WP for each subarea and for each failure type. Performance characteristics of the WP and subsequent release in each subarea are calculated by considering the evolution of such characteristics as climatic conditions, water flux, thermal and chemical conditions, and geologic processes (e.g., seismicity, fault displacement, and igneous activity). Breaching of the WP by human intrusion and the associated release are not considered in the TPA Version 3.2 code.

The geologic setting is composed of the UZ (i.e., geologic media between the ground surface and the water table) and the SZ (i.e., groundwater aquifer beneath the repository, extending to the location of the receptor group). For simplicity, the stratigraphy is assumed laterally continuous and uniform within a subarea, but differing from subarea to subarea. This simplification implies that, in general, flow in the UZ is primarily vertical with little or no lateral diversion of flow along hydrostratigraphic units. The geologic setting also includes features, events, and processes, such as seismicity, tectonism (faulting), and igneous activity (intrusive and extrusive) that may adversely affect the performance of the repository. Seismicity, tectonism, and intrusive igneous activity affect the performance characteristics of the WP and contribute to groundwater releases.

To model flow and transport in the SZ, the TPA conceptual model consists of four distinct streamtubes over the width of the repository footprint normal to UZ flow. Each of the seven streamtubes in the UZ is connected to one of the four streamtubes in the SZ, based on proximity. Radionuclide releases from each of the UZ streamtubes provide the source term to the SZ streamtubes. The SZ streamtubes are treated as separate conduits and have flow velocities that vary along the individual flow paths. The mass flowrate of radionuclides exiting all SZ streamtubes at the well head is used to calculate annual dose to the average member of the receptor group. The annual dose computation accounts for all releases in the groundwater pathway at the location of the receptor group, the spatial extent of the releases in the SZ at the location of the receptor group, the extent of the production zone containing the radionuclides (all radionuclides are assumed released in one production zone), and the influence of the pumping rate attributed to water use by the receptor group.

Direct release of radionuclides to the accessible environment because of an extrusive igneous event is also modeled in the TPA Version 3.2 code. The physical characteristics of the extrusion and the assumption of a uniform distribution of WPs in the repository are used to determine the number of WPs affected by the event. Radionuclides are transported to the receptor location, based on characteristics of the eruption and meteorological conditions. The areal density of radionuclides in the soil, resulting from the deposition of volcanic ash containing SF particles, is then calculated. This soil concentration is used in computing the annual dose to the average member of the receptor group.

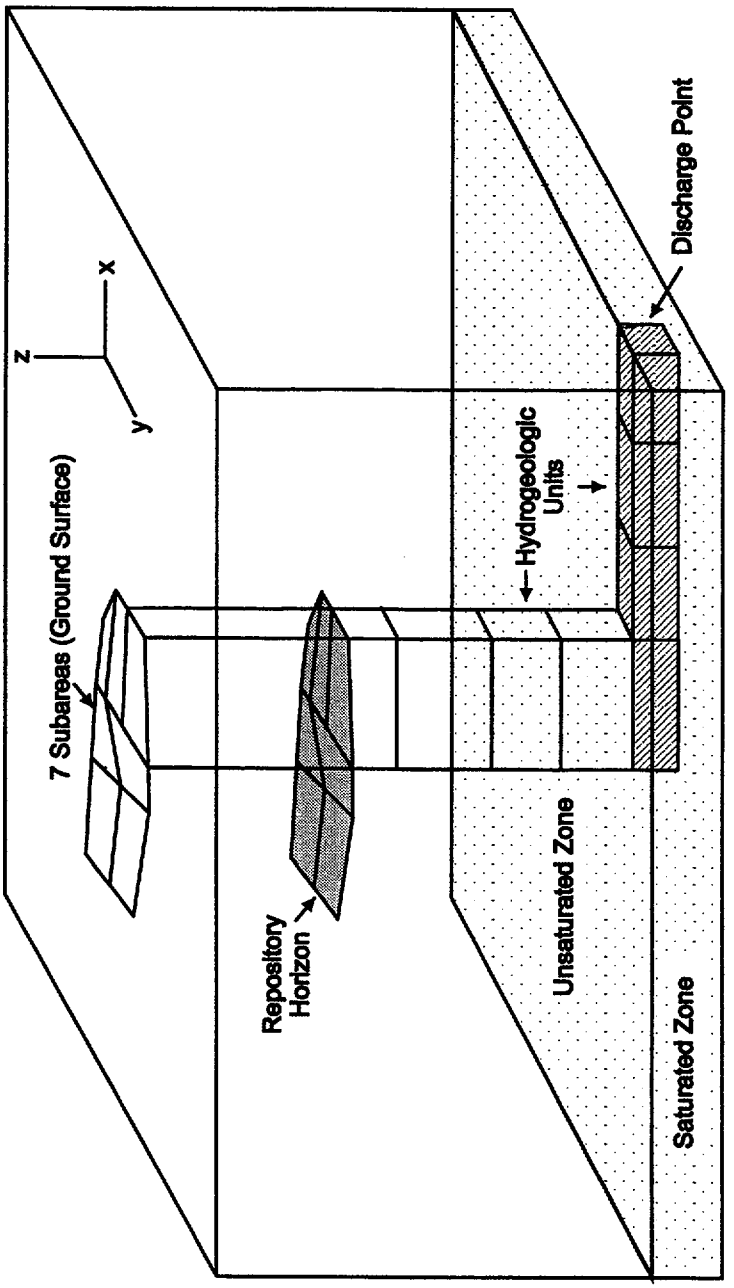

Figure 2-2. Conceptualization of the repository system.

2.2 CONCEPTUAL MODELS IMPLEMENTED IN THE TOTAL-SYSTEM PERFORMANCE ASSESSMENT COMPUTER CODE

In developing the TPA Version 3.2 code, several conceptual models were formulated, integrated, and implemented in various abstracted mathematical models. These basic conceptual models, which describe the interactions and couplings of the physical and chemical processes believed present in a proposed geologic repository at YM, can be grouped into the following generic categories:

- Infiltration and deep percolation;
- Near-field environment;
- Radionuclide releases from the EBS;
- Aqueous-phase radionuclide transport in the UZ and SZ;
- Airborne transport from direct radionuclide releases; and
- Exposure pathways and reference biosphere.

These conceptual models are designed to apply to the current DOE repository design and specific site characteristics of the YM area and provide flexibility for examining alternative designs and uncertainties in site and engineered material performance. In some of these generic categories, alternative conceptual models also have been incorporated into the code.

These conceptual models are used to represent a range of system states, including disruptive events. The consequences of disruptive events (e.g., seismicity, fault displacement, and igneous activity) are evaluated with the TPA Version 3.2 code by assessing the effects on EBS failure (producing releases to groundwater); direct releases of radionuclides (airborne releases to the biosphere); or both. The probability of occurrence of a disruptive event combined with the resulting consequences are used to calculate a risk curve separate from the TPA Version 3.2 code execution.

The following discussion provides a general overview of the key aspects of the major conceptual models implemented in the TPA Version 3.2 code. More detailed descriptions of these models, including the mathematical basis, assumptions, and calculational methodologies, are presented in the TPA Version 3.2 code "User's Guide" (Mohanty and McCartin, 1998).

2.2.1 Infiltration and Deep Percolation

A one-dimensional (1-D) modeling approach is used in the TPA Version 3.2 code to describe the movement of meteoric water at the land surface vertically downward (i.e., without lateral flow) through the UZ, to the repository horizon, and ultimately to the water table. In the 1-D conceptual model, the deep percolation flux (q_{perc}) is constrained to be equal to the shallow infiltration rate (q_{infil}). The annual average q_{infil} is estimated based on

- Present-day shallow-infiltration rate;
- Change in climate with time; and
- Elevation and soil depth over the repository subarea.

Uncertainty in the present-day infiltration rate estimate is accounted for in the TPA Version 3.2 code by treating it as a statistically sampled input parameter. Temporal variations are incorporated by varying the present-day infiltration rate over the 100,000-yr TPI assumed for long-term climatic changes. The effects

of site-specific soil cover thickness and elevation are used to reflect the spatial variation over each of the subareas.

The temporal and spatial variations of q_{infil} were developed through consideration of paleo-climatic information and results from detailed process-level auxiliary analysis (Stothoff, *et al.*, 1997). The q_{infil} response function depends on two independent variables, present-day mean annual precipitation (MAP) and mean annual temperature, as well as the present-day infiltration rate. After computing q_{infil}, the water flux at the repository horizon is then partitioned into

- Water flux diverted around the WP; and
- Water flux entering the failed WP.

Thus, for the purposes of the TPA Version 3.2 code, the net water flux carrying dissolved radionuclides is a fraction of the total water flux arriving at the repository. It is this net water flux that is used in the TPA Version 3.2 code to calculate the radionuclide source term for each subarea.

2.2.2 Near-Field Environment

Physical and chemical processes in the near field of the repository, such as heat transfer, water-rock geochemical interactions, and refluxing of condensate water, are expected to affect WP performance. In the TPA Version 3.2 code, a range of near-field characteristics is depicted in the abstracted mathematical models for heat and water flow and table look-ups for chemical parameters. To estimate WP failure times and radionuclide release rates, the near-field environment is characterized by

- Drift wall rock and WP surface temperatures;
- Relative humidity (RH) (defined in the TPA code as the ratio of vapor pressure at the drift rock wall to the vapor pressure at the WP surface);
- Water chemistry (e.g., pH, chloride concentration, and carbonate ion concentration); and
- Water reflux during the thermal phase.

The average rock temperature in the repository horizon is calculated assuming a conduction-only model (i.e., the time history of temperature for each subarea is calculated accounting for the amount of emplaced waste) and no ventilation in the drifts. The WP surface temperature is calculated using a multimode heat transfer (i.e., conduction, convection, and radiation) model. Vapor pressure is computed using the standard thermodynamic equation relating vapor pressure to temperature.

Estimates of the pH and chloride concentration histories of water films on the WP surface were developed in a separate process-level auxiliary analysis using the multicomponent geochemical module of the MULTIFLO code (Lichtner and Seth, 1996). MULTIFLO was applied to calculate the pH and chloride concentration for water percolating through the matrix of the tuffaceous rock. Because the chloride concentration in the water film is likely to be higher than that in the rock mass, the chloride history is scaled by a statistically sampled parameter that varies between 1 and 30, where 30 scales the peak chloride concentration to its solubility limit. The TPA Version 3.2 code provides the option of either using a look-up table that uses the temperature-dependent pH (not currently used) and chloride concentration generated with

the MULTIFLO code, or specifying constant values in the input file. In general, the user selects code options by changing flag and variable values in the code input file.

The amount of water percolating through the drifts varies over time primarily because of the coupled processes of heat transfer and fluid flow (e.g., vaporization, condensation, and refluxing). Water refluxing produced by these thermohydrologic effects is important during the first few thousand years, after which natural percolation determines the rate of water flow into the repository. Three water reflux models based on bulk flow balances are included in the TPA Version 3.2 code. The first model considers episodic reflux associated with time-dependent perching above the repository. The second model assumes that the volume of refluxing water will always be sufficient to depress the boiling isotherm in fractures and reach the WP during times when the surface temperature exceeds the boiling point of water. In the third model, the degree to which the boiling isotherm is depressed is a function of the temperature, the thickness of the dryout zone, and the volume of reflux water. These functions vary with time. Each reflux model produces estimates of the total water flux into the repository during the thermal period.

2.2.3 Radionuclide Releases from the EBS

In the TPA Version 3.2 code, the performance of a prototypical WP is modeled for each repository subarea, considering the failure time and radionuclide release rates for each of the WP failure categories. When this prototypical WP fails, all WPs in that subarea within a specified failure category are assumed to have failed. The estimation of both WP failure times and liquid releases is dependent on the nature and extent of corrosion, near-field environment, percolation flux in the drift, and external processes that may impose static loads, dynamic loads, or both. WP failures are grouped into three basic categories: (i) corrosion and mechanical; (ii) disruptive event; and (iii) initially defective. After determining the WP failure time, the TPA Version 3.2 code calculates the aqueous-phase radionuclide releases from the WP by considering the dissolution of radionuclides from the SF matrix, advective transport from the WP, and advective and diffusive transport through the invert directly to the UZ beneath the repository.

Corrosion failure of the WP is defined to occur at the time when the inner overpack is fully penetrated by a single pit and the waste form is therefore accessible to water. The abstracted corrosion model uses a conceptual framework that assumes the formation of a water film containing a salt solution but does not explicitly consider water dripping on the container. The corrosion processes considered in the model abstraction are:

- Dry air oxidation;
- Humid air corrosion; and
- Aqueous corrosion.

WP surface temperature and the chloride concentration in the water film influence the mode, and hence, the rate, of corrosion. The predominant mode of corrosion, however, depends on the critical RH as well as the container material. Mechanical failure of the WP is considered the result of fracture of the outer steel overpack from thermal embrittlement arising from prolonged exposure at temperatures sufficiently elevated to cause substantial degradation of mechanical properties.

Disruptive event failures are taken into account by modeling the effects of events such as seismicity, fault displacement, and igneous activity. In the case of seismicity, the drift is assumed to have no backfill that could prevent rockfalls from mechanically loading and deforming the WP. Because the DOE plans to

not emplace WPs within a setback distance from known and well-characterized faults, displacements along yet undetected faults or new faults that exceed a preestablished threshold are assumed to fail WPs within the fault zone. For igneous activity, simulated magmatic intrusions intersecting the repository are assumed to cause WP failure; WPs within a dike but outside the vent hole are assumed to fail and expose the SF to water, whereas those within the vent hole (the diameter of which is a sampled parameter) are assumed entrained in the magma and released directly to the biosphere. For both igneous activity and fault displacement, failures are modeled by superimposing the physical dimensions of the perturbation (i.e., length, width, and orientation of the fault and the igneous intrusion) on the repository footprint to determine the total number of WPs potentially affected in each repository subarea. Separate failure times are calculated for seismicity, fault displacement, and igneous activity. Because multiple seismic events occur during the 10,000- and 100,000-yr TPIs, seismic failure occurrences are collected into four distinct failure times.

In most applications of the TPA Version 3.2 code, it is assumed a small number of WPs is failed at the time of repository closure. These initially failed WPs are attributed to fabrication defects or damage to the WP as a result of improper emplacement. The average number of initially defective WPs is typically assumed to be 0.1 percent[1] of the total number of containers.

Radionuclide releases from the WP are calculated by considering the alteration rate of SF (i.e., rate at which radionuclides in fuel become available for release); radionuclide solubility limits; and transport mechanisms out of the WP. The TPA Version 3.2 code incorporates a number of parameters [e.g., fraction of SF that is wet; particle size of the SF; alteration rate of (UO_{2+x}), and credit for cladding] that control the release of radionuclides from the SF matrix. The effects of the formation of secondary minerals such as schoepite on SF dissolution are treated separately. After radionuclides are leached from the SF waste form, the calculated releases are adjusted to ensure consistency with the radioelement solubility limits. The gap fraction inventory of radionuclides is available for instantaneous release and therefore, may be a major contributor to peak dose.

A parameter value in the code input file is used to specify the fraction of failed WPs that is wetted in the subarea. This value represents the number of failed WPs available to contribute to the source term. To compute the time-dependent source term, the TPA Version 3.2 code provides two alternative conceptual models: (i) a bathtub model—the WP must fill with water to a certain depth (up to the height of the outlet) before the radionuclides are released—and (ii) a flowthrough model—radionuclides are released by water dripping on the waste form and continuing immediately out of the bottom of the container. For the bathtub model, the WP is treated as a stirred tank, with the tank capacity dependent on the statistically sampled water outlet height. Water will fill the WP until the capacity (height) is reached and, thereafter, the amount of water entering the WP will equal the amount of water flowing out. Water leaving the WP transports dissolved radionuclides into the UZ below the repository. The water capacity of the bathtub is assumed unique to the failure modes and to subareas (except for faulting and igneous activity failures). Releases from WPs will travel through the invert before exiting the EBS. If the physical properties of the construction material for the invert are conducive, the radionuclide species could be sorbed, thus reducing the magnitude of radionuclide release from the near field. The flowthrough model is a variant of the bathtub model, except water does not have to first fill the bathtub before release; instead, radionuclides are released as soon as water enters the WP.

[1]Tschoepe, E.C. *et al.* (1994) suggest fabricated metallic component reliabilities of 99.9–99.99 percent.

2.2.4 Treatment of Aqueous-Phase Transport in the Unsaturated and Saturated Zones

Movement of aqueous-phase radionuclides from the repository horizon, through the UZ, SZ, and ultimately to the receptor group, is modeled in the TPA Version 3.2 code, using the streamtube approach described in Section 2.1. Each streamtube encompasses one or more repository subareas and is composed of a vertical section from the repository to the water table and horizontal sections in the SZ. The transport module NEFTRAN II (Olague, *et al.*, 1991) simulates the spectrum of processes (e.g., advection, dispersion, matrix diffusion, sorption, and decay) occurring within individual streamtubes. For the set of radionuclides specified in the code input file, the UZ and SZ modules simulate their vertical transport through the UZ and horizontal transport through the SZ.

Time-dependent flow velocities in the UZ are calculated using the hydraulic properties of each major hydrostratigraphic unit. The UZ transport module simulates the transport of radiocontaminants through either the porous rock matrix or fractures.[2] Radionuclide retardation by chemical sorption in the rock matrix is also included in the model; however, retardation on fracture surfaces is neglected.

Although groundwater flow in the SZ is assumed at steady state, radionuclide transport within individual streamtubes is time-dependent because the source term varies with time. Streamtubes in the SZ exhibit variable cross-sections along the flow path; this variable streamtube geometry was determined from a separate two-dimensional modeling study of the subregional flow (Baca, *et al.*, 1996). The conceptual model of the SZ assumes that flow in the tuff aquifer is in localized conductive zones (i.e., permeable fracture zones) while flow in the alluvium is presumed uniformly distributed in the alluvial aquifer. Although the streamtube approach neglects dilution effects arising from lateral dispersion, credit is taken for sorption in the alluvium, which is likely to retard aqueous-phase transport of many radionuclides. Additionally, matrix diffusion from flowing pores and fractures into the more-or-less stagnant matrix pore water within the rock is included in the SZ transport model.

2.2.5 Airborne Transport from Direct Releases

Radiologic risks associated with the extrusive component of igneous activity are calculated in the TPA Version 3.2 code by modeling airborne releases of radionuclides for simulated extrusive events. The igneous activity module assumes that the magma intercepts WPs, moves upward to the land surface, and then ejects the ash and SF mixture into the atmosphere. The physical characteristics of each simulated extrusion (e.g., vent size, event energetics, and duration) and the atmospheric conditions are treated as statistical parameters in calculations of ash dispersal and deposition patterns, ash blanket thickness, and radionuclide soil concentrations. The three primary factors determining the ash plume geometry and transport rates are:

- Power and duration (of the eruption);
- Wind speed and direction; and
- SF particle sizes.

[2]Transport though rock matrix takes place if the percolation rate, q_{perc}, is less than the hydraulic conductivity of the rock matrix, K_{matrix}, or through fractures when q_{perc} exceeds K_{matrix}.

The ash transport model developed by Suzuki (1983) was modified by Jarzemba, *et al.* (1997) and incorporated into the TPA Version 3.2 code to calculate distribution of the released radionuclides. The time-dependent radionuclide areal densities are calculated taking into account the thickness of the ash blanket, leaching and erosion rates, and radionuclide decay rates. The calculated doses attributed to direct releases are strongly influenced by the time of the event (early events result in larger doses, in part, because of the contribution to the estimated doses from short-lived fission products present in the SF).

2.2.6 Exposure Pathways and Reference Biosphere

Dose calculations are performed in the TPA Version 3.2 code for exposure pathways that consider an average person of a designated receptor group. These calculations express dose in rem/yr or mrem/yr. Alternative receptor groups are currently included in the exposure scenario. One receptor group is a farming community 20 km (12.4 mi) from the repository location whereas the second is a residential community at a specified distance, typically less than 20 km (12.4 mi). The average member of the designated receptor group is assumed exposed to radionuclides transported through the groundwater pathway, air pathway, or both, as a result of direct releases arising from the extrusive component of igneous activity.

Geographic location and lifestyle characteristics assigned to each receptor group are two primary aspects defining the receptor group and are specified in the TPA Version 3.2 code by selection of appropriate input options. In addition, the farming community receptor group is assumed to include persons that use the contaminated water for

- Drinking [i.e., 2 liters per day (0.5 gallons per day)]; and
- Agriculture typical of Amargosa Valley area practices (e.g., growing alfalfa and gardening).

The farming community receptor group is assumed exposed to surface contamination through:

- Consumption of contaminated farm products (i.e., ingestion);
- Breathing air with ash-SF particles (i.e., inhalation); and
- Direct contact.

In contrast, the residential receptor group is assumed composed of persons who use contaminated groundwater only for drinking, but are also exposed to surface contamination (created by ash-SF particle deposition from the extrusive component of igneous activity) through inhalation and direct exposure.

Site-specific dose conversion factors (DCFs) for each radionuclide and pathway are contained in TPA data files. These DCFs are used to convert radionuclide concentrations in the groundwater and soil to doses. The individual DCFs are mean values[3] generated through separate pathway calculations using the GENII-S code (Leigh, *et al.*, 1993). In the groundwater pathway, for example, the DCFs are applied to the concentrations at the well head. Two separate sets of DCFs are included in the TPA Version 3.2 code to represent two distinct reference biospheres associated with the present arid climate (nonpluvial) and the projected future pluvial climate. The determination of whether the climate is nonpluvial or pluvial is based on the Köppen Geiger climate classification model (Strahler, 1969). In addition to computing the dose history for each stochastic simulation, the TPA Version 3.2 code scans these dose calculations to identify the magnitude and timing of the peak dose within a specified TPI.

[3]The justification for using mean values can be found in Mohanty and McCartin (1998).

2.3 BASECASE DEFINITION AND ALTERNATIVE CONCEPTUAL MODELS

The conceptual models available in the TPA Version 3.2 code are briefly presented in the previous sections. The option to evaluate alternatives to the basecase conceptual models is included in the TPA Version 3.2 code. The following sections list the set of conceptual models selected for the basecase studies and also describe the alternatives to the basecase models analyzed for mean input values in Chapter 3 and sampled distributions in Chapter 4.

2.3.1 Basecase

The basecase input data set reflects current repository design features and likely parameter-range estimates for evaluation of processes affecting repository performance. The set of conceptual models that constitutes the basecase against which alternative conceptual models are evaluated in the sensitivity/uncertainty analyses include:

- No cladding protection;
- Dissolution of SF based on J-13 well-water chemistry;
- Bathtub model (i.e., pooling of water in the WP after failure) for determination of water mass balance and fuel wetting of the failed WP; and
- No matrix diffusion of contaminants in the UZ.

A complete list of the input parameters used for the basecase can be found in Appendix A in the TPA Version 3.2 code "User's Guide" (Mohanty and McCartin, 1998). Climate change and seismicity are considered as integral components of the basecase and, therefore, alternative conceptual models to the components are not considered in the analyses.

2.3.2 Alternative Conceptual Models

Various alternative conceptual models are investigated to determine the sensitivity of repository performance to changes in WP design, radionuclide release mechanisms, and radionuclide transport models. These alternative model runs are conducted with the TPA Version 3.2 code and do not include disruptive events (faulting or igneous activity). The alternative models used in this analysis are grouped according to fuel wetting assumptions, fuel-dissolution models, and transport assumptions. For the analyses presented in this report, the repository performance is defined as dose for the mean value data set and as the peak of the expected dose from the multiple-realization results in the TPI.

2.3.2.1 Fuel-Dissolution Models

The TPA Version 3.2 code contains four models (Model 1–Model 4) for the dissolution rate of the SF that has come into contact with water. The basecase model uses Model 2 (Mohanty and McCartin, 1998), which is based on the dissolution rate of SF in J-13 water containing silica and calcium ions. The alternative dissolution models are listed next. Some of the alternatives are combined with fuel wetting alternatives as well.

Fuel-Dissolution Model 1

The first alternative fuel-dissolution model (IModel = 1) has an increased SF dissolution rate at high carbonate concentrations (Mohanty and McCartin, 1998) and reduced silicate and calcium concentrations in the water entering the WP.

Fuel-Dissolution Model 3 (Natural Analog)

In this alternative conceptual model, fuel dissolution and contaminant release rates are based on maximum likely rates inferred from measurements at the Peña Blanca, Mexico, natural analog site (Mohanty and McCartin, 1998). For this alternative, the uranium dissolution rate for fully exposed fuel is 24 kilogram/year (kg/yr) [53 pounds per year (lb/yr)] from the entire repository, but is further limited by the fraction of wetted WPs and the fuel wetting factors. The two factors range from 0 to 1 and are sampled. This alternative conceptual model is invoked by setting IModel = 3.

Fuel-Dissolution Model 4 (Schoepite Dissolution)

The schoepite-alternative conceptual model assumes that all radionuclides released from the SF matrix are captured in the secondary uranium mineral schoepite (Mohanty and McCartin, 1998) and are subsequently released at a limit controlled by schoepite solubility. This model is specified by setting IModel = 4.

2.3.2.2 Fuel-Wetting Assumptions

This grouping includes alternative conceptual models related to the way SF in the WP is contacted by water. These five alternative models use combinations of the flowthrough and dissolution-rate models, and also TPA input parameters for the amount of water and fraction of the subarea wetted by impinging water.

Flowthrough Model with Fuel-Dissolution Model 2

This alternative conceptual model evaluates the flowthrough option in which water enters WPs through corrosion pits but does not pool in the container. In the bathtub model used in the basecase, the fraction of fuel wetted is determined by the bathtub height (determined by the position of the exit port, which is a corrosion pit), which is sampled and ranges from 0 to 1. In the flowthrough model, the fraction of fuel wetted is unrelated to the water level in the WP. Additionally, the fraction of fuel wetted is likely much smaller and depends on poorly understood phenomena such as dripping patterns, surface tension, and vapor-phase wetting. This alternative conceptual model is invoked by specifying a smaller range for the parameter Fmult* (one-tenth of the normal range for the basecase),[4] to simulate a smaller fraction of wet fuel surface. In this model, solubility limits for the radionuclides might become important because of the limited amount of water in contact with the fuel.

[4]Fmult* is the fraction of water, infiltrating to the repository from the unsaturated zone above the repository, that will enter the WP and contribute to the release of radionuclides. Water dripping toward the drifts may be diverted around the drift because of capillary action, may be diverted down the side of the drift, or may not enter the WP for other reasons.

Flowthrough Model with Fuel-Dissolution Model 1

This alternative conceptual model uses the flowthrough model and IModel = 1 (carbonate-dissolution model), which assumes that silicate and calcium will be depleted from much of the water entering the WP by reaction with the fuel and metal in its path.

Focused Flow

The basecase conceptual model assumes that all parts of a repository subarea will receive an equal quantity of infiltrating water. This alternative conceptual model accounts for the possibility that water infiltration reaching the WPs will be focused or funneled by discrete fractures, which will wet some of the WPs more heavily than others. This alternative model is evoked by increasing the range of Fmult* by a factor of 4 (from 0.01–0.2 to 0.04–0.8), while decreasing the fraction of WPs wetted by a factor of one-fourth (from 0–1 to 0–0.25). This has the effect of funneling the same quantity of water for each subarea to one-fourth the number of WPs.

Cladding Credit Plus SF Dissolution Model 1

The basecase conceptual model assumes that once the inner and outer overpack containers have been breached, SF is exposed and available for dissolution and transport. This assumption ignores any protection afforded the fuel from intact and partially failed cladding. In this alternative model, the effect of cladding protection is simulated by setting the SF wetted fraction to a constant value of 0.005 for the entire TPI.

Grain-Size Model with Fuel-Dissolution Model 1

This conceptual model uses the grain size from the uranium dioxide fuel, instead of the particle size, to determine surface area, which leads to a higher dissolution rate because of the increased surface area. This alternative conceptual model combines the fuel-dissolution rate model 1 for relatively fast dissolution by carbonate water, with the large surface area provided by assuming that the fuel surface area is determined by the grain size. Both these assumptions are used in the DOE-TSPA-VA model (U.S. Department of Energy, 1998) for radionuclide release from SF.

2.3.2.3 Transport Alternatives

The transport assumptions in the basecase UZ and SZ conceptual models are investigated with three alternative models. These assumptions affect the releases and time of release from the EBS, UZ, and SZ.

No Retardation of Plutonium (Pu), Americium (Am), and Thorium (Th)

This alternative conceptual model demonstrates the contribution, to repository performance, of retardation of Pu, Am, and Th in the geosphere, and the effect on the groundwater doses if this sorption were removed. Once released from failed WPs, Pu, Am, and Th are assumed to travel at the same speed as water through the EBS, UZ, and SZ to the receptor location. This alternative model is invoked by setting equilibrium coefficients (K_d) to zero and retardation coefficients (R_d) to unity for these elements. This model is a gross approximation of potential contribution from colloids that could move through the geosphere unretarded if filtration processes were not considered.

No-Invert Model

The TPA Version 3.2 code contains a model that takes into account the effect of flow and retardation through the invert material beneath the WPs. This function is normally activated. The no-invert alternative model negates the effect of the invert. This is accomplished by setting the variable *InvertBypass* equal to 1 in the code input file.

Matrix Diffusion

This conceptual model assumes that matrix diffusion will occur in the tuff SZ transport legs where there is fracture flow. Matrix diffusion is specified by setting the parameter *DiffusionRateSTFF* as a loguniform distribution ranging from 0.01 to 1.0 yr^{-1}. Two other factors involved in the matrix diffusion alternative are the immobile porosity and the retardation coefficients in the immobile phase. The default values in Appendix A of the TPA Version 3.2 code "User's Guide" (Mohanty and McCartin, 1998) are used to evaluate this conceptual mode.

3 ANALYSIS OF TOTAL-SYSTEM BEHAVIOR

In this chapter, the relationships between repository performance and the key input parameters and intermediate results are presented. The mean values and distributions for the uncertain TPA input parameters are summarized in Tables 3-1 to 3-18.

In the single-realization case, mean values for the TPA input parameters are used and the results evaluated over the 10,000- and the 100,000-yr TPIs. The single-realization simulation establishes a baseline to investigate the behavior of the total system at the process level (e.g., WP lifetime and SZ travel time) and the repository performance as measured by groundwater dose. Additionally, the repository performance is related to the key input parameters and intermediate results in a deterministic mode.

After the discussion of results from the single-realization simulation, a description of the variability in the TPA results from multiple realizations is presented. The variability in the behavior of the total system at the process level and the repository performance are analyzed in multiple realizations using distributions for the TPA input parameters. For example, the variability in dose is related to the release rate from the EBS. Both the single- and multiple-realization basecase analyses provide background information and form the framework to evaluate and quantify the sensitivity of repository performance to TPA input parameters presented in Chapter 4. After the multiple-realization results, the TPA outputs from alternative conceptual models and disruptive events are presented. This chapter concludes with a discussion of a methodology used to calculate risks from the disruptive events.

3.1 SINGLE-REALIZATION DETERMINISTIC ANALYSES

This section examines repository behavior for a single realization to illustrate how a component influences both the dose and the behavior of other components. For the single realization, all input parameters are specified at mean (or expected) values. It should be noted that the annual dose obtained from using the mean value data set most likely will not be the same as the expected annual dose (which is the performance measure) obtained from multiple-realizations because of the nonlinear dependency of dose on input parameters.

The general representation of waste emplacement at YM is a total of 62,800 Metric Tons Uranium (MTUs) in an area of 3,060,000 meters^2 (m^2) [approximately 3,000 m (1.9 mi) long and 1,000 m (0.6 mi) wide]. Assuming a payload of 9.76 MTU per WP and an equivalence between the SF and other types of wastes, such as DOE waste and glass waste, approximately 6,427 WPs will be needed for waste disposal. The initial inventory activity is approximately 7.4×10^{18} Becquerel (Bq) [200×10^6 Curies (Ci)]. WPs with a 5.682-m (18-6 ft) length and a 1.802-m (5.9-ft) diameter are emplaced in drifts 5 m (16.5 ft) in diameter, spaced 22.5 m (73.8 ft) apart. The average age of the SF is 26 yr. The descriptions of the mean values for the key parameters used in various process-level calculations are presented in each of the following sections.

3.1.1 Unsaturated Zone Flow

Detailed modeling (Stothoff, 1999) suggests that climate conditions could significantly affect the flow of water in the UZ and into the repository. As a consequence, the amount of water contacting a WP, which affects the release rate of radionuclides from the EBS and the transport of the radionuclides in the UZ, may also be significantly influenced.

In the TPA Version 3.2 code,[5] precipitation is assumed to vary from present-day to pluvial conditions over a period of 100,000 yr. For the mean value data set, Figure 3-1 shows the MAP changes from about 160 to 330 mm/yr (0.52 to 1.08 ft/yr), whereas the infiltrating water enters the UZ from 5 to 110 mm/yr (0.016 to 0.36 ft/yr). Based on the Köppen Geiger system of climate classification (Strahler, 1969) implemented in the TPA code to determine the onset of the pluvial period, approximately 90 percent of the 100,000-yr TPI is characterized by pluvial conditions and 10 percent of the time is represented by the present-day climate.

For higher flow rates, there are generally larger releases because of the greater amount of water available to dissolve and transport radionuclides out of the WP. Increasing flow rates in the UZ are not only expected to transport a larger mass of radionuclides from the EBS, but also lead to higher doses. The mean values of the parameters used to calculate the time-varying infiltration rates in the UZ are presented in Table 3-1.

3.1.2 Near-Field Environment

The near-field thermal conditions may alter the flow of water into the repository, which influences the quantity of water that contacts, dissolves, and transports the SF out of the EBS. The near-field chemical environment in conjunction with the thermal environment affects WP corrosion and determines quantity and time history of water entering the WP. These near-field conditions and the flow of water onto the WPs are discussed in the following sections.

3.1.2.1 Repository-Scale Thermohydrology

Radioactive decay of SF generates heat that perturbs ambient percolation conditions. The heat evaporates water and creates a dryout zone around the drift. Above the repository horizon, the water vapor condenses and flows back toward the repository, thus creating a reflux zone. The reflux zone is maintained until the near-field temperature falls below boiling. When the temperature falls below boiling or water from the condensate zone penetrates the dryout zone, water flows into the drift. Water entering the drift may impinge on the WP and contribute to WP corrosion failure. After the WP fails, water contacts the SF and is transported out of the EBS into the UZ.

Of the three reflux models in the TPA code indicated in the previous chapter, the third model was used in the basecase. This model estimates the depth that water will penetrate the boiling isotherm as a function of dryout zone thickness and the volume of water flowing from the condensate zone. Table 3-2 presents the mean values of parameters used in the reflux calculations.

Figure 3-2 presents, except for early times, subarea-to-subarea variations in the volume of water contacting WPs, which behave similarly to the infiltration rates in Figure 3-1. Figure 3-2 also shows slight differences in the seepage flux between subareas and a consistency in the general behavior of the seepage flux for all seven subareas with subarea 3 having the largest seepage flux attributable to the effects of elevation and soil thickness.

[5]The specific version of the code used in developing this chapter is 3.2.3.

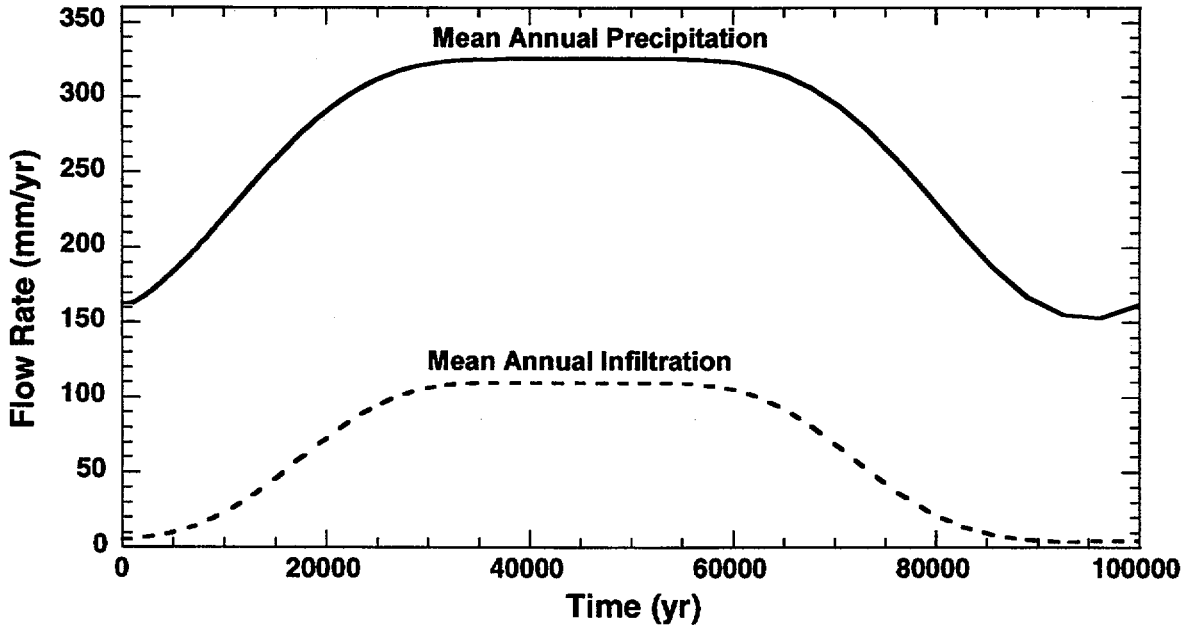

Figure 3-1. Mean annual precipitation and infiltration at the repository horizon averaged over all subareas and encompassing both the current and pluvial periods for the mean value data set.

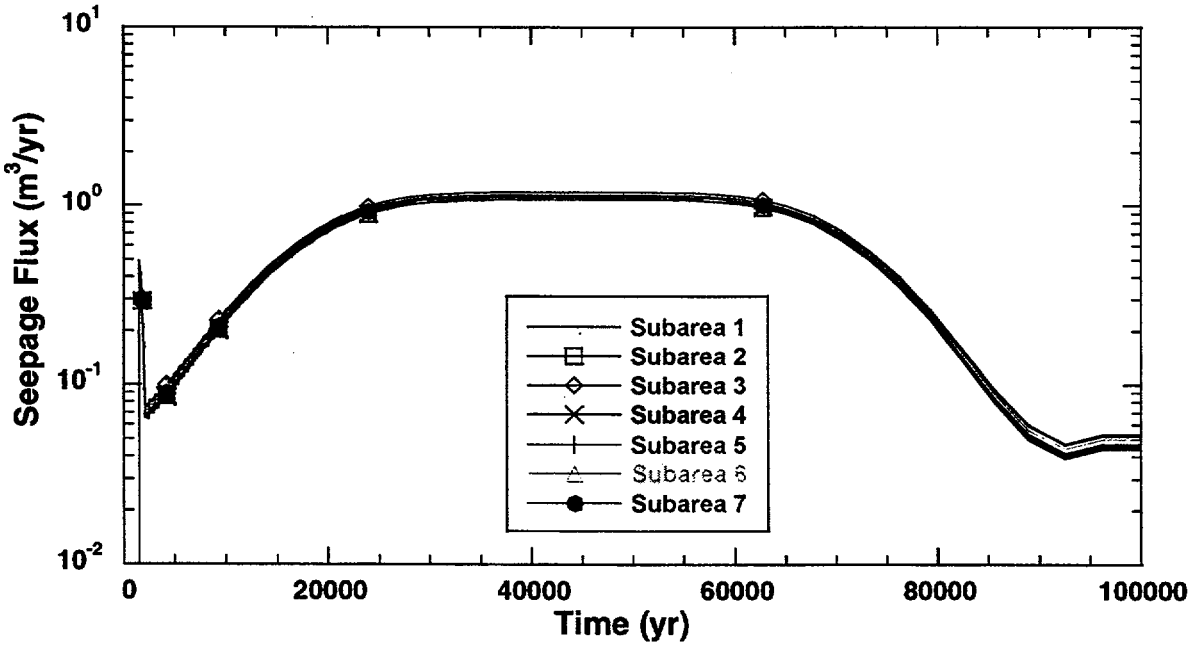

Figure 3-2. Effect of the thermal perturbation on the near field seepage rate in each subarea for the mean value data set.

Table 3-1. Mean values and sampled distributions of parameters for infiltration calculations

Parameter	Mean Value	Distribution
Areally averaged mean annual infiltration for the initial (current) climate	5.50 mm/yr	Uniform; 1.0, 10.0
Mean average precipitation multiplier at glacial maximum	2.00	Uniform; 1.5, 2.5
Mean average temperature increase at glacial maximum	−7.50 °C	Uniform; −10.0, −5.0

Table 3-2. Mean values and sampled distributions of parameters for determining repository-scale and drift-scale thermohydrology (The hyphen in the last column indicates a constant value for the parameter distribution.)

Parameter	Mean Value	Distribution
Length of reflux zone	2.00×10^{1} m	—
Maximum flux in reflux zone	1.00×10^{-9} m/s	—
Perched bucket volume per subarea-area	5.00×10^{-1} m^3/m^2	—
Fraction of condensate removed	1.00×10^{-4} /yr	Log-uniform; 1.0×10^{-8}, 1.0
Fraction of condensate toward repository	5.00×10^{-1} /yr	Uniform; 0.0, 1.0
Fraction of condensate toward repository removed	1.00×10^{-4} /yr	Log-uniform; 1.0×10^{-8}, 1.0
Density of water at boiling	9.61×10^{2} kg/m^3	—
Enthalpy of phase change for water	2.40×10^{6} J/kg	—
Temperature gradient in vicinity of boiling isotherm	5.05×10^{1} K/m	Uniform; 1.0, 100.0
Ambient repository temperature	2.00×10^{1} °C	—
Mass density of Yucca Mountain rock	2.58×10^{3} kg/m^3	—
Specific heat of Yucca Mountain rock	8.40×10^{2} J/(kg-K)	—
Thermal conductivity of Yucca Mountain rock	2.00 W/(m-K)	Uniform; 1.8, 2.2
Emissivity of drift wall	8.00×10^{-1}	—
Emissivity of waste package	7.00×10^{-1}	—
Thermal conductivity of floor	6.00×10^{-1} W/(m-°C)	—
Effective thermal conductivity of unbackfilled drift	9.00×10^{-1} W/(m-°C)	—
Time of emplacement of backfill	1.00×10^{5} yr	—
Effective thermal conductivity of backfill	6.0×10^{-1} W/(m-°C)	—
Thermal conductivity of inner stainless steel wall	1.50×10^{1} W/(m-°C)	—
Thermal conductivity of outer carbon steel wall	5.00×10^{1} W/(m-°C)	—
Effective thermal conductivity of basket and spent fuel in waste package	1.00 W/(m-°C)	—
Elevation of repository horizon	1.07×10^{3} m	—
Elevation of ground surface	1.40×10^{3} m	—

The spike in Figure 3-2 at early times illustrates a large change in the seepage flux that occurs because of a higher thermal perturbation. Although this thermal perturbation takes place before to corrosion failures, the modified infiltration rate could affect releases from initially defective failures or seismically induced failures. The duration of the thermal perturbation is small compared with long simulation periods such as 10^5 yr; however, it may be significant for the 10,000-yr TPI. The subarea average infiltration rate in the UZ is provided in Figure 3-3. Water flowing into the drift and water entering the WP are also illustrated in this figure. The effects of the thermal perturbation on the flow rate are evident in this figure for approximately 3000 yr. Once the infiltration into the repository begins, the rate increases by a factor of approximately 5 compared with the ambient infiltration rate. The thermal augmentation of flow for the mean values data-set case lasts about 1000 yr. Significant infiltration into the repository is delayed until approximately 2000 yr. Afterward, the thermal effects no longer influence the UZ flow above the repository.

3.1.2.2 Drift-Scale Thermohydrology

WP surface temperature, drift wall temperature, and WP surface RH are computed for each subarea. The mean TPA input parameters used to compute these values are presented in Table 3-2. Figure 3-4 illustrates the subarea-to-subarea differences in the WP surface temperature, and Figure 3-5 shows WP surface RH. For the mean value data set presented in Table 3-2, the highest temperature of approximately 150 °C (302 °F) is observed at about 100 yr. The temperature remains above ambient temperature even at 100,000 yr. Subareas 1 and 2 are the largest subareas and subarea 7 is the smallest, located away from the center of the repository and with an elongated shape. Thus, in subareas 1 and 2, WPs cool much more slower compared with subarea 7. Subarea 7 exhibits the greatest differences in temperature and RH when compared with subareas 1 through 6.

Subarea-dependent temperature and RH values from the near field are also used by the WP degradation model to determine the WP failure time. Consequently, the WP failure time may be different for each subarea. For the drift-scale thermohydrology, the climatic conditions were considered irrelevant because fluid flow was not modeled in the temperature and RH calculations. Fluid flow was not accounted for in the temperature and RH calculations, because its effect was found to be insignificant in the detailed calculations using equivalent continuum modeling conducted outside the TPA code.

3.1.2.3 Near-Field Geochemical Environment

The near-field geochemical environment is represented by the time-dependent chloride concentration that interacts with the WP and wasteform inside the drift. The parameters available to the TPA analysis are the chloride concentration, oxygen partial pressure, the solution pH, and the total dissolved carbonate. Figure 3-6 shows the time history of chloride concentration used by the TPA program, which was calculated with the MULTIFLO (Lichtner and Seth, 1996) computer program and supplied in tabular form to the TPA code. The chloride concentration is calculated based on an initial fluid composition corresponding to J-13 well water and represents the time-dependent composition of water available at the drift wall. The chloride multiplication factor in Table 3-3 (mean value of 15.5) modifies the time-dependent chloride concentration curve presented in Figure 3-6. The chloride multiplication factor is intended to account for the uncertainty in estimating the water chemistry; the parameter values (chloride concentration) and MULTIFLO results are considered to be the lower bound for chloride concentration.

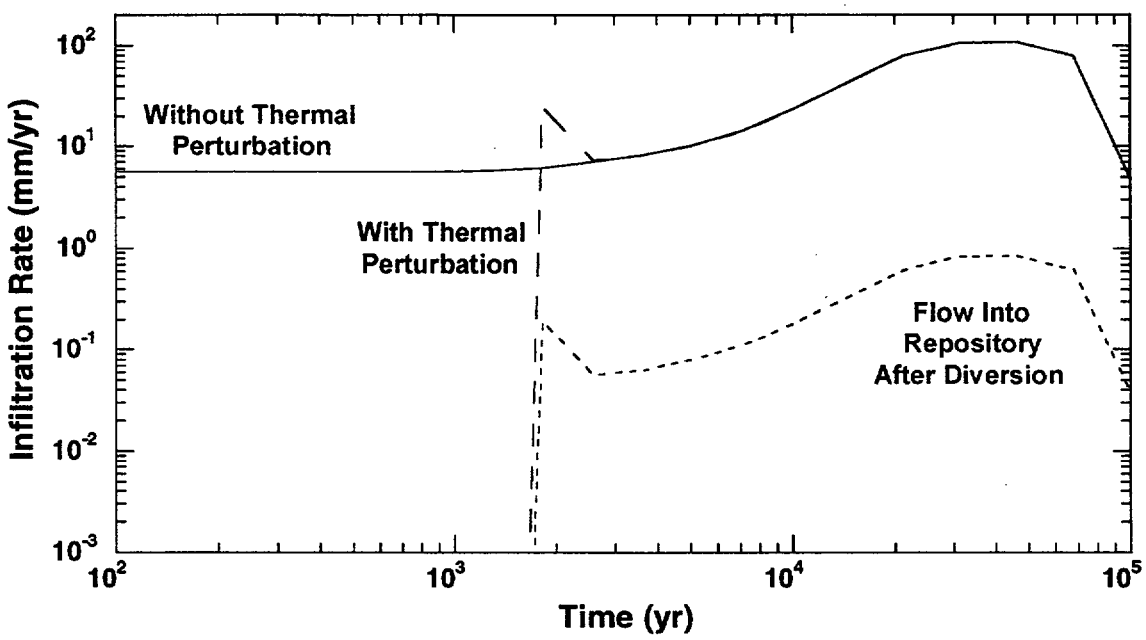

Figure 3-3. Subarea average infiltration rate, flow into the drift, and amount of water entering the WP for the mean value data set.

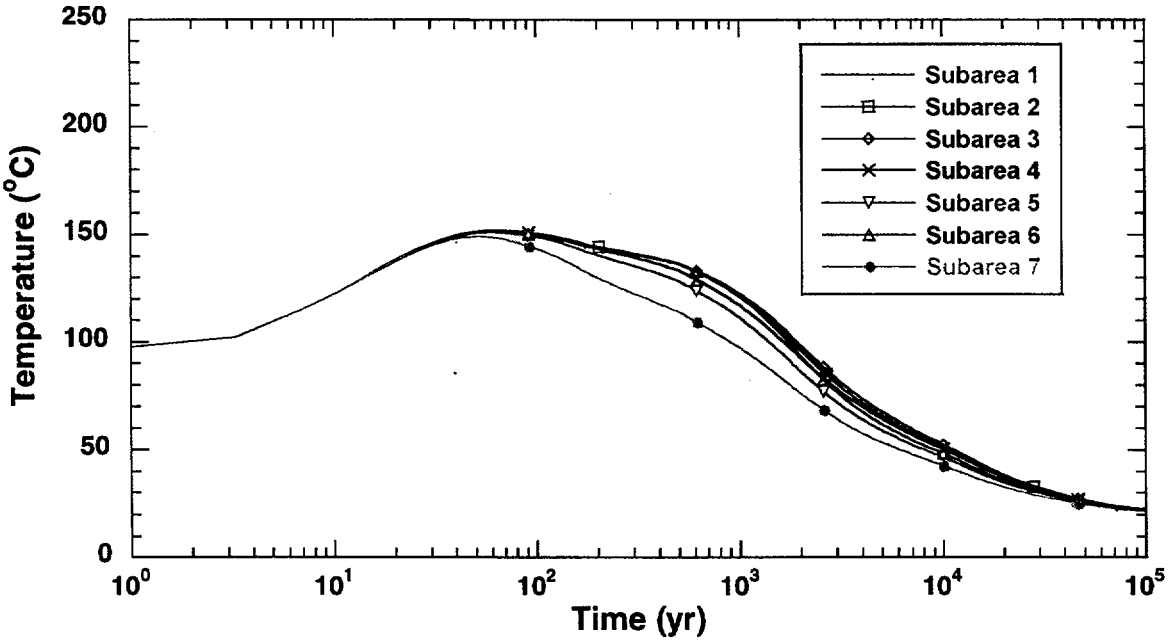

Figure 3-4. WP surface temperature in each subarea for the mean value data set.

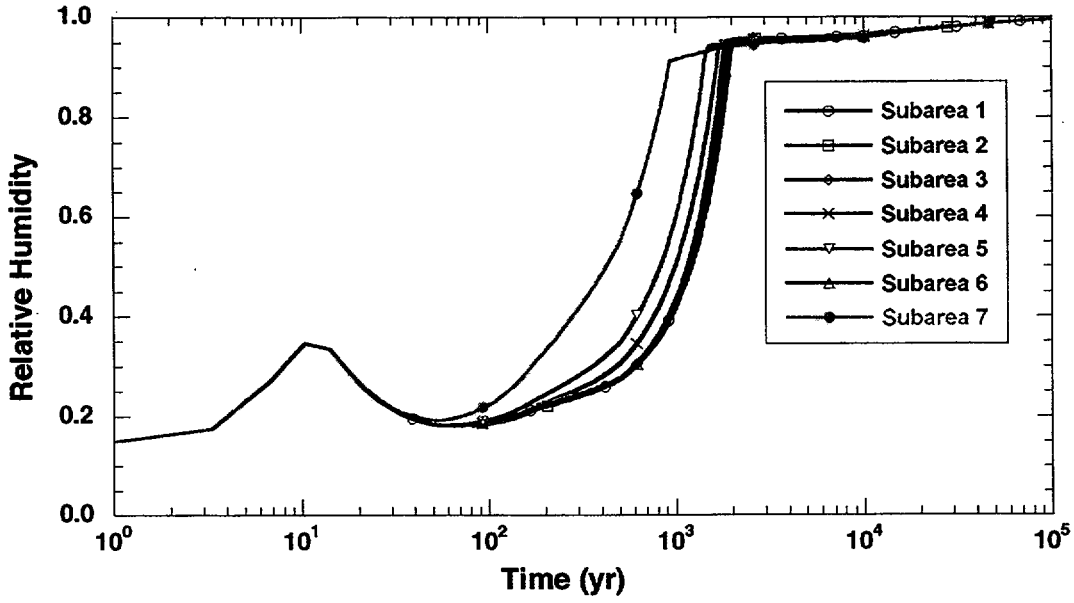

Figure 3-5. WP surface relative humidity in each subarea for the mean value data set.

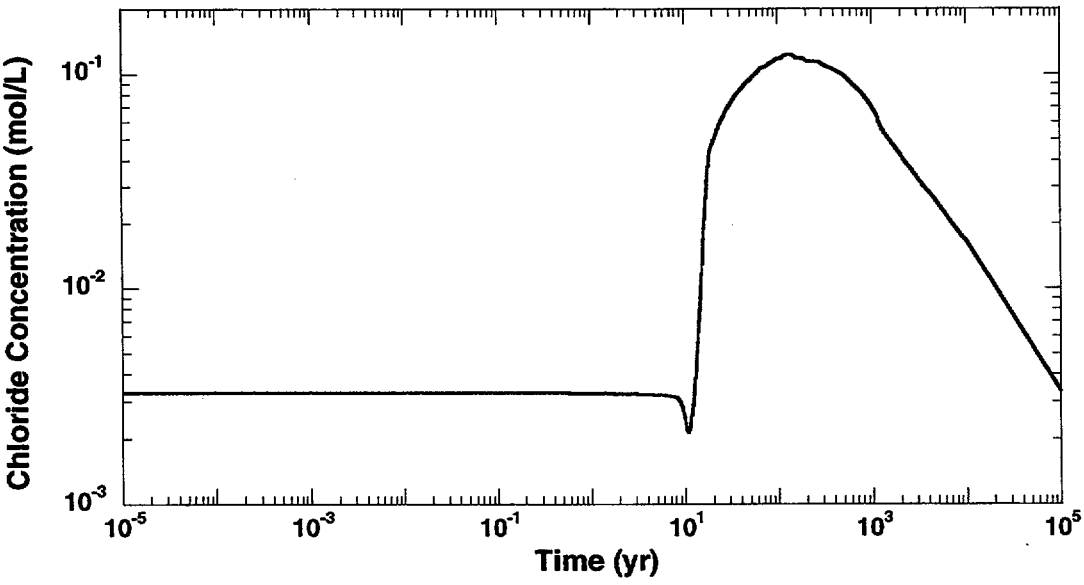

Figure 3-6. Time history of chloride concentration computed by MULTIFLO

Table 3-3. Parameters for determining the corrosion failure of WPs

Parameter	Mean Value	Distribution
Outer waste package thickness	1.00×10^{-1} m	—
Inner waste package thickness	2.00×10^{-2} m	—
Metal grain radius	1.38×10^{1} μm	—
Grain boundary thickness	7.00×10^{-4} μm	—
Dry oxidation constant	1.00×10^{-5}	—
Critical relative humidity humid air corrosion	5.50×10^{-1}	—
Critical relative humidity aqueous corrosion	8.00×10^{-1}	Normal; 0.75, 0.85
Thickness of water film	2.00×10^{-3} m	Uniform; 0.001, 0.003
Boiling point of water	9.70×10^{1} °C	—
Outer overpack E_{rp} intercept	-6.20×10^{2}	—
Temperature coefficient of outer pack E_{rp} intercept	4.70×10^{-1}	—
Outer overpack E_{rp} slope	-9.52×10^{1}	—
Temperature coefficient of outer pack E_{rp} slope	8.80×10^{-1}	—
Inner overpack E_{rp} intercept	1.14×10^{3}	Uniform; 1040.0, 1240.0
Temp coef of inner pack E_{rp} intercept	0.00	—
Inner overpack E_{rp} slope	0.00	—
Temp coef of inner pack E_{rp} slope	0.00	—
Outer waste package beta kinetics parameter for oxygen	7.50×10^{-1}	—
Outer waste package beta kinetics parameter for water	5.00×10^{-1}	—
Inner waste package beta kinetics parameter for oxygen	7.50×10^{-1}	—
Inner waste package beta kinetics parameter for water	5.00×10^{-1}	—
Outer waste package rate constant for oxygen reduction	3.80×10^{12} C-m/m/yr	—
Outer waste package rate constant for water reduction	1.60×10^{-1} C-m/m^2/yr	—
Outer waste package activation energy for oxygen reduction	3.73×10^{4} J/mol	—
Outer waste package activation energy for water reduction	2.50×10^{4} J/mol	—
Inner waste package rate constant for oxygen reduction	3.00×10^{10} C-m/mol/yr	—
Inner waste package rate constant for water reduction	3.2 C-m/m^2/yr	—
Inner waste package activation energy for oxygen reduction	4.0×10^{4} J/mol	—
Inner waste package activation energy for water reduction	2.50×10^{4} J/mol	—

Table 3-3. Parameters for determining the corrosion failure of WPs (cont'd)

Parameter	Mean Value	Distribution
Passive current density for waste package outer overpack	3.15×10^5 C/m^2/yr	—
Passive current density for waste package inner overpack	4.15×10^4	Uniform; 2.0×10^4, 6.3×10^4
Measured galvanic couple potential	-4.60×10^{-1}	—
Coefficient for localized corrosion of outer overpack	4.76×10^{-3}	Uniform; 8.66×10^{-4}, 8.66×10^{-3}
Exponent for localized corrosion of outer overpack	4.5×10^{-1}	—
Humid air corrosion rate	1.16×10^{-5} m/yr	—
Localized corrosion rate of inner overpack	2.5×10^{-4} m/yr	—
Fractional coupling strength	0.0	—
Factor for defining choice of critical potential	0.0	—
Critical chloride concentration for first layer	3.0×10^{-4} mol/L	—
Critical chloride concentration for second layer	1.00 mol/L	—
Chloride multiplication factor	1.55×10^1	Uniform; 1.0, 30.0
Reference pH	9.0	—
Waste package surface scale thickness	0.0 m	—
Tortuosity of scale on waste package	1.0	—
Porosity of scale on waste package	1.0	—
Yield strength	2.05×10^2 MPa	—
Safety factor	1.4	—
Fracture toughness	2.50×10^2 MPa/m^2	—

Note: mol/L— moles per liter
MPa—megapascal

3.1.3 WP Degradation

Because radionuclide releases begin only after WP failure, the lifetime of a WP significantly affects repository performance. The WP degradation rate is strongly dependent on the behavior of the inner and outer container materials. The inner and outer WP materials are specified as carbon steel and Alloy C-22, respectively, based on the DOE TSPA-VA design (U.S. Department of Energy, 1998). The mean values of the parameters used in computing the WP failure time are presented in Table 3-3. Figure 3-7 provides a time evolution of the WP wall thinning and shows WP failure occurring at about 16,500 yr. The two distinct lopes in this figure correspond to the different corrosion rates for the carbon steel and Alloy C-22 materials. The transition point corresponds to the penetration of the outer overpack at approximately 1700 yr. The figure indicates that an order of magnitude longer WP life is attributable to the inner overpack rather than the outer overpack.

Figure 3-8 shows that, for the mean value data set, 31 WPs are initially defective at year zero. The number of initially defective failures ranges from one to nine WPs in the seven subareas. No seismically

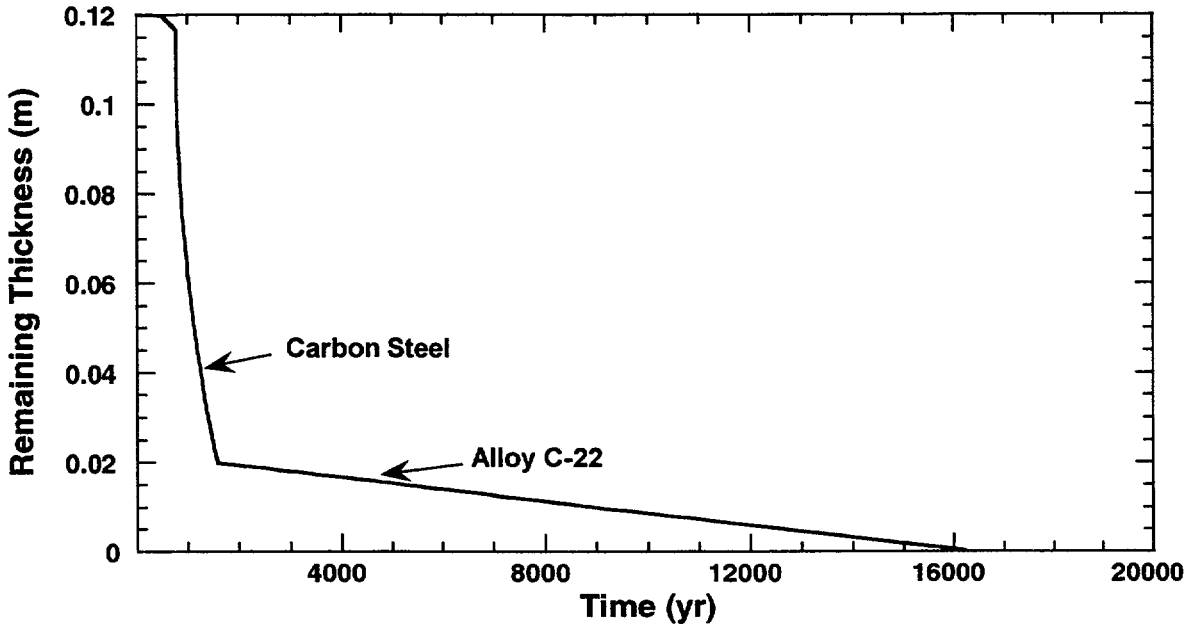

Figure 3-7. WP wall thickness as a function of time for the mean value data set.

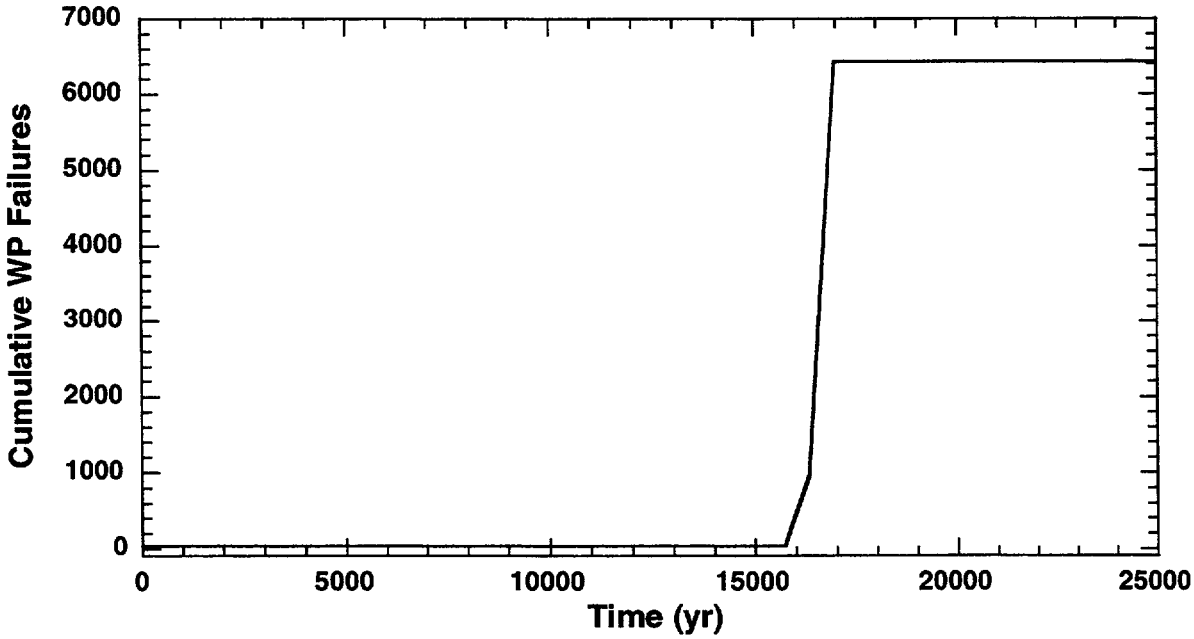

Figure 3-8. Cumulative number of failed WPs for the mean value data set.

induced failure occurs for the mean value data set. The first corrosion failures take place in subareas 5 and 7. A total of 928 WPs fail in these subareas at 16,300 yr. The next corrosion failure occurs in subareas 1 to 4, and 6, with a total of 5468 WPs failing at 17,000 yr.

3.1.4 Releases from WP

After WP failure, radionuclide releases are modeled assuming advective mass transfer out of the WP from incoming water. The volume of water contacting the SF is computed from a combination of flow in the near-field environment and two flow factors. The first flow factor represents the fraction of dripping water, which may be focused to reach the WP. The second flow factor represents the fraction of the water reaching the WP that enters the WP. The flow rate into the WP is used in the bathtub model to determine radionuclide release rates. The mean value parameters used in the calculation of radionuclide release rates from the EBS are presented in Tables 3-4 and 3-5.

Because radionuclides have different chemical, physical, and biological properties that affect the mobilization and radiotoxicity, not every radionuclide in the SF is an important contributor to dose. Furthermore, because modeling all radionuclides in the SF significantly increases the computation time, a screening process employing criteria such as contribution to dose was used to determine a list of 11 radionuclides. The 11 radionuclides and the decay chains evaluated in the TPA analysis are presented in Table 3-6.

3.1.4.1 Cladding Degradation

Cladding must fail for water to contact the SF. Because of lack of adequate knowledge, no explicit mechanism for cladding failure is included in the TPA code. To capture the potential effect of cladding degradation, however, a fraction of the rods inside a WP may be specified to have failed at the time of WP failure. In the basecase, cladding failure is specified at 100 percent of the fuel rods, indicating no cladding protection for the SF (see Table 3-4).

3.1.4.2 SF Dissolution and Mobilization

SF dissolution is modeled by defining rate equations for the SF exposed after WP failure and cladding degradation. The rate equation is based on laboratory data in the presence of calcium (Ca) and silicon (Si). The data follow an Arrhenius-type trend that uses the time-varying temperature as the independent parameter. The dissolution rate is calculated from a mass balance on the water flowing into the WP. Because the flow rate is subarea-dependent, the dissolution rate varies from subarea to subarea.

The average temperature of the WP surface, calculated in the drift-scale thermohydrology model, is used in the dissolution rate equation. This assumption that the temperature of the WP surface is close to the temperature at the interior of the WP is justified because by the time the WP fails from corrosion (the dominant failure mechanism) at around 17,000 yr, the thermal effects have subsided. The surface area of the SF available for dissolution is about 746 m^2 (8000 ft^2) based on the SF particle size, grain density, and the SF wetted fraction.

As with SF dissolution, the mobilization of the SF also depends on the initial inventory instantaneously released from the gap between SF and cladding into the contacting water as soon as the WP fails. Radionuclide gap fractions are presented in Table 3-7.

Table 3-4. Parameters used in determining radionuclide releases from the engineered barrier system

Parameter	Mean	Distribution
Flow model flag (0 = bathtub, 1 = flow through)	0.00	—
Flow convergence/divergence factor	1.73×10^{-1}	Lognormal; 0.01, 3.0
Flow multiplication factor	4.47×10^{-2}	Lognormal; 0.01, 0.2
Subarea wet fraction	5.0×10^{-1}	Uniform; 0.0, 1.0
Initial failure time	0.00 yr	—
Defective fraction of waste packages per cell	5.05×10^{-3}	Uniform; 1.0×10^{-4}, 1.0×10^{-2}
Number of SEISMO waste package failure intervals	4.00	—
Beginning of seismic waste package failure intervals	0, 2000, 5000, 10,000 yr	—
Waste package internal volume	4.83 m^3	—
Flow onset temperature	9.99×10^{2} °C	—
Spent fuel density	1.06×10^{4} kg/m^3	—
Surface area model	1.00	—
Spent fuel dissolution model	2.00	—
Oxygen partial pressure	2.10×10^{-1} atm	—
Negative log10 carbonate concentration	3.71 mol/L	—
User leach rate	2.50×10^{-6} kg/yr/m^2	—
Initial radius of spent fuel particle	1.85×10^{-3} m	Normal; 7.0×10^{-4}, 3.0×10^{-3}
Radius of spent fuel grain	1.25×10^{-5}	—
Cladding correction factor	1.0	—
Subgrain fragment radius of UO_2 particle after transgranular fracture	1.25×10^{-6} m	Normal; 5.0×10^{-7}, 2.0×10^{-6}
Thickness of cladding	6.1×10^{-4} m	—
Spent fuel ^{14}C inventory of spent fuel	7.2×10^{-4} Ci/kg	—
Clad ^{14}C inventory of spent fuel	4.89×10^{-4} Ci/kg	—
Zirconium oxide and crud ^{14}C inventory of spent fuel	2.48×10^{-5} Ci/kg	—
Gap and grain boundary inventory of spent fuel	6.2×10^{-6} Ci/kg	—
Spent fuel wetted fraction for all failure types	5.0×10^{-1}	Uniform; 0.0, 1.0
Invert bypass (0 = use ebsfilt, 1 = bypass ebsfilt)	0	—
Invert rock porosity	3.0×10^{-1}	—
Invert thickness	7.5×10^{-1} m	—
Invert diffusion coefficient	4.4×10^{-5} m^2/yr	—
Invert matrix permeability	2.0×10^{-17} m^2	Lognormal; 2.0×10^{-18}, 2.0×10^{-16}
Unsaturated zone minimum velocity change factor (fraction)	4.0×10^{-1}	

Table 3-4. Parameters used in determining radionuclide releases from the engineered barrier system (cont'd)

Parameter	Mean	Distribution
Invert RD		—
^{241}Am	3.00×10^{3}	—
^{14}C	6.10×10^{1}	—
^{36}Cl	1.00	—
^{245}Cm	6.00×10^{3}	—
^{129}I	7.00	—
^{237}Np	1.20×10^{3}	—
^{239}Pu	3.00×10^{3}	—
^{79}Se	1.00	—
^{99}Tc	1.00	—
^{230}Th	3.00×10^{3}	—
^{234}U	6.01×10^{2}	—

Table 3-5. Distributions of solubility limits

Radionuclide	Mean Value (kg/m^3)	Distribution (kg/m^3)
^{241}Am	1.20×10^{-4}	Uniform; 2.4×10^{-8}, 2.4×10^{-4}
^{14}C	1.40×10^{1}	—
^{36}Cl	3.60×10^{1}	—
^{245}Cm	2.40×10^{-4}	—
^{129}I	1.29×10^{2}	—
^{237}Np	2.14×10^{-2}	Log triangular; 1.2×10^{-3}, 3.4×10^{-2}, 2.4×10^{-1}
^{239}Pu	1.21×10^{-4}	Uniform; 2.4×10^{-6}, 2.4×10^{-4}
^{79}Se	7.90×10^{1}	—
^{99}Tc	9.93×10^{1}	—
^{230}Th	2.30×10^{-4}	—
^{234}U	7.60×10^{-3}	—

Table 3-6. Radionuclide decay chains

Chain Number	Chain
1	$^{245}Cm \rightarrow {}^{241}Am \rightarrow {}^{237}Np$
2	^{239}Pu
3	$^{234}U \rightarrow {}^{230}Th$
4	^{129}I
5	^{99}Tc
6	^{14}C
7	^{79}Se
8	^{36}Cl

Table 3-7. Initial inventory, gap inventory, and half-life of radionuclides in spent nuclear fuel for groundwater release

Radionuclide	Inventory at 10 yr from Reactor (Ci/WP)	Gap Inventory (%)	Half-life (yr)
^{241}Am	1.60×10^{4}	0	4.32×10^{2}
^{14}C	1.30×10^{1}	10	5.73×10^{3}
^{36}Cl	1.14×10^{-1}	12	3.01×10^{5}
^{245}Cm	1.22	0	8.50×10^{3}
^{129}I	2.88×10^{-1}	6	1.57×10^{7}
^{237}Np	2.80	0	2.14×10^{6}
^{239}Pu	3.01×10^{3}	0	2.41×10^{4}
^{79}Se	3.71	6	6.50×10^{4}
^{99}Tc	1.20×10^{2}	1	2.13×10^{5}
^{230}Th	1.26×10^{-3}	0	7.70×10^{4}
^{234}U	1.10×10^{1}	0	2.45×10^{5}

3.1.4.3 Transport in the EBS

The TPA code models advective transport out of the WP and advective and diffusive transport through the invert below the WP. Two different flow rates are used in these transport calculations. The volumetric flow rate of water into the WP is calculated by scaling the seepage flux into the drift with the surface area of the pits. The volumetric flux through the invert is based on the volume of water entering the drift rather than the volume of water entering the WP.

Inside the WP, high solubility nuclides released from the solid matrix are carried out of the WP. However, low-solubility nuclides precipitate out of solution if released from the solid matrix at a concentration exceeding the carrying capacity of water (or solubility limit of a particular nuclide). The volume of water available for dissolution of waste is the amount of water in the failed WP and the difference between the volume of water flowing in and out of the failed WP. Table 3-5 provides solubility limits of the radio-elements evaluated in the TPA Version 3.2 code.

In the invert, advective and diffusive transport is modeled through 0.75 m (2.5 ft) of concrete having a 30-percent porosity. The determination of whether flow through the invert occurs in the matrix or fractures is based on the invert matrix permeability and the average flow rate of water through the invert. Radionuclide sorption is modeled in the concrete invert, and the mean values of the R_ds are presented in Table 3-4, together with values for other parameters used to compute transport in the EBS. Colloidal transport of radionuclides is not considered in this calculation.

3.1.5 UZ Transport

In UZ transport calculations, the NEFTRAN II code (Olague, *et al.*, 1991) models 1-D advection and retardation of radionuclides with chain decay. Inputs to the UZ transport model are the release rates of radionuclides from the EBS, the time-varying flow results from the UZ shown in Figure 3-1, and the chemical and physical properties of the hydrostratigraphic units between the repository and the water table (see Figure 3-9 and Table 3-8).

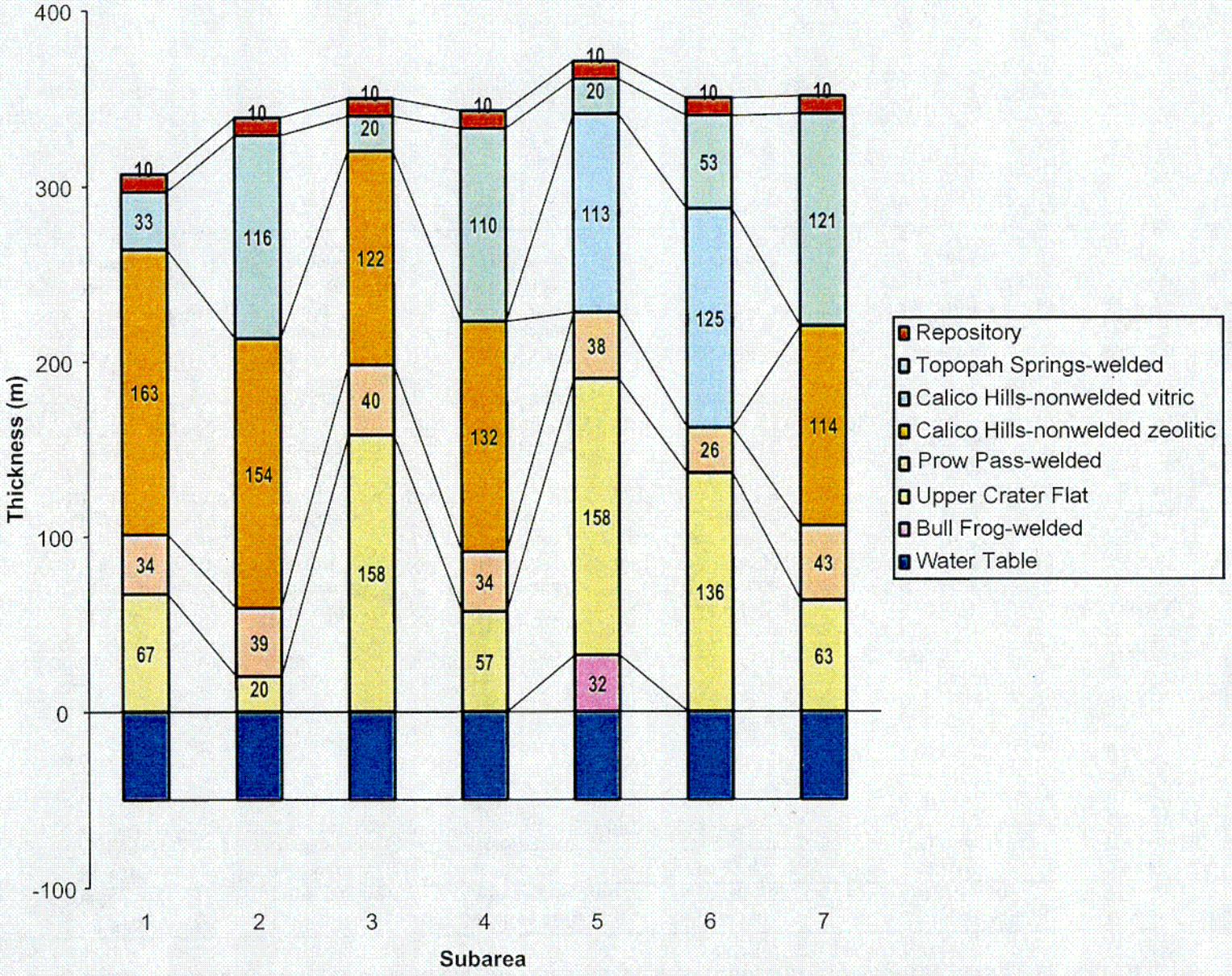

Figure 3-9. Thickness of subarea stratigraphic units.

C01

Table 3-8. Mean values and sampled distributions of sorption coefficient, K_d (m^3/kg), parameters. (Other parameters for UZ radionuclide transport are also included. The dash in the last column indicates a constant value for the parameter distribution.)

Element	Bull Frog welded unit	Calico Hills nonvitric unit	Calico Hills nonzeolitic unit	Prow Pass welded unit	Topopah Spring welded unit	Upper Crater Flat unit
Am	3.89×10^{3} (Lognormal; 4.1, 3.7×10^{6})	1.25×10^{4} (Lognormal; 1.3×10^{1}, 1.2×10^{7})	1.15×10^{4} (Lognormal; 1.2×10^{1}, 1.1×10^{7})	9.09×10^{3} (Lognormal; 9.5, 8.7×10^{6})	3.99×10^{3} (Lognormal; 4.2×10^{1}, 3.8×10^{6})	9.54×10^{3} (Lognormal; 1.0×10^{1}, 9.1×10^{6})
C	0.00 —	0.00 —	0.00 —	0.00 —	0.00 —	0.00 —
Cl	0.00 —	0.00 —	0.00 —	0.00 —	0.00 —	0.00 —
Cm	0.00 —	0.00 —	0.00 —	0.00 —	0.00 —	0.00 —
I	0.00 —	0.00 —	0.00 —	0.00 —	0.00 —	0.00 —
Np	5.61×10^{-4} (Lognormal; 1.5×10^{-6}, 2.1×10^{-1})	1.78×10^{-3} (Lognormal; 4.8×10^{-6}, 6.6×10^{-1})	1.62×10^{-3} (Lognormal; 4.4×10^{-6}, 6.0×10^{-1})	1.34×10^{-3} (Lognormal; 3.6×10^{-6}, 5.0×10^{-1})	5.93×10^{-4} (Lognormal; 1.6×10^{-6}, 2.2×10^{-1})	1.40×10^{-3} (Lognormal; 3.8×10^{-6}, 5.2×10^{-1})
Pu	6.95×10^{1} (Lognormal; 2.3×10^{-2}, 2.1×10^{1})	2.18 (Lognormal; 7.1×10^{-2}, 6.7×10^{1})	1.99 (Lognormal; 6.5×10^{-2}, 6.1×10^{1})	1.63 (Lognormal; 5.3×10^{-2}, 5.0×10^{1})	7.11×10^{-1} (Lognormal; 2.3×10^{-2}, 2.2×10^{1})	1.71 (Lognormal; 5.6×10^{-1}, 5.2×10^{1})
Se	9.49×10^{-5} (Lognormal; 3.0×10^{-7}, 3.0×10^{-2})	6.32×10^{-5} (Lognormal; 2.0×10^{-7}, 2.0×10^{-2})	4.74×10^{-5} (Lognormal; 1.5×10^{-7}, 1.5×10^{-2})	9.49×10^{-5} (Lognormal; 3.0×10^{-7}, 3.0×-10^{-2})	9.49×10^{-5} (Lognormal; 3.0×10^{-7}, 3.0×10^{-2})	9.49×10^{-5} (Lognormal; 3.0×10^{-7}, 3.0×10^{-2})
Tc	0.00 —	0.00 —	0.00 —	0.00 —	0.00 —	0.00 —
Th	3.36×10^{-1} (Lognormal; 4.7×10^{-5}, 2.4×10^{3})	1.07 (Lognormal; 1.5×10^{-4}, 7.6×10^{3})	9.47×10^{-1} (Lognormal; 1.3×10^{-4}, 6.9×10^{3})	7.92×10^{-1} (Lognormal; 1.1×10^{-4}, 5.7×10^{3})	3.46×10^{-1} (Lognormal; 4.8×10^{-5}, 2.5×10^{3})	8.06×10^{-1} (Lognormal; 1.1×10^{-4}, 5.7×10^{3})
U	2.02×10^{-5} (Lognormal; 1.0×10^{-9}, 2.6)	6.55×10^{-5} (Lognormal; 1.3×10^{-9}, 3.3)	6.00×10^{-5} (Lognormal; 1.2×10^{-9}, 3.0)	4.90×10^{-5} (Lognormal; 9.6×10^{-10}, 2.5)	2.15×10^{-5} (Lognormal; 4.2×10^{-10}, 1.1)	5.10×10^{-5} (Lognormal; 1.0×10^{-9}, 2.6)

Table 3-8. Mean values and sampled distributions of sorption coefficient, K_d (m^3/kg), parameters. (Other parameters for UZ radionuclide transport are also included. (cont'd)

Parameter	Mean	Distribution
Matrix Permeability		
Topopah Springs–welded	2.00×10^{-19} m^2	Lognormal; 2.0×10^{-20}, 2.0×10^{-18}
Calico Hills–nonwelded vitric	2.00×10^{-14} m^2	Lognormal; 2.0×10^{-15}, 2.0×10^{-13}
Calico Hills–nonwelded zeolitic	5.00×10^{-18} m^2	Lognormal; 5.0×10^{-19}, 5.0×10^{-17}
Prow Pass–welded	1.00×10^{-17} m^2	Lognormal; 1.0×10^{-18}, 1.0×10^{-16}
Upper Crater Flat	3.00×10^{-18} m^2	Lognormal; 3.0×10^{-19}, 3.0×10^{-17}
Bull Frog–welded	2.00×10^{-19} m^2	Lognormal; 2.0×10^{-20}, 2.0×10^{-18}
Unsaturated Fracture Zone	1.94×10^{-17} m^2	Lognormal; 1.8×10^{-18}, 2.1×10^{-16}
Matrix Porosity		
Topopah Springs–welded	1.20×10^{-1}	–
Calico Hills–nonwelded vitric	3.30×10^{-1}	–
Calico Hills–nonwelded zeolitic	3.20×10^{-1}	–
Prow Pass–welded	2.80×10^{-1}	–
Upper Crater Flat	2.80×10^{-1}	–
Bull Frog–welded	1.20×10^{-1}	–
Unsaturated Fracture Zone	1.20×10^{-1}	–
Matrix Beta		
Topopah Springs–welded	1.50	–
Calico Hills–nonwelded vitric	1.30	–
Calico Hills–nonwelded zeolitic	2.30	–
Prow Pass–welded	1.50	–
Upper Crater Flat	1.40	–
Bull Frog–welded	1.70	–
Unsaturated Fracture Zone	2.30	–
Matrix Grain Density		
Topopah Springs–welded	2.46×10^3 kg/m^3	–
Calico Hills–nonwelded vitric	2.26×10^3 kg/m^3	–
Calico Hills–nonwelded zeolitic	2.40×10^3 kg/m^3	–
Prow Pass–welded	2.54×10^3 kg/m^3	–

Table 3-8. Mean values and sampled distributions of sorption coefficient, K_d (m^3/kg), parameters. (Other parameters for UZ radionuclide transport are also included. (cont'd)

Parameter	Mean	Distribution
Matrix Grain Density		
Upper Crater Flat	2.42×10^3 kg/m^3	–
Bull Frog–welded	2.57×10^3 kg/m^3	–
Unsaturated Fracture Zone	2.63×10^3 kg/m^3	–
Fracture Permeability		
Topopah Springs–welded	8.00×10^{-13} m^2	Lognormal; 8.0×10^{-15}, 8.0×10^{-11}
Calico Hills–nonwelded vitric	8.00×10^{-13} m^2	Lognormal; 8.0×10^{-15}, 8.0×10^{-11}
Calico Hills–nonwelded zeolitic	6.00×10^{-13} m^2	Lognormal; 6.0×10^{-15}, 6.0×10^{-11}
Prow Pass–welded	6.00×10^{-13} m^2	Lognormal; 6.0×10^{-15}, 6.0×10^{-11}
Upper Crater Flat	6.00×10^{-13} m^2	Lognormal; 6.0×10^{-15}, 6.0×10^{-11}
Bull Frog–welded	3.00×10^{-13} m^2	Lognormal; 3.0×10^{-15}, 3.0×10^{-11}
Unsaturated Fracture Zone	1.00×10^{-12} m^2	Lognormal; 1.0×10^{-13}, 1.0×10^{-11}
Fracture porosity for all units	3.16×10^{-3}	Lognormal; 1.0×10^{-3}, 1.0×10^{-2}
Fracture beta for all units	3.00	–
Matrix and fracture longitudinal dispersivity as a fraction of unit	1.00×10^{-1}	–

The water table elevation remains constant in the TPA calculations. Thus, the thickness of the UZ does not change with time even during the pluvial climate. Sorption in fractures is neglected because of the fast travel times, whereas sorption in the matrix is modeled using the sorption coefficients presented in Table 3-8. The effects of matrix diffusion on transport in the UZ are not modeled.

Figure 3-10 shows the release rate for ^{36}Cl. Because ^{36}Cl moves unretarded, comparison of the times of the release rates in this figure indirectly illustrate the UZ and SZ travel times. The EBS and UZ release rates are nearly the same, indicating that the UZ does not significantly delay groundwater transport.

3.1.6 SZ Flow and Transport

For each subarea, radionuclide transport out of the EBS and into the UZ and the SZ can be conceptualized as occurring in a single streamtube that originates in the repository, extends to the water table, and continues to the receptor location. In the SZ, streamtubes begin at the water table directly below the repository and continue to the receptor location. Each subarea in the repository is assigned to the nearest streamtube. Subareas 1 and 2 are mapped to streamtube D, subareas 3 and 4 are mapped to streamtube, B and subareas 5, 6, and 7 are mapped to streamtube A. Figure 3-11 shows the subareas and streamtubes used for the SZ transport model, and Table 3-9 provides the length of the SZ flow path by subarea. The groundwater travel times (GWTT) from the point where the radionuclides enter the SZ to the receptor location are 6000 yr for subareas 1 and 2 (streamtube D); 2700 yr for subareas 3 and 4 (streamtube B); and 2800 yr for subareas 5, 6, and 7 (streamtube A). Large variations in the GWTT are primarily the result of variations in the streamtube length, width, and flow rates. There are no subareas mapped to streamtube C, consequently, streamtube C, which contains 26 percent of the total SZ flow, serves to dilute the concentration of radionuclides in the groundwater. The total SZ flow rate in all the streamtubes is 2.56×10^5 m^3/yr (9.04×10^6 ft^3/yr). The relative contributions of streamtubes A, B, and D to the total SZ flow are 27, 29, and 18 percent.

The release rate at the outlet of the streamtubes is determined using the sum of the release rates from all the streamtubes and is dependent on the time-varying concentration at the inlet. Figure 3-10 shows the SZ release rates for ^{36}Cl, which is not retarded in the SZ. When compared with the time of peak UZ release rate, this figure also indicates the GWTT through the SZ is on the order of a few thousand years.

The source term for the SZ transport model is the time-varying radionuclide release rate from the UZ calculations. Other inputs to the SZ transport model include the physical and chemical properties of the tuff and alluvium and the streamtube flow rates, widths, and lengths. The mean values for the SZ input parameters are presented in Table 3-9.

3.1.7 Dose to the Receptor Group

The receptor location for the basecase data set is 20 km (12.4 mi) from the repository. At 20 km (12.4 mi), the mean value for the pumping rate is 1.21×10^7 m^3/yr (4.3×10^8 ft^3/yr), which is sufficient to capture the entire contaminant plume. Because the TPA code assumes the volume of water pumped is constant throughout the TPI, values for the concentration of the well water exhibit the same behavior as the SZ release rates. For example, to convert from ^{36}Cl release rates in Figure 3-10 to concentration, the release rates are divided by the well pumping rate to compute the well-water concentrations.

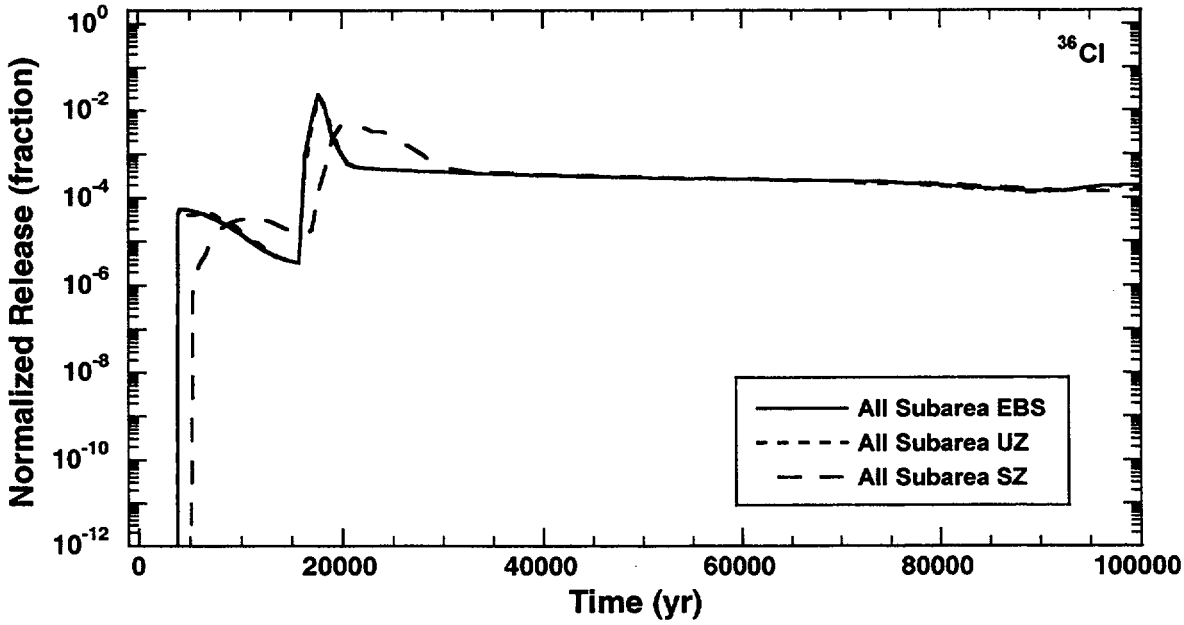

Figure 3-10. ^{36}Cl normalized release rates from the EBS, UZ, and SZ for the mean value data set.

The groundwater dose is determined by multiplying the concentration of the nuclides in the pumped water with the DCF. The mass of radionuclides captured by pumping is diluted in the volume of water extracted from the pumping well and converted from a groundwater concentration to a dose using DCFs. The dose to an individual of the receptor group originates from drinking and irrigation water used by an average adult living in Amargosa Valley. The groundwater pathway DCFs for the 11 radionuclides used in the basecase mean value data set are summarized in Table 3-10.

3.2 RESULTS FROM THE MEAN VALUE DATA SET

This section illustrates the behavior of the total system with the mean value of parameters and how the individual dose is influenced by the various subsystem models and parameters. Time history plots of key system parameters for both doses and release rates at various subsystem boundaries are presented in this section for the mean value single-realization case.

Subarea	Streamtube
1	D
2	D
3	B
4	B
5	A
6	A
7	A

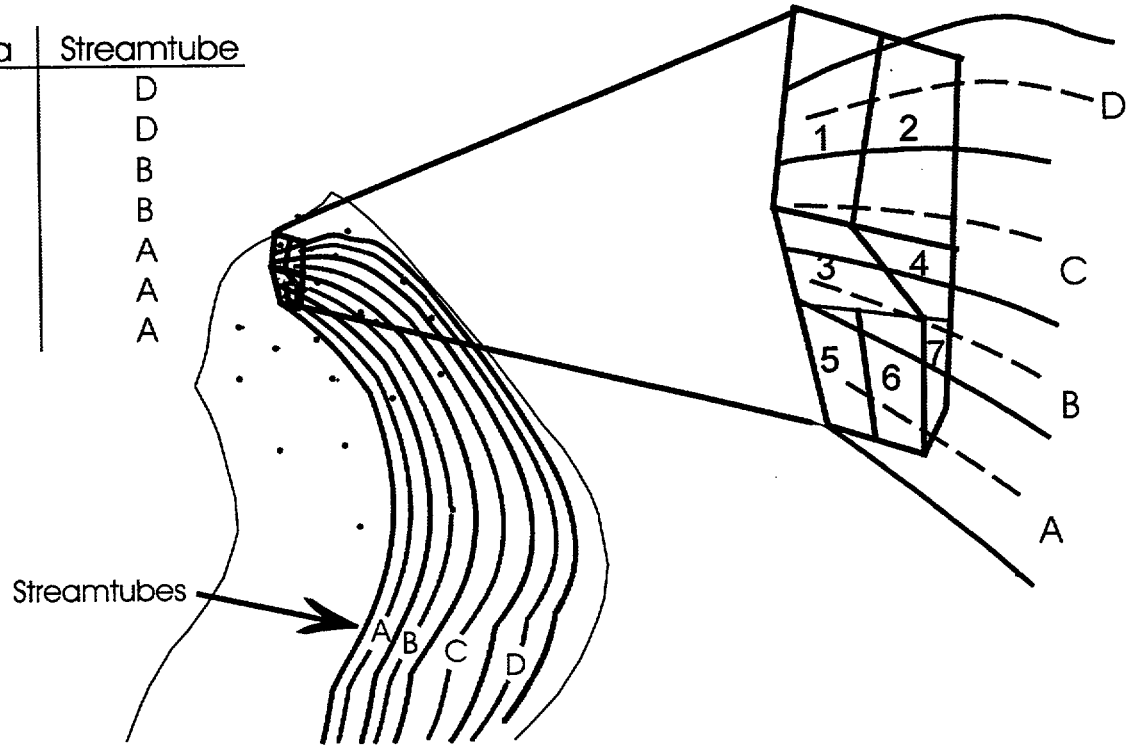

Figure 3-11. SZ streamtubes assigned to each subarea.

Table 3-9. Parameter values used for SZ flow and radionuclide transport in TPA

Parameter	Mean	Distribution
Mixing zone dispersion fraction	1.00×10^{-2}	—
Tuff dispersion fraction	1.00×10^{-2}	—
Alluvium dispersion fraction	1.00×10^{-1}	—
Tuff fracture porosity	3.16×10^{-3}	Log-uniform; 1.0×10^{-3}, 1.0×10^{-2}
Alluvium matrix porosity	1.25×10^{-1}	Uniform; 1.0×10^{-1}, 1.5×10^{-1}
Immobile R_d for tuff for ^{241}Am	1.80×10^{4}	Not used because matrix diffusion = 0
Immobile porosity for tuff	1.00×10^{-2}	—
Diffusion rate for tuff	0.00	—
Fracture R_d for tuff for all nuclides	1.00	—
Min residence time for tuff	1.00×10^{1} yr	—
Min residence time for alluvium	1.00×10^{1} yr	—
Well pumping rate at receptor group at 20 km	8.75×10^{6} gal/day	—
Mixing zone thickness at 20 km	1.25×10^{2} m	—
Alluvium Matrix R_d		
^{241}Am	7.14×10^{7}	Lognormal; 7.5×10^{4}, 6.8×10^{10}
^{14}C	1.00	—
^{36}Cl	1.00	—
^{245}Cm	7.50×10^{4}	—
^{129}I	2.00	Log-uniform; 1.0, 4.0
^{237}Np	6.24×10^{1}	Lognormal; 1.0, 3.9×10^{3}
^{239}Pu	1.28×10^{4}	Lognormal; 4.2×10^{2}, 3.9×10^{5}
^{79}Se	2.24×10^{1}	Log-uniform; 1.0, 500.0
^{99}Tc	5.48	Log-uniform; 1.0, 30.0
^{230}Th	9.25×10^{3}	Lognormal; 1.9, 4.5×10^{7}
^{234}U	1.38×10^{2}	Lognormal; 1.0, 1.9×10^{4}
Streamtube Flow Properties	**Length (m)**	**Streamtube**
Subarea 1	29,200	D
Subarea 2	28,600	D
Subarea 3	25,200	B
Subarea 4	24,600	B
Subarea 5	23,400	A
Subarea 6	23,000	A
Subarea 7	22,500	A

Table 3-10. Biosphere dose conversion factors for groundwater at the 20-km receptor location

Radionuclide	Nonpluvial DCF (rem/year)/(Ci/m^3)	Pluvial DCF (rem/year)/(Ci/m^3)
^{241}Am	6.11×10^6	4.31×10^6
^{14}C	1.35×10^4	8.60×10^3
^{36}Cl	4.52×10^4	3.02×10^4
^{245}Cm	6.32×10^6	4.51×10^6
^{129}I	1.27×10^6	7.90×10^5
^{237}Np	9.01×10^6	6.43×10^6
^{239}Pu	6.00×10^6	4.30×10^6
^{79}Se	2.51×10^4	1.68×10^4
^{99}Tc	4.74×10^3	3.29×10^3
^{230}Th	9.32×10^5	6.61×10^5
^{234}U	5.06×10^5	3.66×10^5

The dose to an average individual residing 20 km (12.4 mi) downgradient of the repository is presented in Figure 3-12 for radionuclides with doses greater than 10^{-8} mSv/yr (10^{-6} mrem/yr). The results are presented for the first 10,000 and 100,000 yr, respectively. The period of 100,000 yr is chosen so that the effects of one cycle of the pluvial climate and the effects of WP corrosion, which occur after the 10,000-yr TPI, can be studied.

A peak total dose of about 2×10^{-8} Sv/yr (0.002 mrem/yr) was calculated during the 10,000-yr TPI. The dose is dominated in the 10,000-yr TPI by ^{129}I and ^{36}Cl, which are nonsorbing nuclides with relatively long half-lives. For the 100,000-yr TPI, a peak total dose of 3×10^{-6} Sv/yr (0.3 mrem/yr) occurred at 23,000 yr, and the dose was dominated by the nuclides ^{129}I, ^{99}Tc, and ^{36}Cl. A discussion of the TPA results from the 10,000- and 100,000-yr TPIs, with and without the faulting and igneous activity disruptive events, follows in the next two sections.

3.2.1 10,000-Year Releases and Dose

As evident from Figure 3-8 and explained in Section 3.1.3, all basecase releases in 10,000 yr would arise from initially defective WP failures. Although initially defective failure takes place at the zero year, releases do not occur until approximately 3400 yr later. Before 3400 yr, refluxing water enters and fills the failed WP. Once the WP fills, water overflows from the WP, and radionuclides leave the failed WP.

The time histories of radionuclide releases at the downgradient boundaries of the EBS, the UZ, and the SZ are provided in Figure 3-13. In general, the release rates from the EBS in Figure 3-13(a) for the soluble radionuclides drop within a few years after the peak release, because of radioactive decay and because the removal of radionuclides from the WP decreases the inventory available for release. Other radionuclides, such as ^{234}U, ^{237}Np, ^{239}Pu, and ^{230}Th, which are less soluble, and have relatively longer half-lives, exhibit increasing release rates in the 10,000-yr TPI. The radionuclide ^{241}Am also has a low solubility; however, with a relatively short half-life of 432 yr, the release rate decreases to match the release rate of its parent ^{245}Cm and establishes secular equilibrium.

There is no initial increase in the EBS release rates observed from the instantaneous release of the gap fraction inventory. Moreover, climatic change from current to pluvial conditions could be a key event

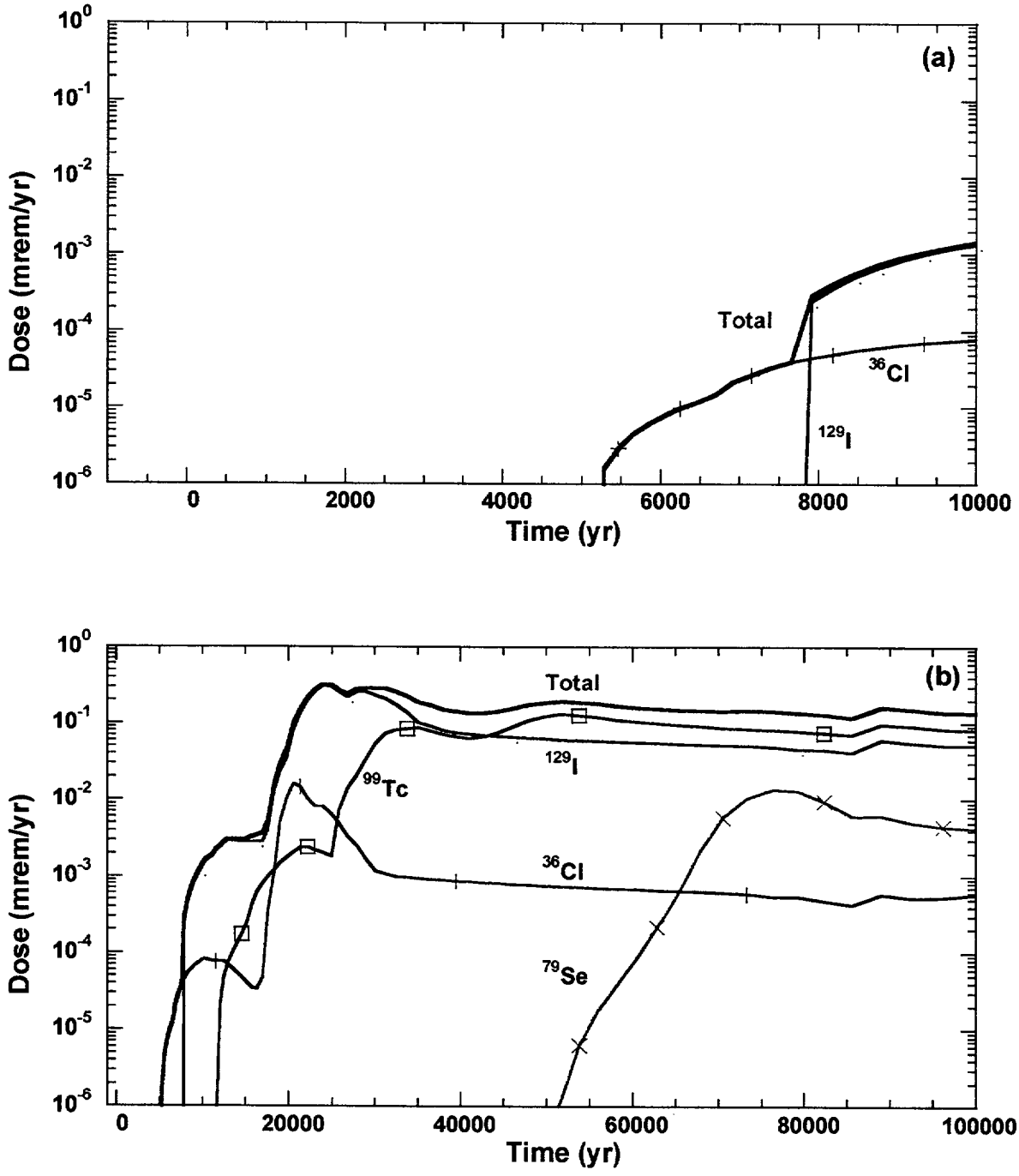

Figure 3-12. Groundwater dose to an average individual as a function of time at the receptor location 20 km (12.4 mi) downgradient of the repository, for the mean value data set in the: (a) 10,000-yr, and (b) 100,000-yr, time periods of interest.

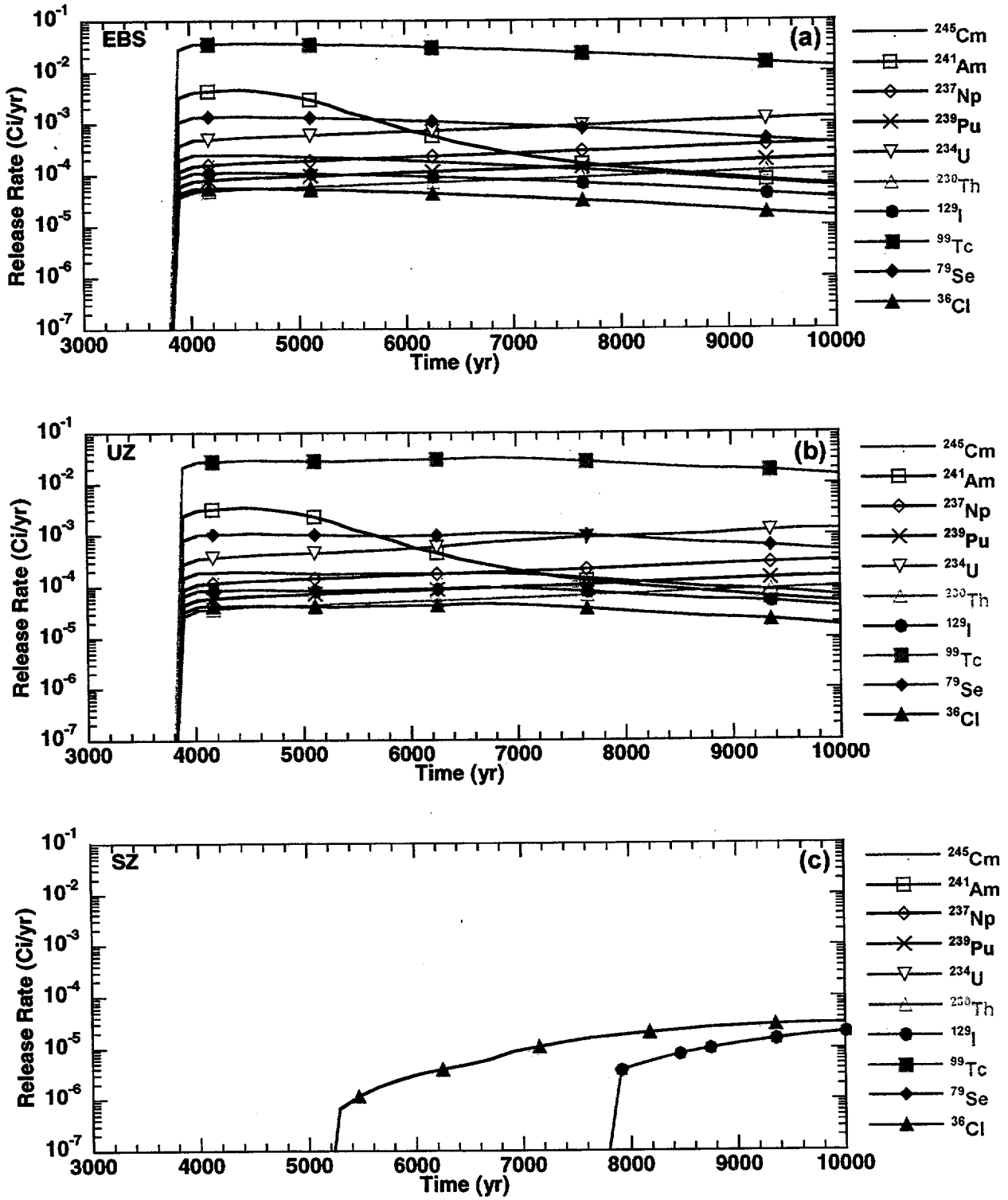

Figure 3-13. Release rates in the 10,000-yr time period of interest from the: (a) EBS (b) UZ; and (c) SZ for the mean value data set.

that affects performance. The increase in infiltration rate over the 10,000-yr TPI shown in Figure 3-1 does not result in increased release rates from the EBS for the highly soluble radionuclides, although an effect is evident for the less soluble radionuclides, as discussed previously.

The similarity between EBS and UZ releases shown in Figures 3-13(a) and (b) indicates the UZ as modeled does not significantly influence the releases into the SZ. One might expect the UZ to delay the transport of radionuclides, because the radionuclides must be transported 300 m (984 ft) from the repository to the water table.

The GWTT through the UZ is only 20 yr (i.e., fracture flow) for all subareas except subareas 5 and 6, which have a travel time of about 1400 yr (i.e., matrix flow). Consequently, for subareas 1 through 4 and subarea 7, which encompass almost 80 percent of the SF inventory, the UZ does not delay radionuclide transport subsequent to release from the EBS. For the remaining 20 percent of the SF inventory, the 1400-yr GWTT is relatively small compared with the 10,000-yr TPI.

The SZ illustrated in Figure 3-13(c) reveals releases of only ^{99}Tc, ^{129}I, and ^{36}Cl in the 10,000-yr TPI. As provided in Table 3-9, these radionuclides have the weakest sorbing properties in the SZ alluvium. The SZ release rates presented in Figure 3-13(c) can also be compared with Figure 3-13(b) to evaluate the effects of flow and transport in the SZ. The GWTT computed using the streamtube flow rates and lengths in the SZ is about 3700 yr. However, sorption in the alluvium significantly increases the travel time for most of the radionuclides.

As illustrated in Figure 3-12(a), the groundwater pathway dose at 10,000 yr is dominated by ^{129}I and ^{36}Cl. These nuclides contribute the most to dose because of no or little retardation during transport, a large initial inventory, long half-lives compared to the 10,000-yr time frame of interest, relatively large DCFs, and high solubilities. Tables 3-5 and 3-7 through 3-10 provide a summary of the mean values for these parameters. To obtain a perspective of the magnitude of the dose, a total dose of 10^{-11} Sv/yr (1 nanorem/yr) does not appear until 4500 yr in the time evolution of dose curve in Figure 3-12(a). Furthermore, the SZ release rate for ^{129}I corresponding to 74,0000 Bq/yr (2 μCi/yr) does not occur until 6,500 yr, at which time the dose from ^{129}I is 1/10th of a μrem/yr. The only nuclides that contribute more than 10^{-11} Sv/yr (1 nanorem/yr) to dose in 10,000 yr are ^{129}I and ^{36}Cl, which exhibit the peak doses at the end of the 10,000-yr-TPI.

The dose histories for a particular faulting event and a particular igneous event are presented in Figures 3-14(a) and (b). It must be made very clear that the purpose of the following discussion is not to compare the incremental risk posed by the faulting crust or the igneous event, but rather to illustrate the behavior of the underlying model abstractions for faulting and igneous activity. To determine the risk, one would need to multiply the additional doses caused by faulting and igneous activity by their respective annual probabilities of occurrence (5×10^{-6} and 1×10^{-7}). For the mean value data set, there are no faulting events because the mean value of the threshold displacement is greater than the mean value of the credible displacement along a fault. However, if the threshold is made smaller than the mean value of the credible displacement, the faulting event occurs at about 4900 yr and causes the failure of 162 WPs. Figure 3-14(a) shows that the groundwater dose from the forced faulting event is approximately twice the dose without a faulting event at 10,000 yr. The difference between the results arises solely from the release of SF from WPs failed by faulting.

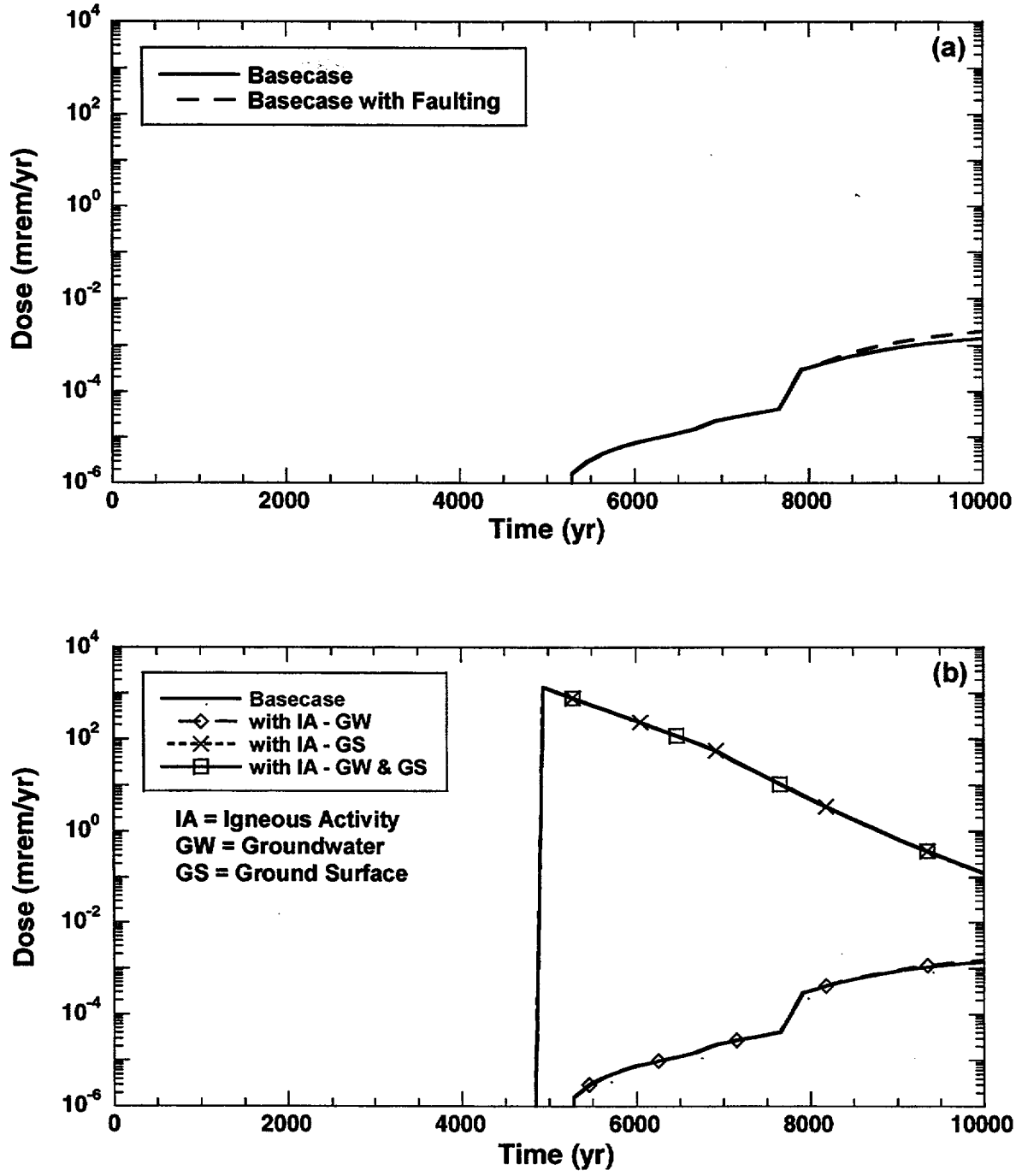

Figure 3-14. Groundwater dose in 10,000-yr time period of interest with and without: (a) faulting; and (b) igneous-activity disruptive events, for the mean value data set, without probability weighting. (The ground-surface dose is shown for releases caused by extrusive igneous activity.)

The groundwater dose from igneous activity in Figure 3-14(b) behaves similarly to the dose from faulting events. The increase in groundwater dose from igneous activity is smaller than that for faulting events because only 31 WPs are failed by the intrusive igneous activity compared with 162 WPs failed by the faulting event in the mean value single-realization case. Extrusive igneous events also result in a peak ground-surface dose of about 0.01 Sv/yr (1,000 mrem/yr) at 4900 yr, which is the time of the volcanic event, and the dose exponentially decreases thereafter.

The following section presents a discussion of the TPA results from the 100,000-yr TPI for dose, release rates, and other intermediate values such as corrosion failure time. The results for the 100,000-yr TPI are different from the results for the 10,000-yr TPI, partly because all WPs fail from corrosion before 17,000 yr.

3.2.2 100,000-Year Releases and Dose

Figure 3-8 provides the performance of the EBS showing the number of failed WPs during the 100,000-yr TPI. Initially defective failures in all subareas account for 31 WPs, whereas of those remaining, 928 WPs in subareas 5 and 7 fail from corrosion at 16,300 yr; and 5468 WPs in subareas 1, 2, 3, 4, and 6 fail from corrosion at 17,000 yr. Thus, all 6427 WPs in the repository fail by 17,000 yr. Table 3-3 provides a summary of the TPA input parameters that determine the WP failure time.

The release rate histories for all 11 radionuclides at the three boundaries (i.e., EBS, UZ, and SZ presented in Figure 3-15) reflect the time required for the initially defective WPs to fill with water (3400 yr) and release radionuclides, together with the corrosion failure time of 17,000 yr. The WPs failed by corrosion fill relatively faster and release radionuclides relatively faster compared with initially defective failures, because the thermal reflux period has passed and the pluvial period has taken effect. The first peak releases begin at about 4000 yr, and the second peak occurs before 20,000 yr. Just as with the 10,000-yr TPI in Figure 3-13, release rates for radionuclides are impacted by sorption coefficients, half-lives, initial inventories, solubilities, and DCFs. Values for these parameters are presented in Tables 3-5 and 3-7 through 3-10.

When water starts to leave the WP after it has filled with water, the releases of ^{99}Tc, ^{129}I, and the other highly soluble radionuclides represent the accumulation of the radionuclides in water that occurs as the WP fills. The peak releases for these highly soluble radionuclides occur after the WP fills with water at 3400 yr. As seen in Figure 3-15 for the less soluble radionuclides such as ^{237}Np, the release rate peaks at the end of the 10,000-yr TPI. This implies that the solubility limit is controlling the release rate. Because ^{237}Np leaves the WP at the solubility limit, the release rate from the WP is proportional to the rate of water flow through the WP. With a half-life of 2.14×10^6 yr, the ^{237}Np inventory is available for release throughout the simulation period. This effect is observable in Figure 3-15(a), from 3400 yr to the corrosion failure time at 17,000 yr. After 17,000 yr, radionuclide releases decrease (i.e., not solubility-limited) following the peak releases at approximately 17,000 yr. The decrease in release rates for the radionuclides with low solubilities can be attributed to high flow rates during the pluvial period. ^{239}Pu is another actinide that is solubility-limited in ambient YM pore waters. Therefore, release rates from the EBS should be similar to ^{237}Np as shown in Figure 3-15(a).

The plot in Figure 3-15(b) represents the release rates from the seven subareas summed over all nuclides at the water table. Comparison of the EBS and UZ release rates in Figures 3-15(a) and (b) shows that the UZ has little delaying effect, not only on the transport of ^{99}Tc, a nonsorbing nuclide, but also on the

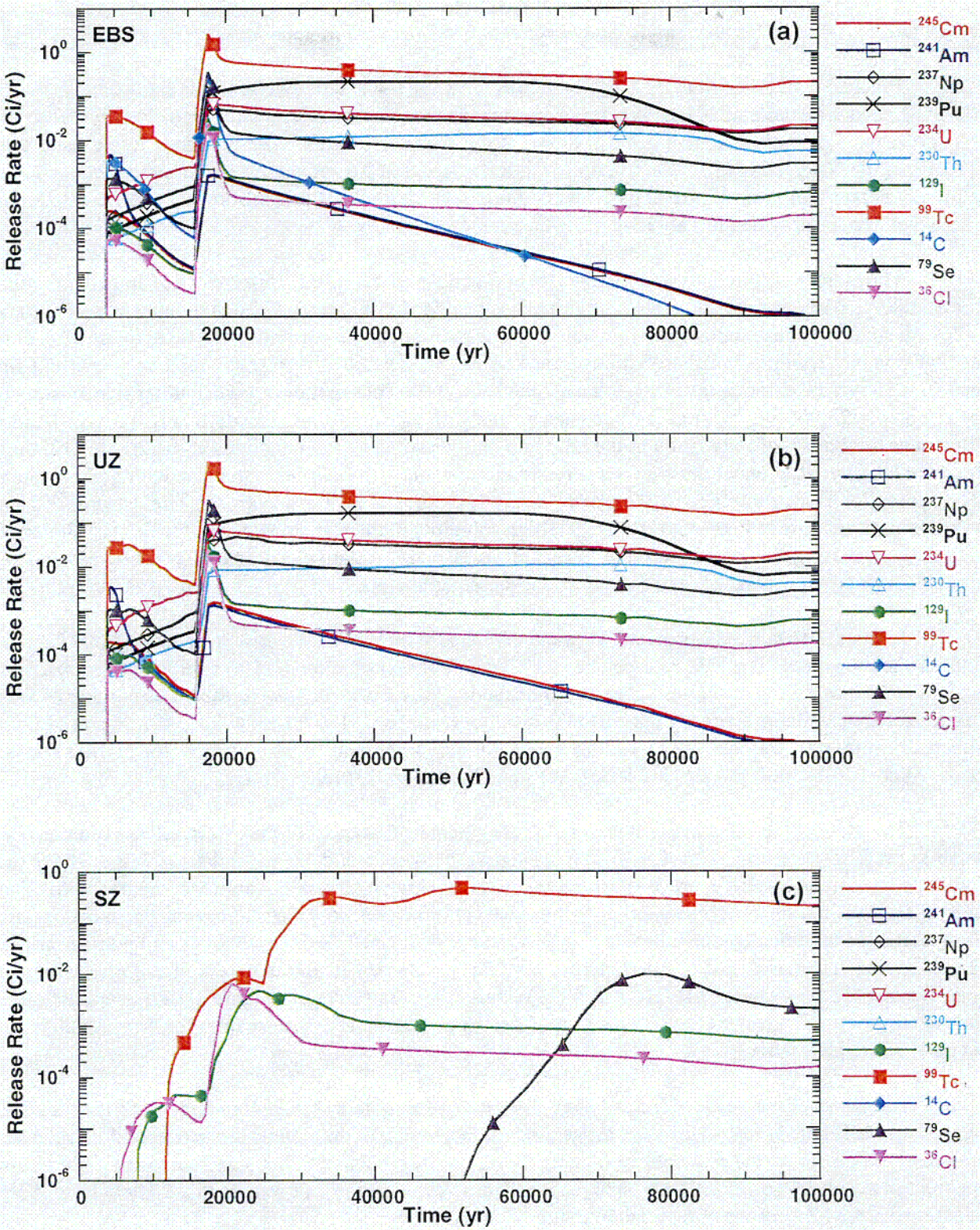

Figure 3-15. Release rates in 100,000 yr from the: (a) EBS; (b) UZ; and (c) SZ for the mean value data set.

C02

transport of the other 10 radionuclides. As discussed in the previous section, the UZ does not significantly affect the release rates because flow mainly occurs in fractures with no retardation.

Figure 3-15(c) illustrates the performance of the SZ in the 100,000-yr TPI. The figure shows the SZ release rates at a distance of 20 km (12.4 mi) from the repository. In the SZ, sorption significantly affects the release rates. The only radionuclides that arrive at the receptor location with a release rate greater than 37 Bq/yr (10^{-6} Ci/yr) are ^{99}Tc, ^{79}Se, ^{129}I, and ^{36}Cl. Retardation of the remaining seven radionuclides in the alluvium delays their time of arrival past the 100,000-yr TPI. The SZ alluvium sorption coefficients for all radionuclides are provided in Table 3-9.

The radionuclides contributing to the 100,000-yr dose are completely different than those dominating the 10,000-yr dose. For the 100,000-yr TPI, the dose provided in Figure 3-12(b) is dominated by ^{99}Tc and ^{129}I, with smaller contributions from ^{36}Cl and ^{79}Se. The radionuclide contributing the most to the peak dose at 23,000 yr is ^{129}I, with minor contributions from ^{99}Tc and ^{136}Cl. Although ^{136}Cl has a relatively long half-life at 3.01×10^5 yr, the chloride inventory is small (see Table 3-7). Thus, although contributing significantly to peak dose at 23,000 yr, ^{36}Cl rapidly becomes an insignificant contributor to dose. Figure 3-12(b) also illustrates the impact of retardation in the alluvium on the arrival of radionuclides at the 20-km (12.4-mi) receptor location. Radionuclides with lower retardation factors arrive earlier than those with higher values. The retardation factors for ^{36}Cl, ^{129}I, ^{99}Tc, and ^{79}Se are 1, 2, 5.5, and 22.4, respectively. The reasons ^{99}Tc and ^{129}I dominate the dose in Figure 3-12(b) are: (i) high solubility in the water contacting the SF; (ii) almost no retardation; (iii) large initial inventory; (iv) long half-lives; and (v) relatively large DCFs. Tables 3-5 and 3-7 through 3-10 provide summaries of the values for these parameters.

Figures 3-16 and 3-17 present ^{99}Tc and ^{237}Np release rates and ^{99}Tc dose, respectively, by subarea and for the repository. The EBS release rates for ^{99}Tc and ^{237}Np in Figure 3-16(a) exhibit similar behavior with the subareas having the largest inventory contributing the most to the total release. The number of WPs in each subarea, which are directly related to the inventory, are 1663; 1767; 855; 472; 654; 738; and 278, for subareas 1 through 7, respectively. Subareas 1 and 2 are the largest subareas and show the highest release rates, whereas subarea 7 contains the fewest WPs and has the lowest release rates.

The plots of the UZ releases in Figure 3-16(b) indicate that the ^{99}Tc and ^{237}Np release rates are the same as the EBS releases in Figure 3-16(a) in all subareas except 5 and 6. Only subareas 5 and 6 have the Calico Hills nonvitric unit (Figure 3-9), which has relatively high matrix permeability compared with other units. At the infiltration rate corresponding to the mean value data set, only matrix flow can occur in this unit. Flow occurs in the fractures for subareas 1, 2, 3, 4, and 7, with GWTTs of about 20 yr and no retardation. However, for subareas 5 and 6, the transport of ^{237}Np is retarded in the matrix and the effects of the time-varying UZ flow change the ^{99}Tc and ^{237}Np release rates. As evident in Figure 3-16(b), retardation in the matrix produces a greater effect on the ^{237}Np UZ release rates than the release rates for ^{99}Tc, which is not retarded in the UZ matrix.

The SZ release rates for ^{99}Tc in Figure 3-16(c) exhibit a delay when compared with the ^{99}Tc UZ release rates in Figure 3-16(b). However, the general characteristics of the engineered barrier and UZ releases are preserved insofar as the peak releases arising from initially defective failures and corrosion failures are apparent in the plot. The variability by subarea is also consistent for the ^{99}Tc release rates. There is no ^{237}Np release from the SZ because of retardation in the SZ alluvium.

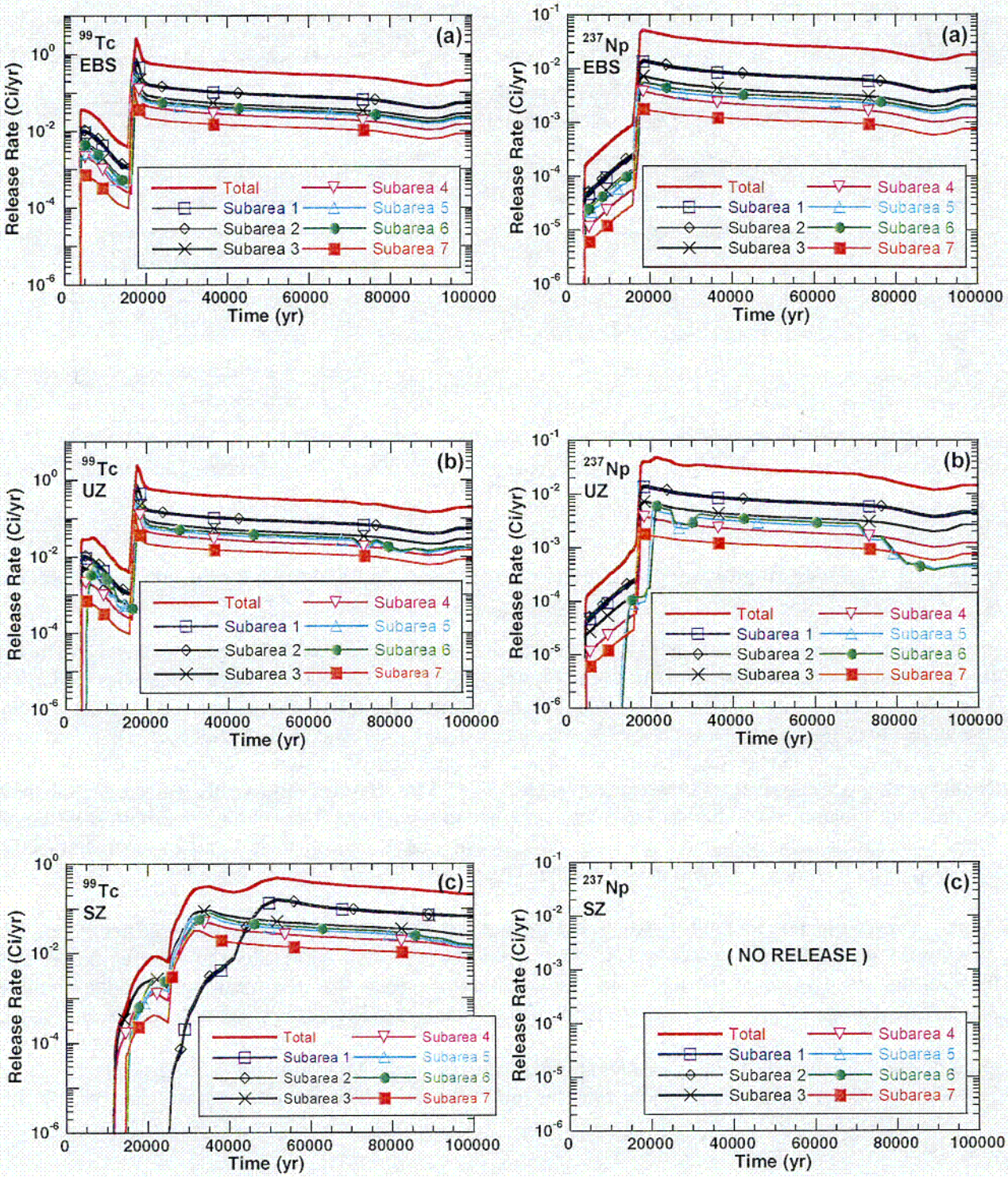

Figure 3-16. ^{237}Np and ^{99}Tc total release and releases by subarea in 100,000 yr from the: (a) EBS; (b) UZ; and (c) SZ for the mean value data set.

C03

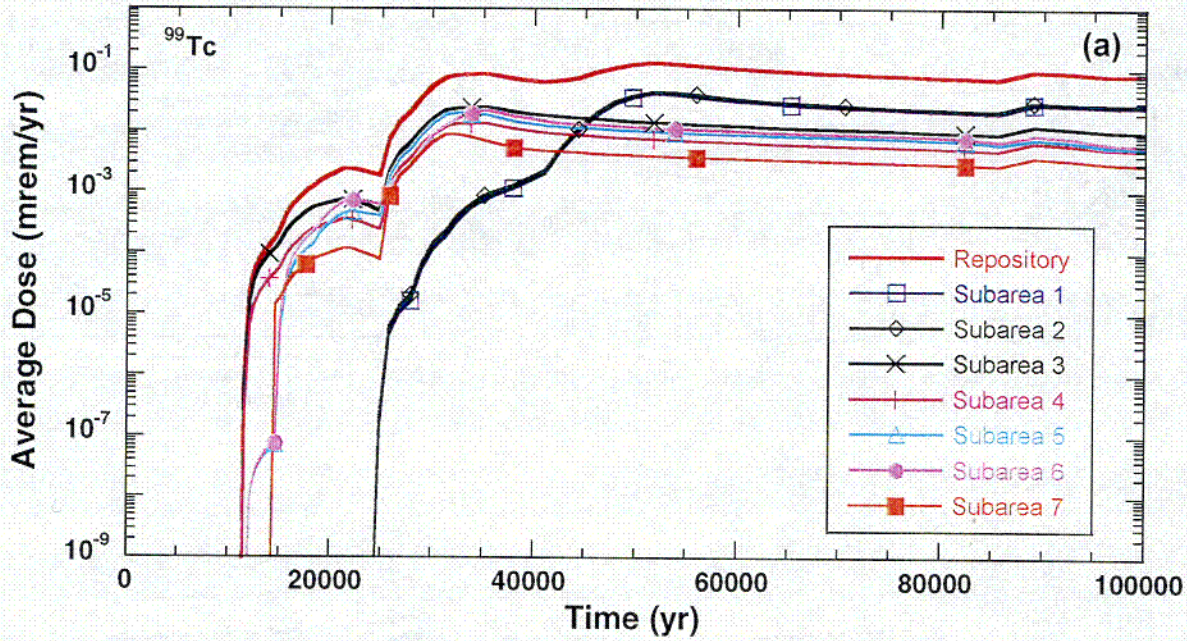

Figure 3-17. ^{99}Tc groundwater doses, total and by subarea, in 100,000 yr, for the mean value data set.

The groundwater doses for ^{99}Tc by subarea are shown in Figure 3-17. The general characteristics of this plot match the SZ release rates for ^{99}Tc in Figure 3-16(c). For 100,000 yr, the subareas with the largest ^{99}Tc release rates and dose in Figure 3-17 contain the greatest amount of SF (i.e., the subareas listed from the largest to the smallest amount of SF are subareas 2, 1, 3, 6, 5, 4, and 7). The effects of GWTT on dose at the receptor location is evident in Figure 3-18 with the peak dose from subareas 1 and 2 arriving at about 20,000 yr after peak doses from subareas 3 through 7. The SZ travel times vary by subarea because subareas use different streamtubes. Subareas 3 and 4 are assigned to streamtube B and exhibit the shortest SZ travel times, whereas subareas 5, 6, and 7 are assigned to streamtube A, and subareas 1 and 2 use streamtube D. The longest travel times are found in streamtube D (see Table 3-9 for streamtube lengths).

The dose history for faulting events and igneous activity[2] over 100,000 yr is presented in Figure 3-19. As with the results for the 10,000-yr TPI, using the mean value data set results show no faulting events because the mean value of the threshold displacement is greater than the mean value of the credible displacement along a fault. However, if the threshold is made smaller than the credible displacement, the faulting event occurs at about 4900 yr and causes the failure of 162 WPs. Figure 3-19(a) shows that the groundwater dose from the faulting event is approximately twice the dose without a faulting event from about 10,000 to 17,000 yr. After 17,000 yr, the releases from WPs failed by corrosion dominate the groundwater

[6]These results are presented only to show the process-level trends and must be used in proper context, because these are not weighted by appropriate probabilities. The annual probability for the faulting event is 5×10^{-6} and for the igneous event is 1×10^{-7} yr^{-1}.

C04

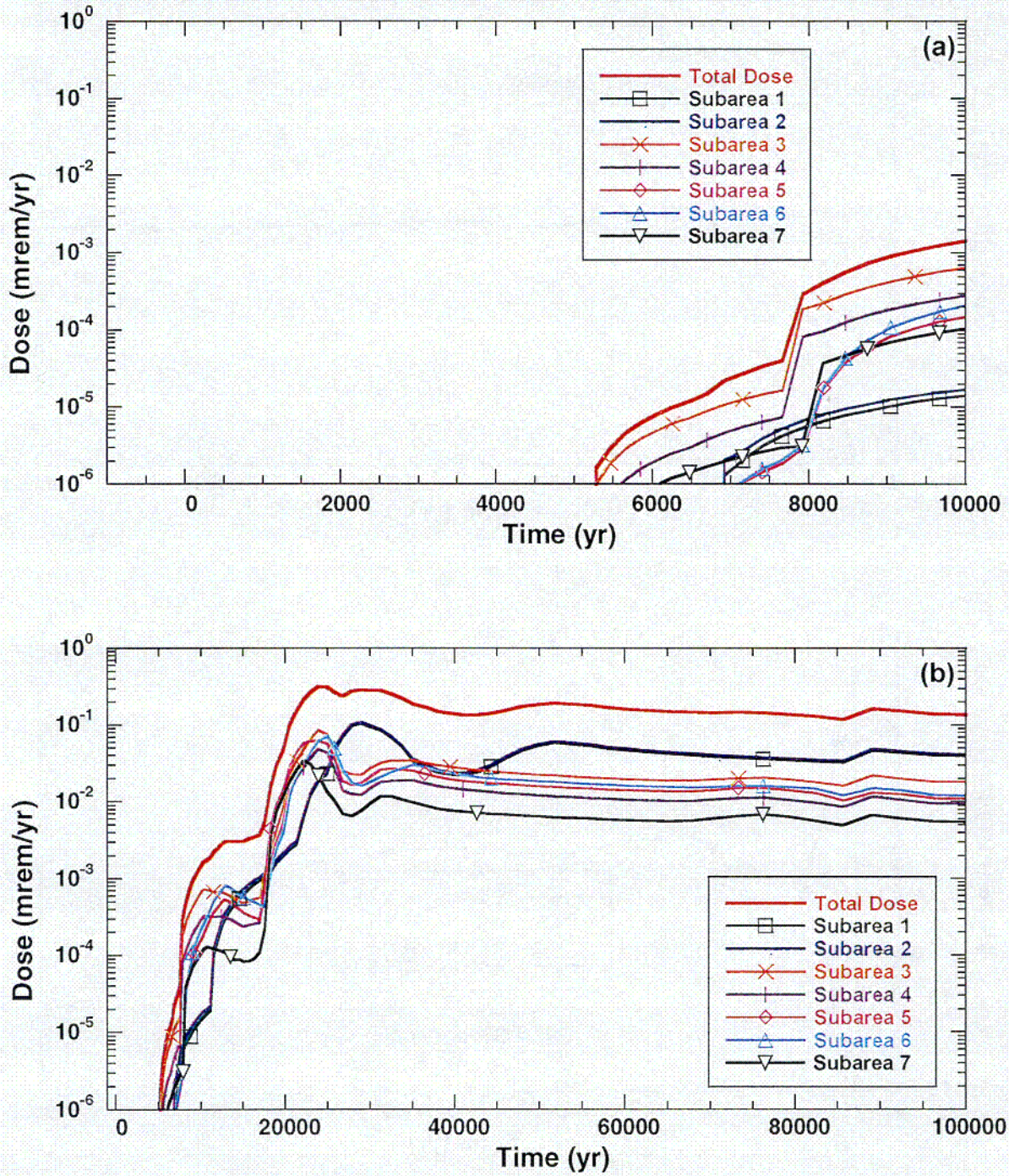

Figure 3-18. Groundwater dose, total and by subarea, in: (a) 10,000, and (b) 100,000 yr, for the mean value data set.

C05

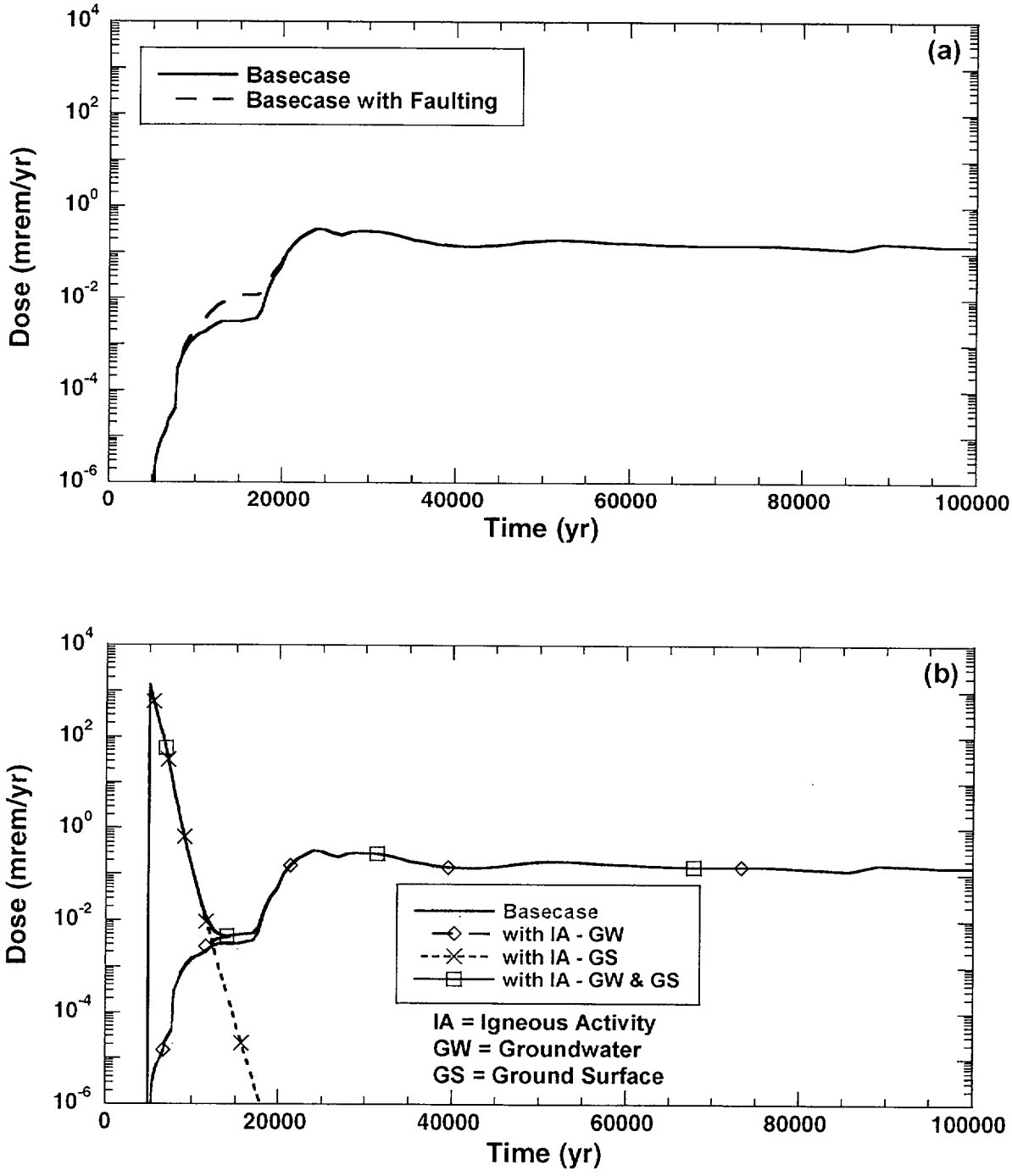

Figure 3-19. Groundwater dose in 100,000 yr with and without: (a) faulting, and (b) igneous activity disruptive events for the mean value data set, without probability weighting. (The ground-surface dose is shown for releases caused by extrusive igneous activity.)

dose, and the results plotted in Figure 3-19(a) of the groundwater dose with and without faulting events are not distinguishably different.

The groundwater dose from igneous activity over the 100,000-yr TPI in Figure 3-19(b) behaves similarly to the dose from faulting events. As with the results for the 10,000-yr TPI, the increase in groundwater dose from igneous activity for 100,000 yr is smaller than that for faulting events because only 31 WPs are failed by the intrusive igneous activity, compared with 162 WPs failed by the faulting event. Extrusive igneous events also result in a ground-surface dose that peaks at about 10 mSv/yr (1000 mrem/yr) when the volcanic events occur at 4900 yr and exponentially decreases thereafter. At about 12,000 yr, the groundwater and ground-surface contributions to dose are equal. From 17,000 yr, when all the WPs have failed by corrosion, through 100,000 yr, groundwater dose dominates the receptor dose. The doses presented in Figure 3-19 are not probability-weighted.

3.3 MULTIPLE-REALIZATION ANALYSIS

The performance of the YM repository is evaluated with a probabilistic approach that comprises results from simulations performed with multiple realizations. This approach uses the probabilistic sampling of input data to compute dose at a receptor location 20 km (12.4 mi) from the repository during time periods of 10,000 and 100,000 yr. Although the deterministic approach (previous section) was presented to illustrate in detail how the behavior of the various components or processes influences other components or dose, the probabilistic approach provides a range of results that shows the variation in the output resulting from the combined effects of the variability in the input data. Also, trends not evident in the results from the deterministic data may become evident in the probabilistic results.

Probabilistic sampling is conducted using Latin Hypercube Sampling (LHS) (Iman, *et al.*, 1980) for the 250 realizations, which is sufficiently large to obtain convergence in results while maintaining computational efficiency. Each realization uses a set of values generated from probability distribution functions specified in the TPA input file. The probability distribution functions are constructed for the input parameters thought to contain uncertainty and variability, using available data and interpretation. Uncertainty arises from a lack of complete information, whereas variability is the natural or inherent variance in the value of a parameter.

The previous section presents TPA results computed with mean values for the distributions specified in the basecase data set. The basecase data set comprises the best available information of the TPA input parameters. In the basecase data set, of the 838 parameters, 592 parameters are defined as constants, and 246 parameters are specified with probability distribution functions. The basis for assigning a constant value or a probability distribution to the parameter depends on various factors. For example, constant values are assigned to parameters that are either well-characterized or have negligible variability. Probability distribution functions are assigned to parameters with either a natural variability or uncertainty that has been observed in data. Expert elicitation also provides a valid basis to assign a constant value or a probability distribution function to a parameter. The selection of the particular distribution type, such as normal, uniform, or beta, depends on the information available for the parameter and may involve either the best fit of data to a distribution or a reasonable assumption of the distribution type. Specification of a probability distribution function in the TPA code consists of a distribution type and limits (e.g., uniform with a minimum of 0 and a maximum of 100, or log-triangular, with a minimum of 1.0×10^{-5}, maximum of 1.0×10^{-1}, and a peak of 1.0×10^{-3}). The impact of assuming a particular distribution for a parameter is evaluated in sensitivity analyses.

When the TPA code is executed for a realization of the parameter vector, dose to the receptor is calculated for realization. The results from all Monte Carlo realizations using the LHS sampler are plotted to evaluate the repository performance. For example, dose to the receptor is presented in a scatterplot of peak dose versus time of peak dose, a time history of average and expected dose for all realizations, and a CCDF of peak dose. The expected dose is computed by averaging the doses at an instant of time from all realizations. The resulting curve is a time-dependent dose curve that represents the expected dose. The peak expected dose is the largest expected dose obtained from the expected dose curve versus time. For example, groundwater dose from a single realization using the mean value data set is shown in Figure 3-18, and the expected dose from multiple realizations is presented in Figure 3-20, which also provides dose from individual realizations. Additionally, the relationship between dose and intermediate results, such as WP failure time, flow of water onto a WP, and radionuclide release rates, is presented for all realizations.

This section provides results from simulations conducted with the TPA Version 3.2 code, using the basecase data set with 250 realizations. For the major components of the TPA code, results are summarized and trends presented. The values and distributions of the TPA parameters in the basecase data set used to generate the multiple-realization results are provided in Tables 3-1 through 3-10, and the correlated parameters with associated correlation coefficients are presented in Table 3-11.

3.3.1 UZ Flow

The variation in the mean, minimum, and maximum infiltration rates is illustrated in Figure 3-21. For the mean infiltration rates, a present-day climate exists from 0 to about 3000 yr, and 89,000 to 100,000 yr, with the pluvial climate occurring between 3000 and 89,000 yr. Figure 3-21 shows that the range from the minimum to the maximum infiltration rates is approximately 1 order of magnitude. This range is related to the TPA input parameter for the initial infiltration rate, which has a uniform distribution from 1 to 10 mm/yr (0.0394 to 0.394 inches/year).

Subarea 3 exhibits the largest infiltration rates, because of higher infiltration at the ground surface above subarea 3 attributable to near-surface processes such as elevation and soil depth, whereas subareas 1, 2, and 4 have the lowest infiltration rates. In any single realization, the largest difference among the subarea infiltration rates is approximately 10 percent. The minimum and maximum pluvial infiltration rates, which occur between about 3000 and 89,000 yr, vary from about 10 to 280 mm/yr (0.394 to 11.02 in/yr) for all realizations and subareas.

In realizations with higher flow rates, there are generally more radionuclides released from the EBS because of a greater amount of water available to dissolve radionuclides. This effect is illustrated in Figure 3-22, which provides scatterplots of the cumulative releases of ^{99}Tc and ^{237}Np in 100,000 yr versus the maximum flow rate into the repository for each realization. The variability in the maximum flow rate is slightly more than 1 order of magnitude, whereas the cumulative release varies over 3 orders of magnitude. Although these releases are solubility limited, there is not a one-to-one relationship with the flow rate because of other parameters such as flow factors and the subarea wet fraction that affect the EBS release rate.

Figure 3-23 shows the trend of higher peak groundwater dose for maximum flow rate in both the 10,000- and 100,000-yr TPIs. Higher flow rates in the UZ transport a larger mass of radionuclides from the EBS and result in higher groundwater dose. Although the peak flow rate varies about 1 order of magnitude, the variability in the peak groundwater dose spans 5 orders of magnitude.

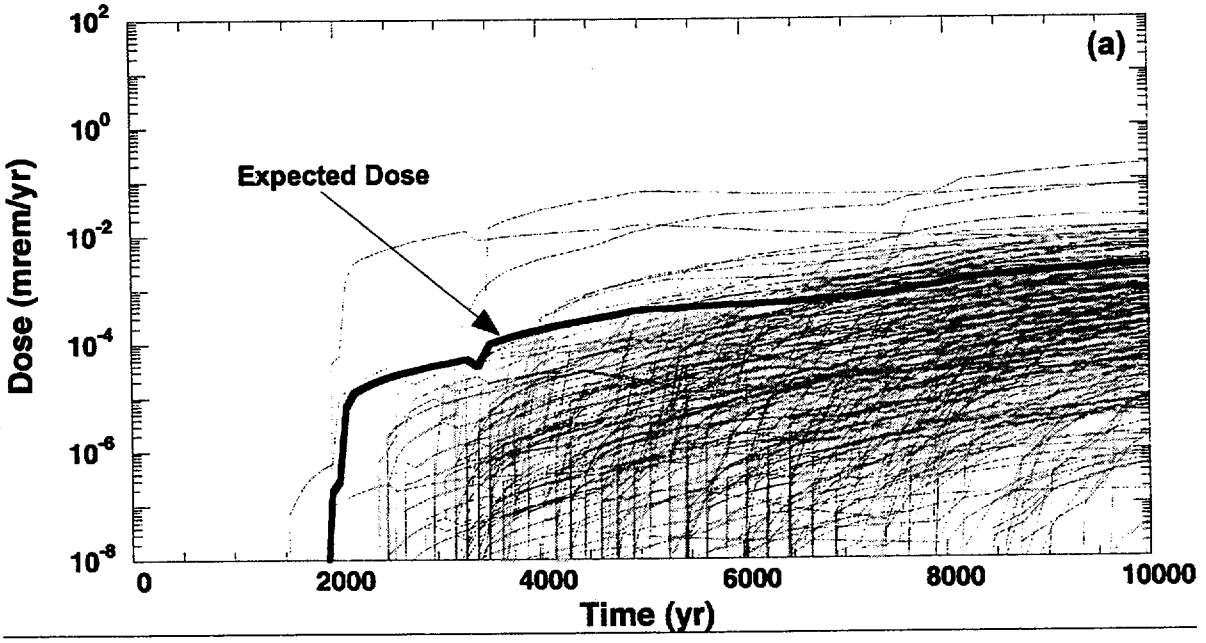

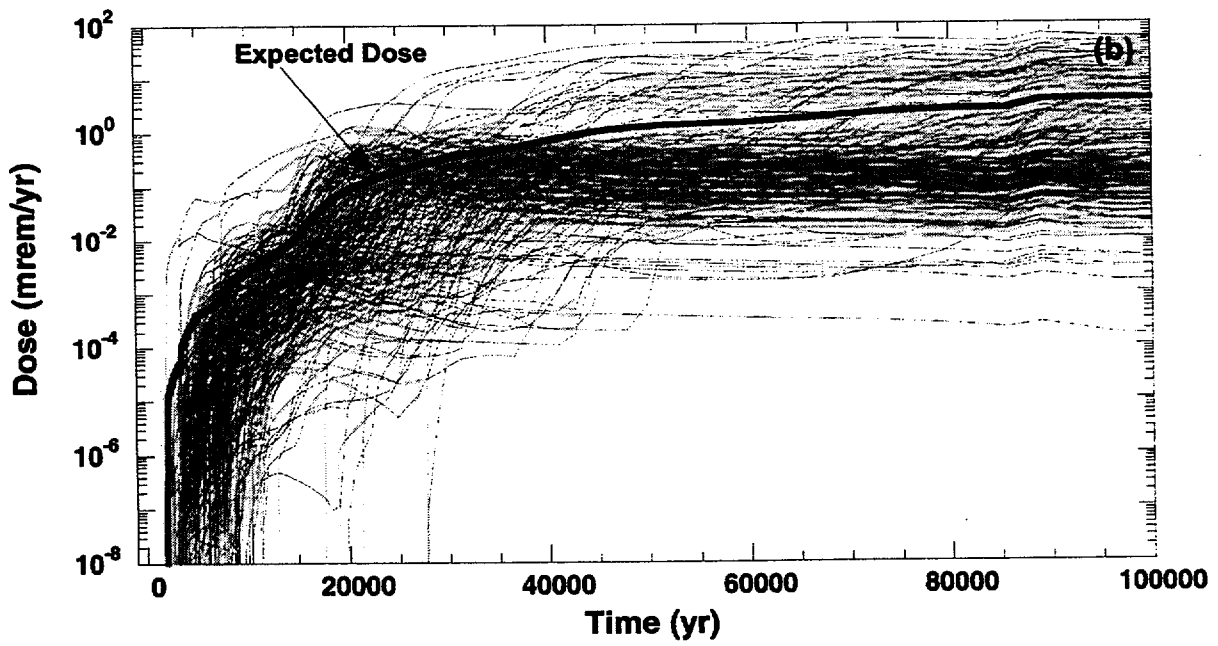

Figure 3-20. Groundwater dose in: (a) 10,000, and (b) 100,000 yr, including the average dose, for 250 realizations.

Table 3-11. Correlated parameters and correlation coefficients for the multiple realizations

Correlated Parameter 1	Correlated Parameter 2	Correlation
SubAreaWetFraction A	realAverageMeanAnnualInfiltrationAtStart[mm/yr]	0.631
SubAreaWetFraction M	atrixPermeability_TSw_[m2]	0.623
FowFactor A	realAverageMeanAnnualInfiltrationAtStart[mm/yr]	0.224
FowFactor M	atrixPermeability_TSw_[m2]	0.13
FowFactor S	ubAreaWetFraction	0.366
AlluviumMatrixRD_SAV_Am	Alluv iumMatrixRD_SAV_Pu	0.964
AlluviumMatrixRD_SAV_Am	Alluv iumMatrixRD_SAV_U	0.346
AlluviumMatrixRD_SAV_Am	Alluv iumMatrixRD_SAV_Np	0.837
AlluviumMatrixRD_SAV_Am	Alluv iumMatrixRD_SAV_Th	0.112
AlluviumMatrixRD_SAV_Pu	Alluv iumMatrixRD_SAV_U	0.489
AlluviumMatrixRD_SAV_Pu	Alluv iumMatrixRD_SAV_Np	0.881
AlluviumMatrixRD_SAV_Pu	Alluv iumMatrixRD_SAV_Th	0.109
AlluviumMatrixRD_SAV_Np	Alluv iumMatrixRD_SAV_Th	0.260
AlluviumMatrixRD_SAV_Np	Alluv iumMatrixRD_SAV_U	0.610
AlluviumMatrixRD_SAV_Th	Alluv iumMatrixRD_SAV_U	0.165

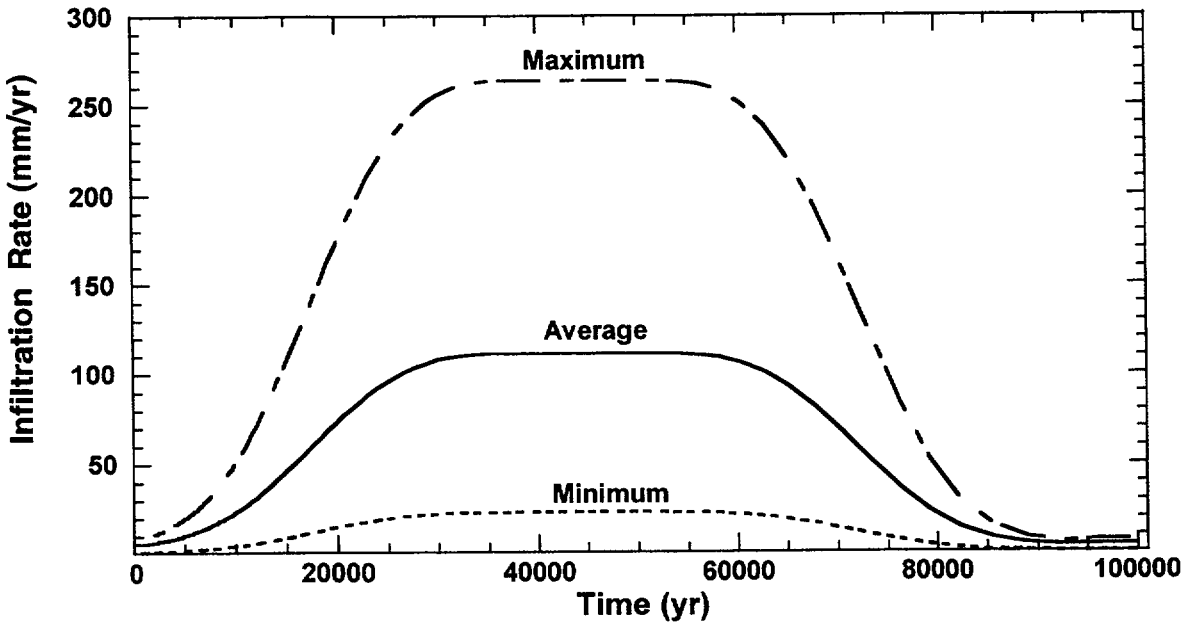

Figure 3-21. Mean, maximum, and minimum infiltration rates in the UZ for each subarea. (The subarea mean infiltration rate is averaged over all 250 realizations.)

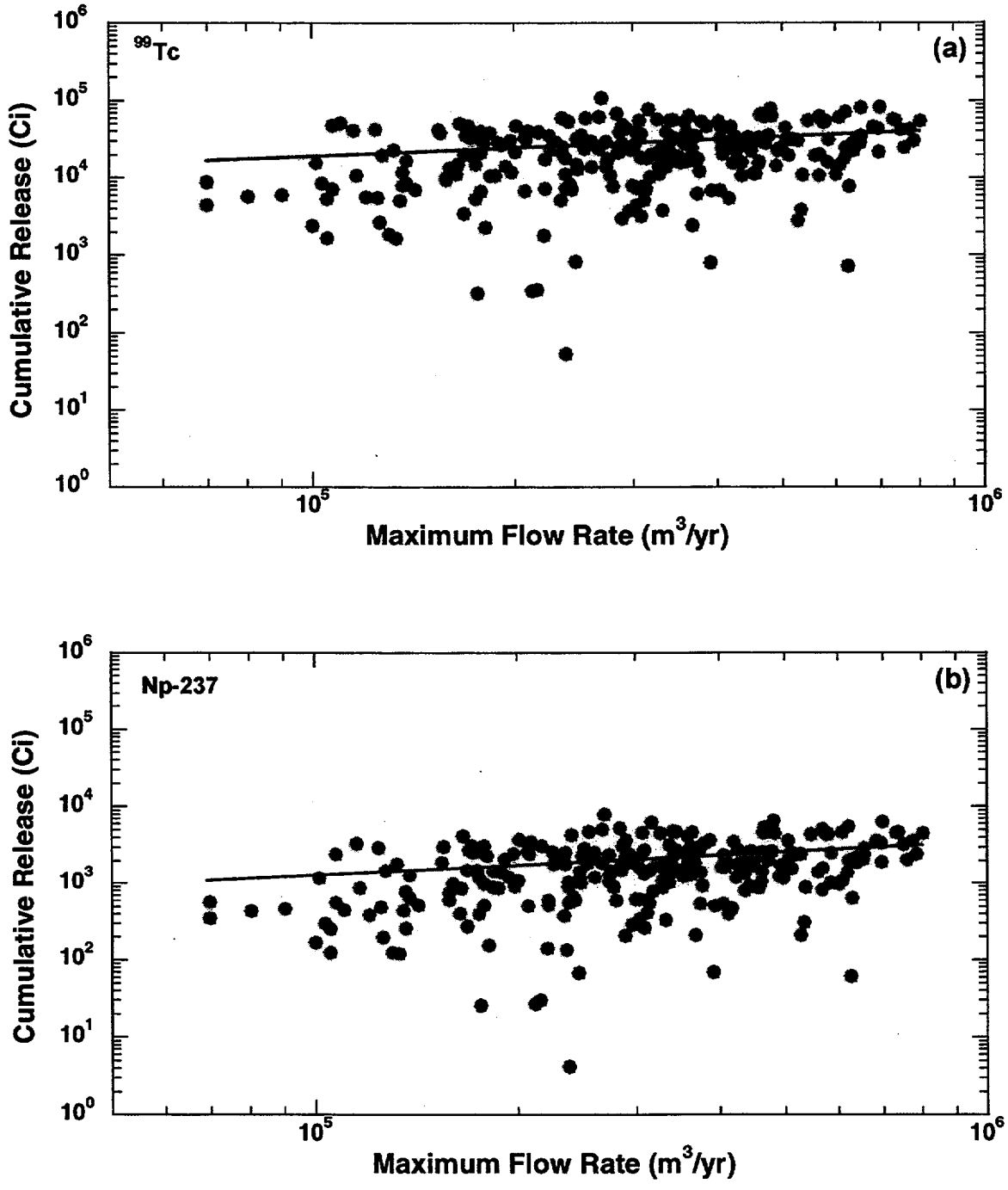

Figure 3-22. Cumulative release rates of ^{99}Tc and ^{237}Np from the EBS plotted with the maximum flow rate of water into the repository, for 250 realizations.

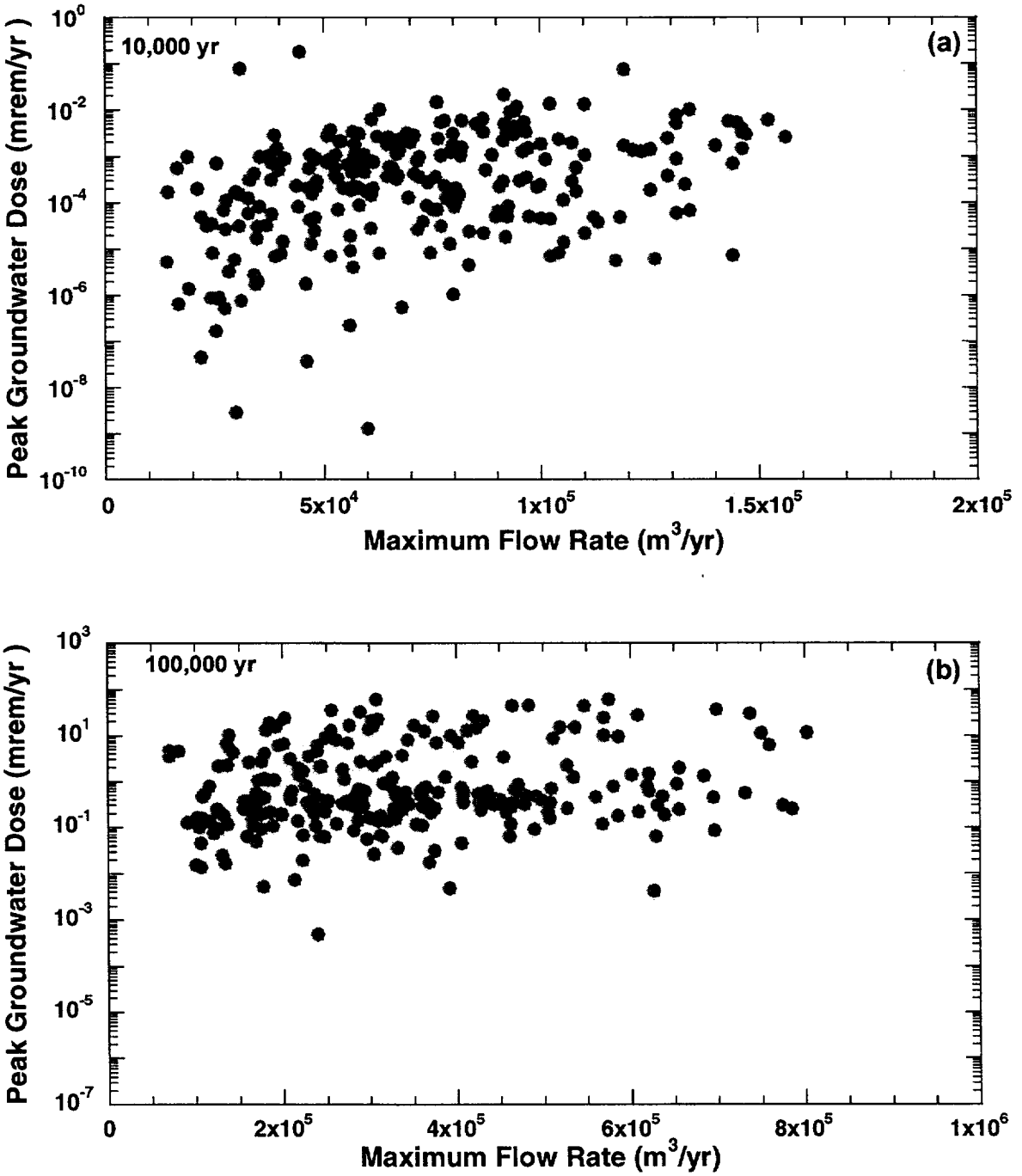

Figure 3-23. Peak groundwater dose in: (a) 10,000, and (b) 100,000 yr, plotted with the maximum flow rate of water into the repository, for 250 realizations.

3.3.2 Near-Field Environment

The time history of average WP temperature is provided in Figure 3-24(a), for each subarea. The subarea variability in the WP temperature from 10,000 and 100,000 yr is small compared with the difference in temperatures exhibited over about 100–10,000 yr, with a maximum difference in average WP temperature about 10 °C (50 °F) at 1,000 yr. In the 100–10,000-yr TPI, the greatest amount of heat is generated from the radioactive decay of SF.

Figure 3-24(b) shows the average, minimum, and maximum WP temperatures for subarea 1. The range between the minimum and maximum temperatures is about 10 °C (50 °F) at 100–1000 yr. Subareas 2–7 exhibit the same general variability in the average, minimum, and maximum WP temperatures as subarea 1. Inasmuch as the variation from the average temperature among the subareas is less than 5 percent in Figure 3-24, the parameters sampled in the basecase data set do not have a large influence on the range of computed WP temperatures. This small difference could affect corrosion calculations because the corrosion rate is sensitive to the WP temperature.

3.3.3 WP Degradation

In the basecase data set, the outer and inner overpack materials for the WP are specified as carbon steel and Alloy C-22, respectively, consistent with the DOE TSPA-VA design (U.S. Department of Energy, 1998). Figure 3-25 presents results from all realizations and the expected failure curve of WPs failed by corrosion for the probabilistic case. The WP failure times by corrosion range from about 11,000 to 46,000 yr, with an average corrosion failure time, for 250 realizations, of approximately 20,000 yr. There are no WPs failing from corrosion before 10,000 yr. It should be noted that effects of welds and closures, which could substantially decrease WP failure time, have not been considered in this calculation.

The relationship between average WP failure time and both the peak groundwater dose and the time of the peak groundwater dose is presented in Figure 3-26. The variability in the peak groundwater dose in Figure 3-26(a) ranges over 5 orders of magnitude, whereas the average WP failure time is 11,000–46,000 yr. An overall trend of decreasing peak groundwater dose with increasing average WP failure time is observable in this figure. When the WP failure time is delayed, more of the SF inventory decays and the transport time through the UZ and SZ is delayed. Thus, the peak groundwater dose is generally expected to be lower for larger WP failure times.

The average WP failure time and time of peak groundwater dose are provided as a scatterplot in Figure 3-26(b). In all instances, the peak groundwater dose occurs after the average WP failure time for 100,000-yr analyses. However, for approximately one-half the realizations, the peak groundwater dose occurs at times greater than 90,000 yr.

3.3.4 WP Release

Water transports radionuclides out of the WP and into the UZ and SZ to the receptor location. Thus, the flow rate of water in the UZ should be positively correlated with the release from the EBS. The relationships between the flow of water into the WP and the release of ^{99}Tc and ^{237}Np are illustrated in Figure 3-22. Furthermore, higher release rates contribute to greater peak groundwater doses, as shown in Figure 3-27, for ^{99}Tc and ^{237}Np, in subarea 1. The subarea 1 release rates presented in these figures are representative of release rates from subareas 2 through 7. The ^{99}Tc and ^{237}Np peak release rates and time of

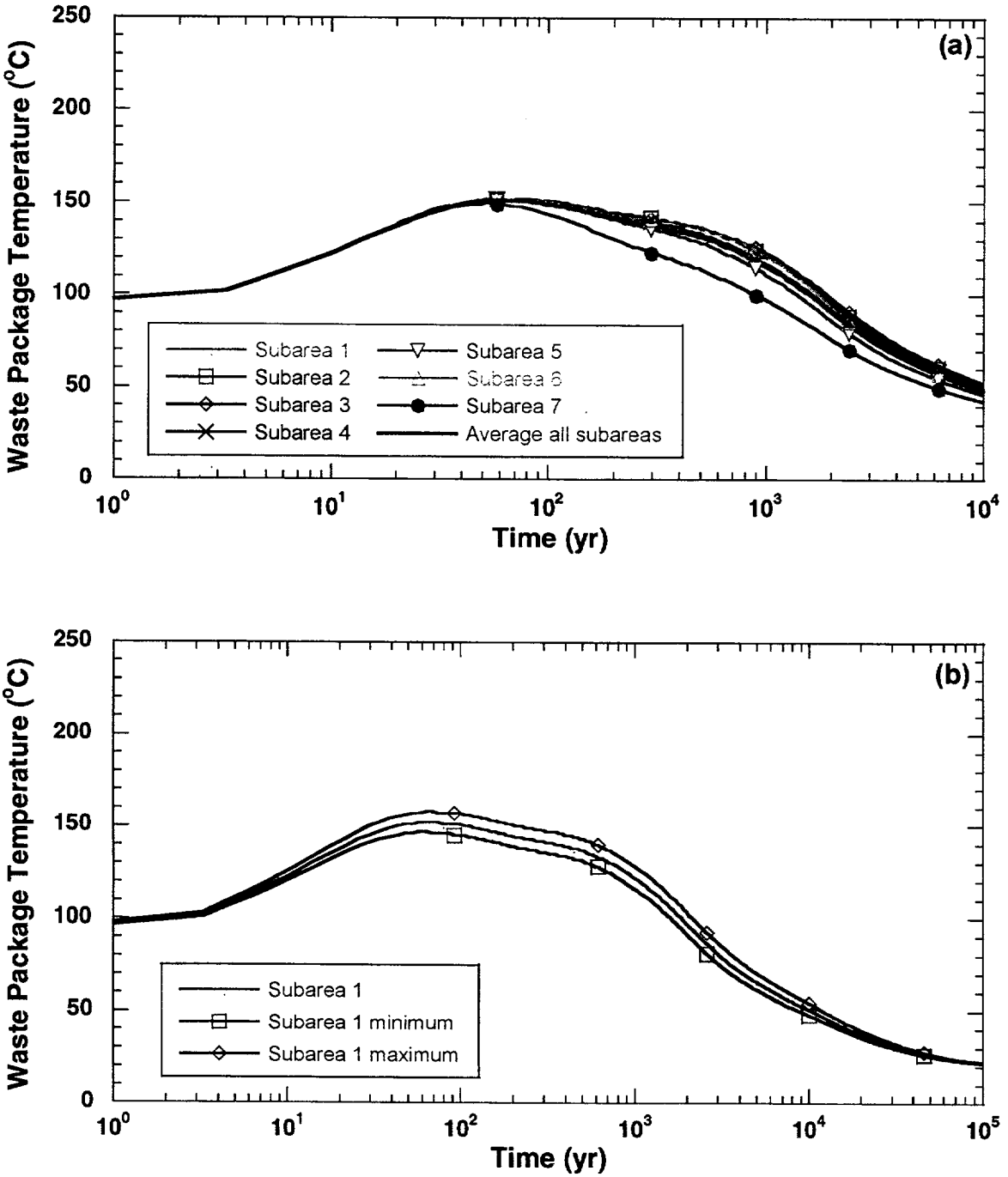

Figure 3-24. WP surface temperature: (a) averaged over the repository and for each subarea and (b) in subarea 1; the average, minimum, and maximum values, for 250 realizations.

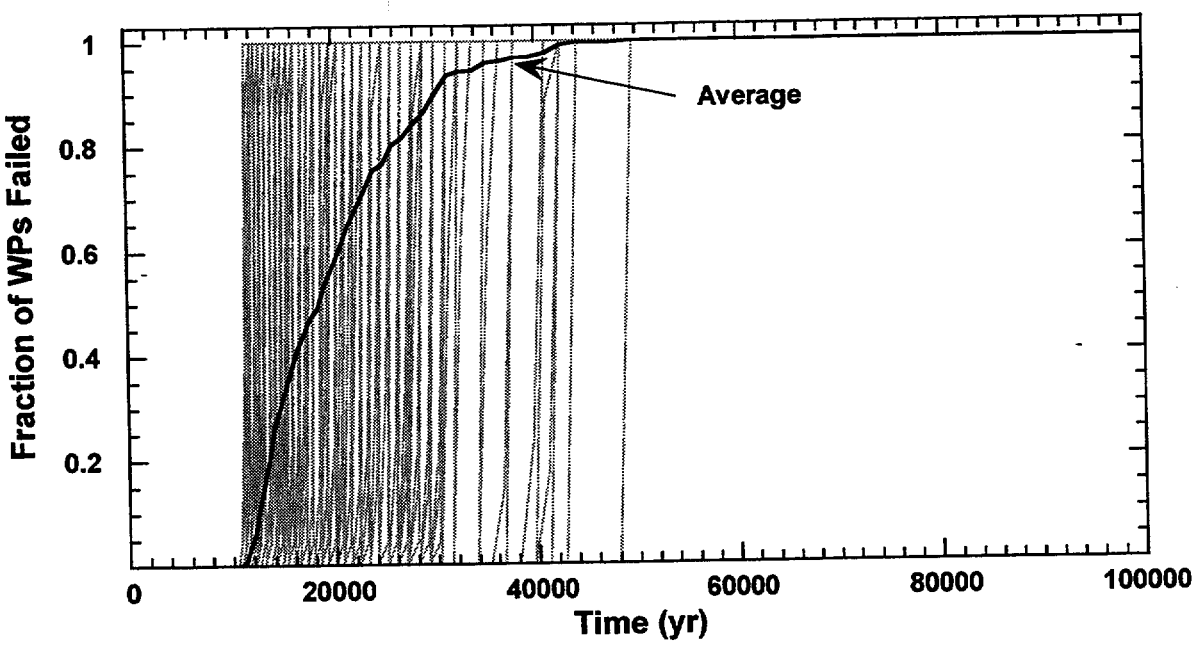

Figure 3-25. Fraction of Wps failed by corrosion for each of the 250 realizations, and the average fraction of failed WPs.

the peak release rates are presented in Figure 3-28. This figure shows that nearly all the ^{99}Tc and ^{237}Np peak releases occur between 11,000 and 46,000 yr, when WPs fail by corrosion. The variability in the peak release rates is slightly less than that for the groundwater dose. The peak release rates of ^{99}Tc and ^{237}Np vary over 3 to 4 orders of magnitude, whereas the peak groundwater dose exhibits over 5 orders of magnitude variability. Factors that influence the radionuclide transport from the EBS to the receptor location, such as well pumping rate and retardation, cause a greater variability in the groundwater dose than the release rate from the EBS.

Figure 3-29 provides the release rate of ^{99}Tc from subarea 1 for 10,000 and 100,000 yr. The results in this figure demonstrate that the variability in the EBS release rates is greater in the first 10,000 yr than in the period between 10,000 and 100,000 yr. It appears that the variability can be attributed to factors such as lower flow rates at times less than 10,000 yr, initially defective failures, and time to fill up the WP. Releases before to 10,000 yr are from initially defective and seismic failures, whereas the peak releases observed after 10,000 yr result mainly from corrosion failures. The magnitude of the releases extends over 4 to 5 orders of magnitude and arises partly from the variability in the flow rate into the EBS.

The cumulative release of radionuclides from the EBS is plotted in Figure 3-30, along with the initial inventory and the UZ and SZ releases. This graph reveals that more radionuclides are released relatively early, with most of the releases occurring during the first 50,000 yr. Radionuclides with a combination of the higher solubility, half-life, and initial inventory, such as ^{99}Tc, exhibit the largest release rates. Source depletion and radioactive decay result in lower releases toward the end of the 100,000-yr TPI.

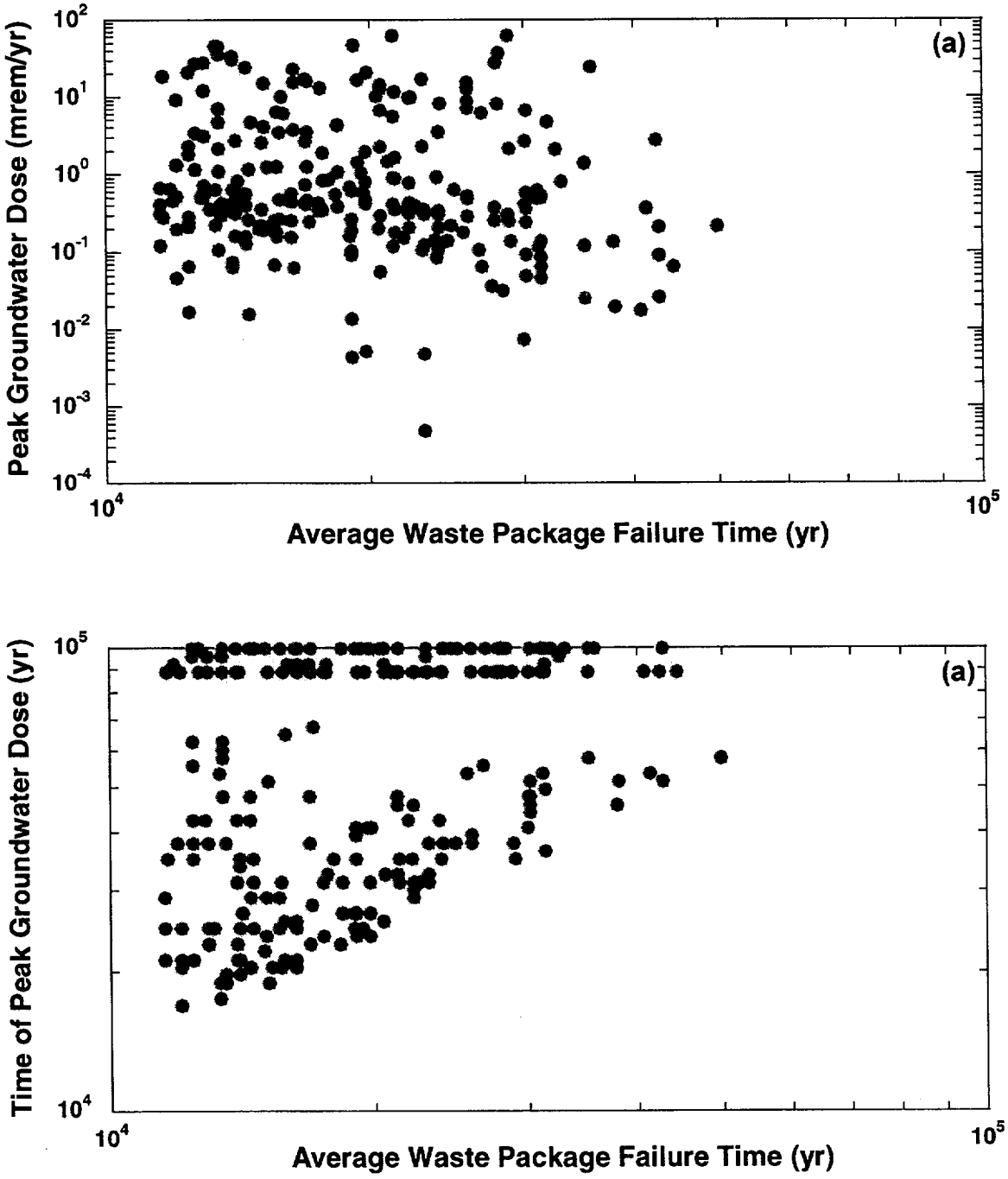

Figure 3-26. Average WP failure time by corrosion plotted with: (a) peak groundwater dose; and (b) time of the peak groundwater dose, for 250 realizations.

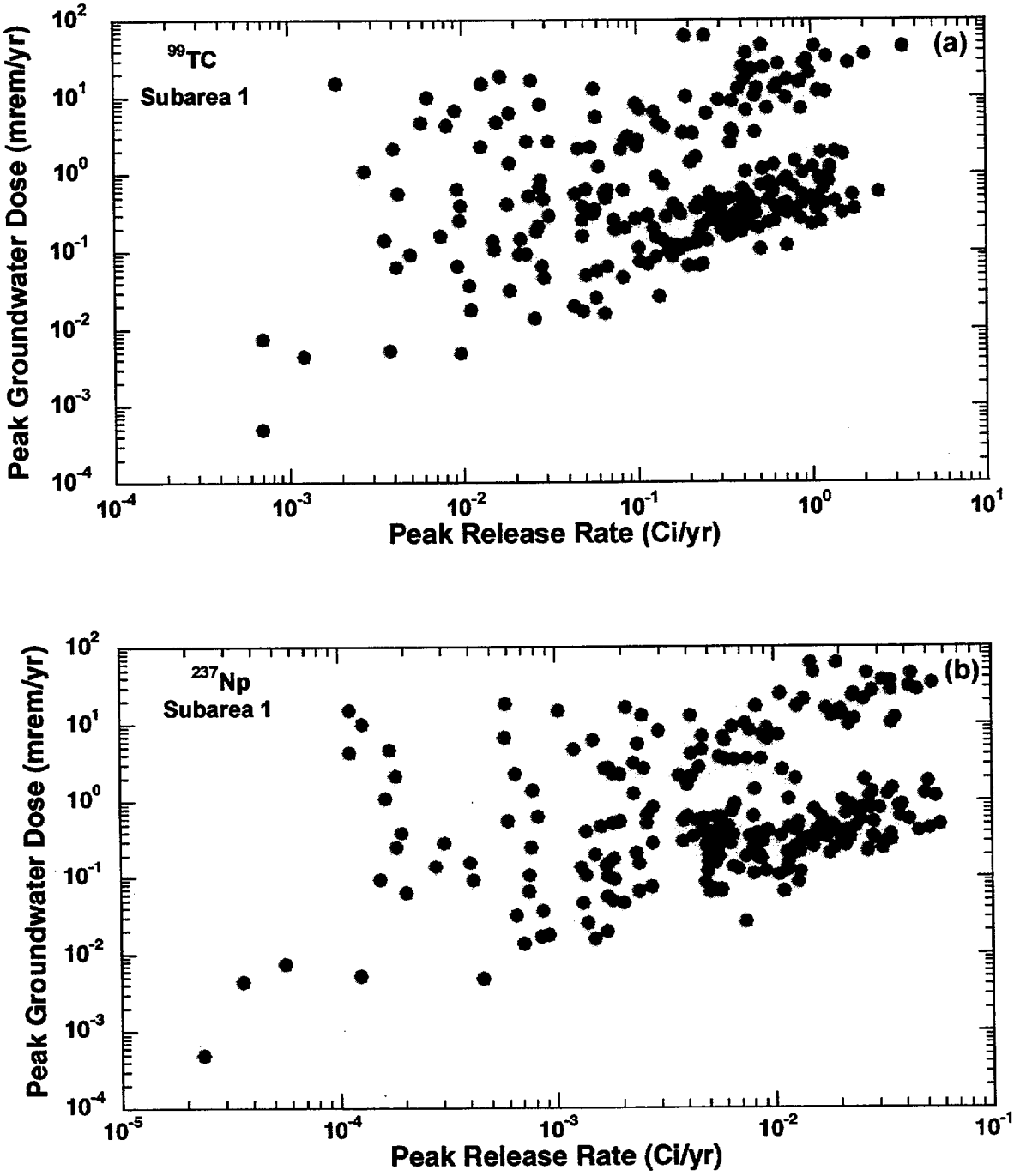

Figure 3-27. Peak groundwater dose, and the: (a) ^{99}Tc, and (b) ^{237}Np, peak release rates from subarea 1, for 250 realizations.

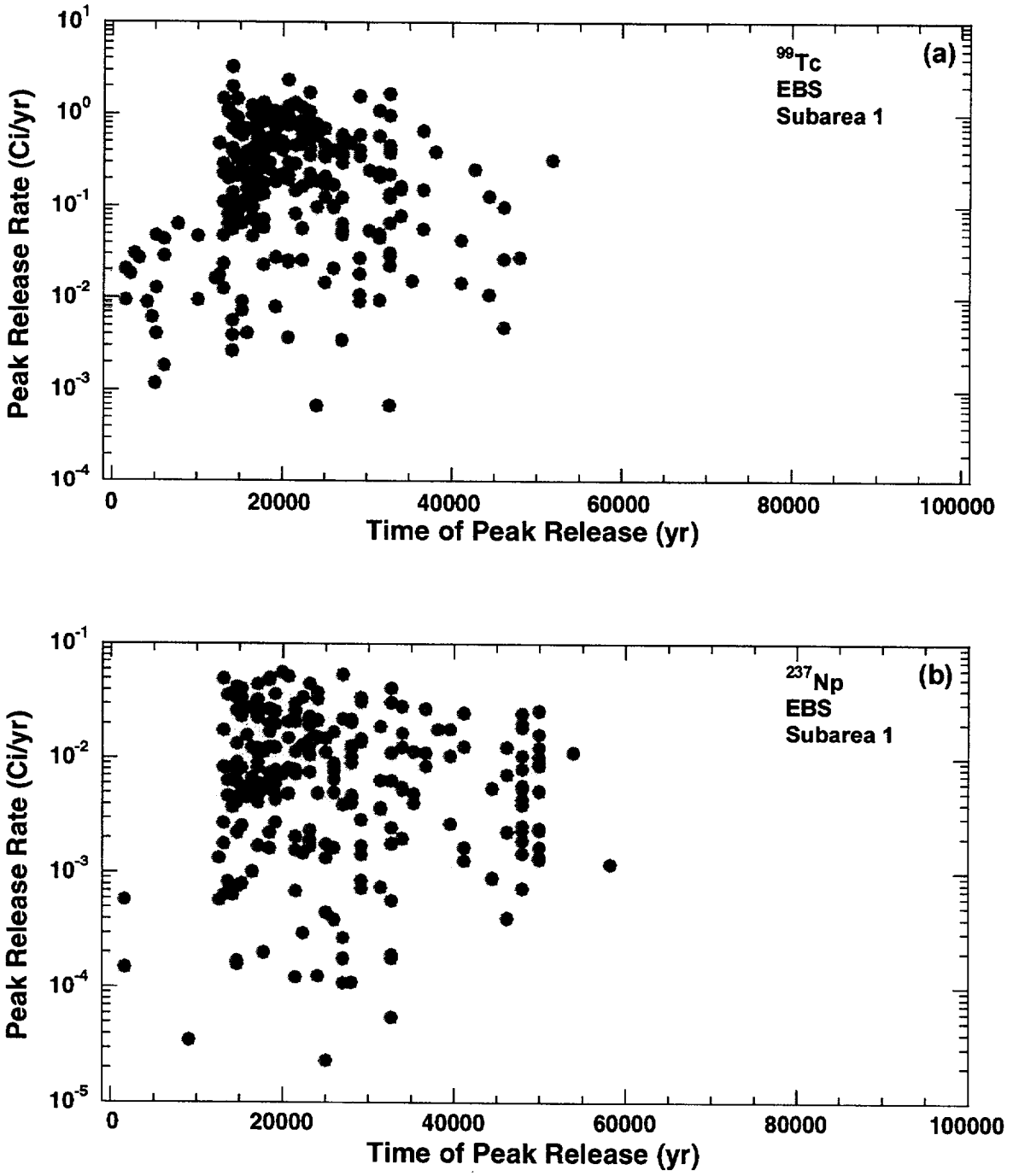

Figure 3-28. Peak release rates from the EBS and time of the peak release for: (a) ^{99} Tc, and (b) ^{237}Np, in 250 realizations.

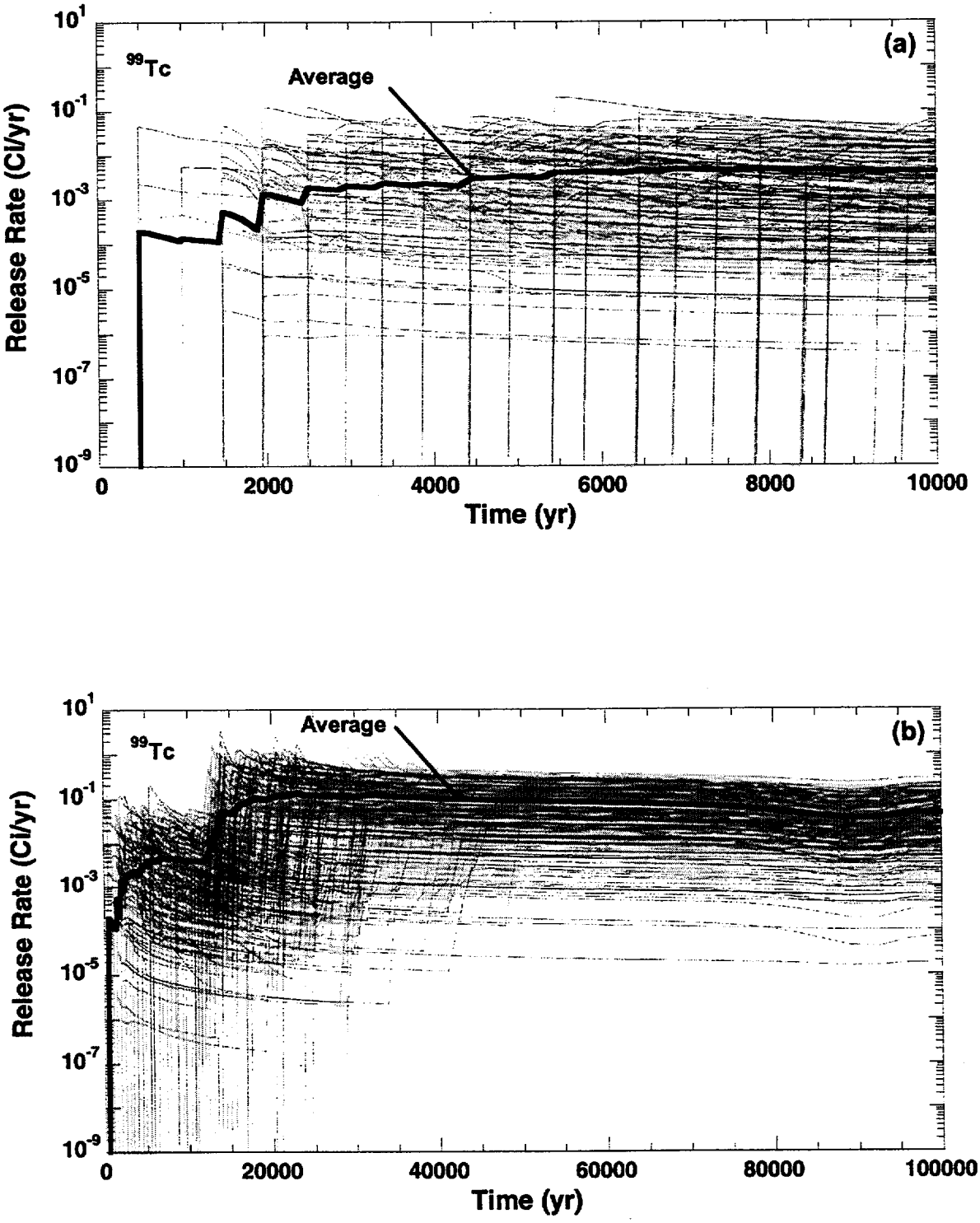

Figure 3-29. ^{99} Tc release rates from the EBS over: (a) 10,000, and (b) 100,000 yr, including the average release rate, in subarea 1, for 250 realizations.

3.3.5 UZ Transport

Figure 3-31 presents ^{99}Tc, ^{237}Np, and ^{239}Pu average release rates for the basecase data set. In the first 10,000 yr, releases are from initial WP failures. The failure of WPs from corrosion begins after 10,000 yr and an increase in the release rates is evident in Figure 3-31, from 10,000 to 20,000 yr, with the peak average release rate for 250 realizations occurring at approximately 20,000 yr.

The results in Figure 3-30 indicate that the UZ releases are only slightly less than the EBS releases and suggest that the effects of the hydrostratigraphic units beneath the repository on the radionuclide release rates are not significant.

Figure 3-32 provides the ^{99}Tc release rate from the UZ, for subarea 1, from 10,000 and 100,000 yr. When compared with the EBS release rates in Figure 3-29, these results demonstrate that the movement of ^{99}Tc through the UZ is not significantly different. As with the EBS, releases from the UZ before 10,000 yr are from initially defective and seismic failures, whereas the peak releases observed after 10,000 yr result mainly from corrosion failures. The magnitude of the releases extends over 4 to 5 orders of magnitude and arises partly from the variability in the flow rate into the EBS.

The conclusion that the UZ has a small effect on the EBS release rates is further supported by the results for the relatively short UZ GWTTs shown in Figure 3-33. The average UZ travel time is about 530 yr with a range 200–1200 yr, which is small, compared with the 10,000- and 100,000-yr TPIs. Differences in the travel times arise from distributions specified in the basecase data set for the porosities of the hydrostratigraphic units below the repository and for the climate conditions used to determine the UZ flow rates.

3.3.6 SZ Flow and Transport

Release rates from the SZ are presented in Figure 3-34 for ^{99}Tc, ^{237}Np, and ^{239}Pu. The ^{99}Tc, ^{237}Np, and ^{239}Pu UZ and SZ release rates can be significantly different because of the flow path length and retardation in the SZ alluvium. The path length thickness in the SZ alluvium ranges from 8000 to 12,000 m, whereas the UZ path length is about 300 m (984 ft). Saturated zone retardation occurs in the alluvium. For UZ retardation to occur, flow needs to be in the matrix. Because UZ flow is mainly in fractures, UZ retardation has little effect on delaying radionuclide transport. Additionally, the average retardation factors for Tc, Np, and Pu are 1, 9, and 10,000 in the UZ matrix; and 5, 62, and 13,000 in the SZ alluvium, respectively. Consequently, the longer flow path, combined with greater retardation, has a larger effect on the SZ release rates than on the UZ release rates. These effects are apparent in the UZ and SZ release rates plotted in Figures 3-31 and 3-34. Compared with the releases from the UZ, ^{99}Tc and ^{237}Np releases are smaller from the SZ and, because of a larger retardation factor, there is no Pu released from the SZ in 100,000 yr.

The effect of retardation and of the flow path length, on the ^{99}Tc SZ release rates for subarea 1, from 10,000 and 100,000 yr, is evident, when comparing Figure 3-35 with the UZ release rates in Figure 3-32. Higher retardation factors increase the SZ travel time and shift the release rate to the right (i.e., later time).

The average GWTT in the SZ is approximately 3680 yr, compared with about 500 yr for the UZ (see Figure 3-33). For each subarea, the minimum travel times vary from 2130 to 4730 yr, whereas the maximum travel times range from 3320 to 7240 yr. Table 3-12 provides a summary of the average, minimum, and

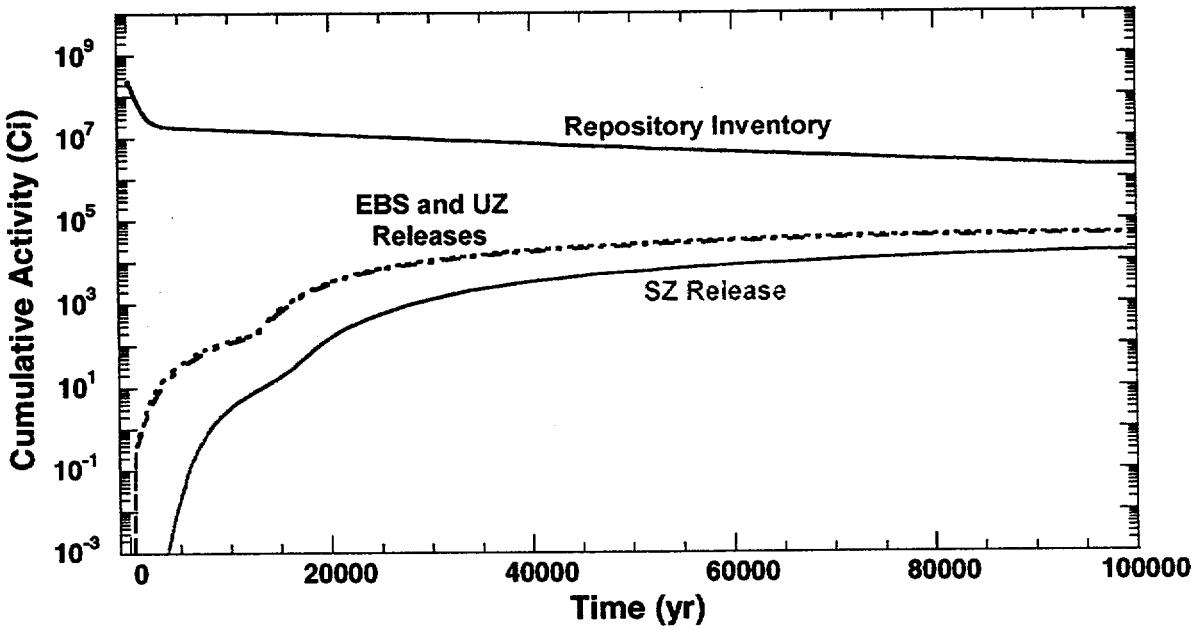

Figure 3-30. Cumulative releases from the EBS, the UZ, and the SZ, together with the initial inventory in the repository.

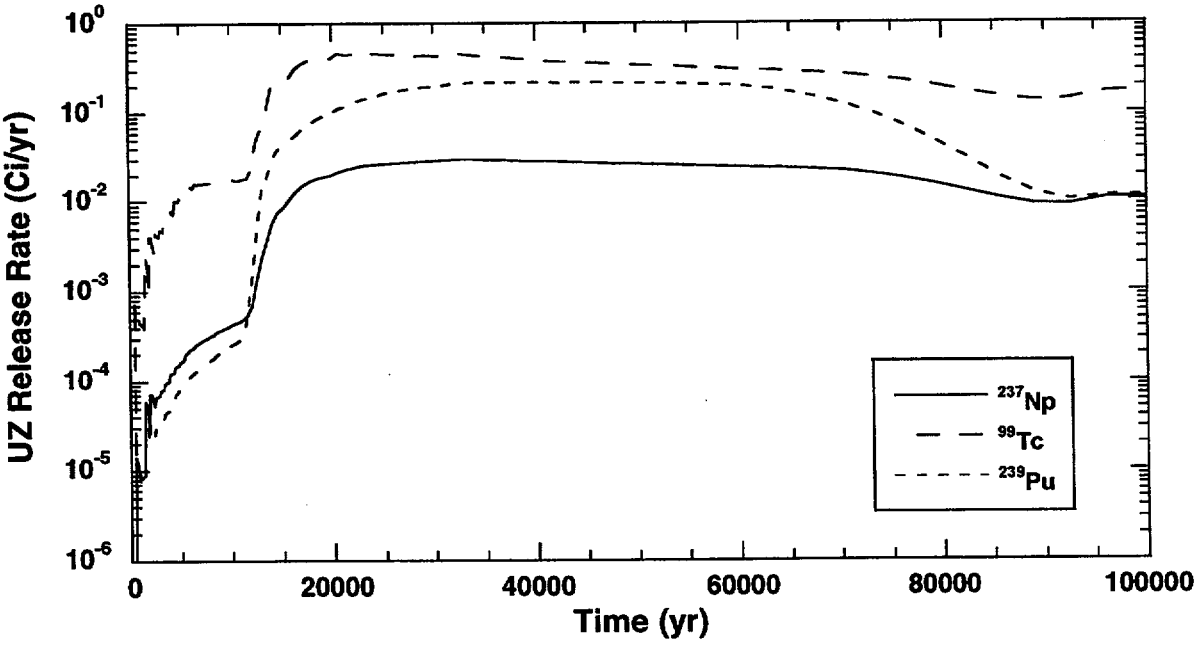

Figure 3-31. UZ average release rates of ^{99}Tc, ^{237}Np, and ^{239}Pu, for 250 realizations.

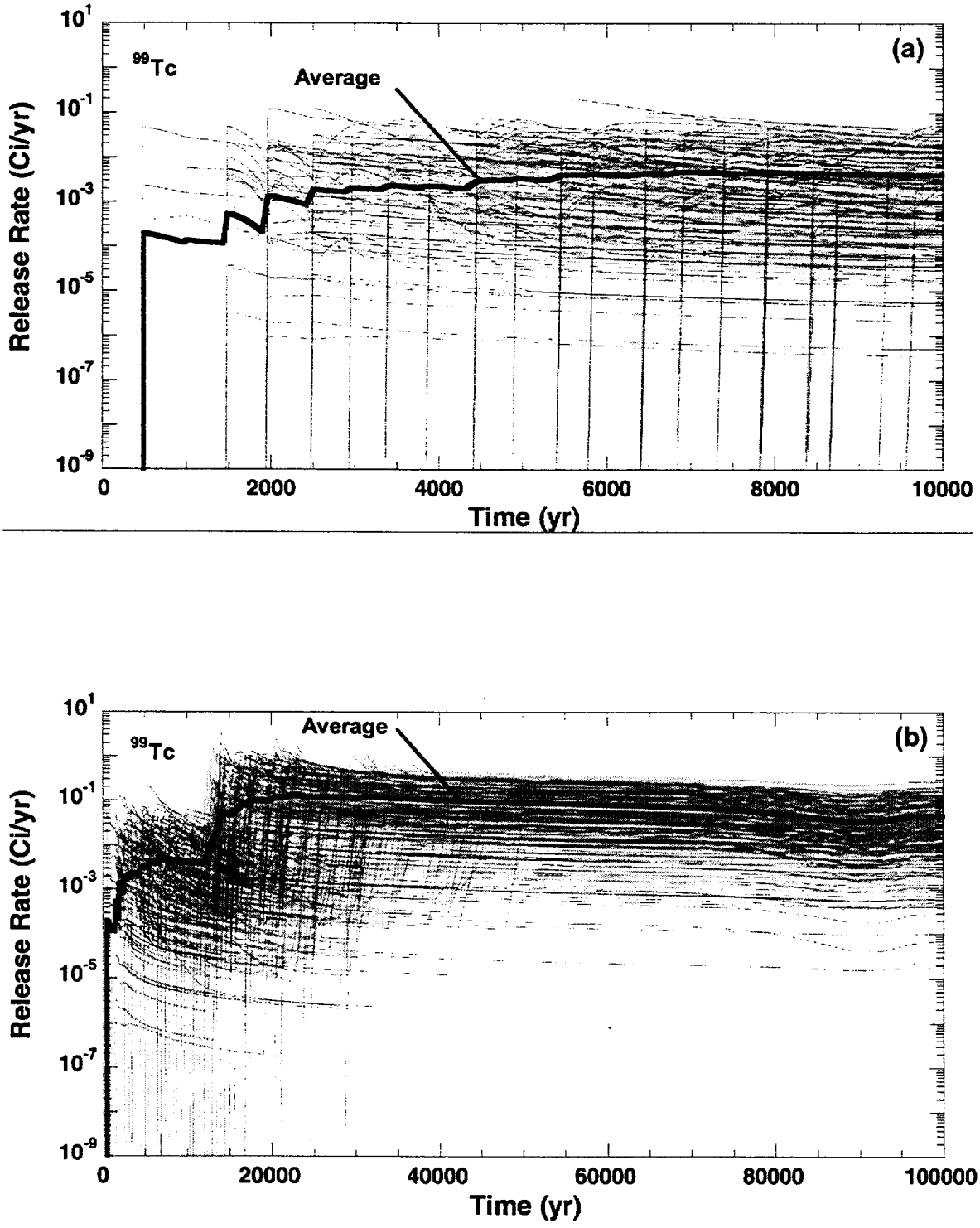

Figure 3-32. UZ release rates of ^{99}Tc over: (a) 10,000, and (b) 100,000 yr, including the average release rate, in subarea 1, for 250 realizations.

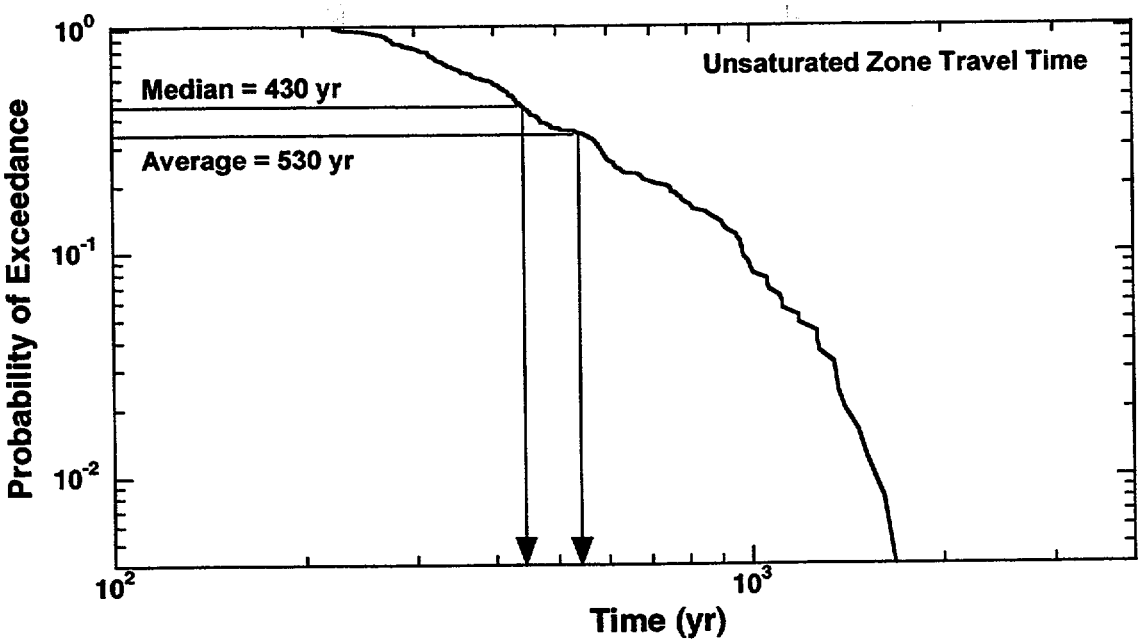

Figure 3-33. CCDF function of UZ groundwater travel times, for 250 realizations.

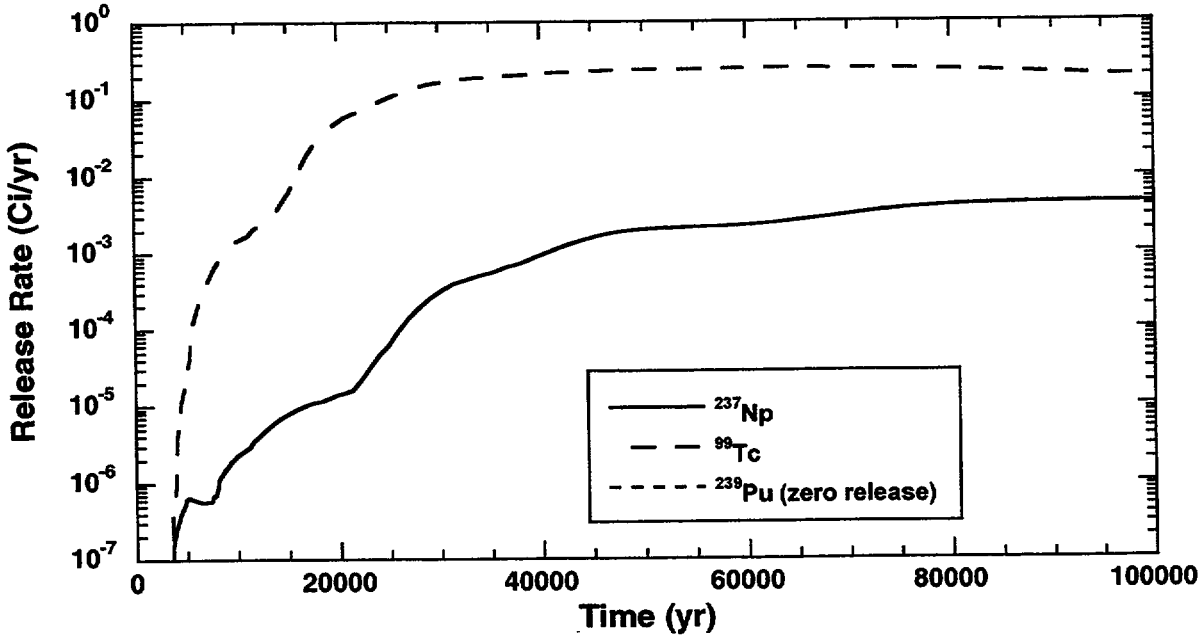

Figure 3-34. SZ average release rates of ^{99}Tc, ^{237}Np, and ^{239}Pu, for 250 realizations.

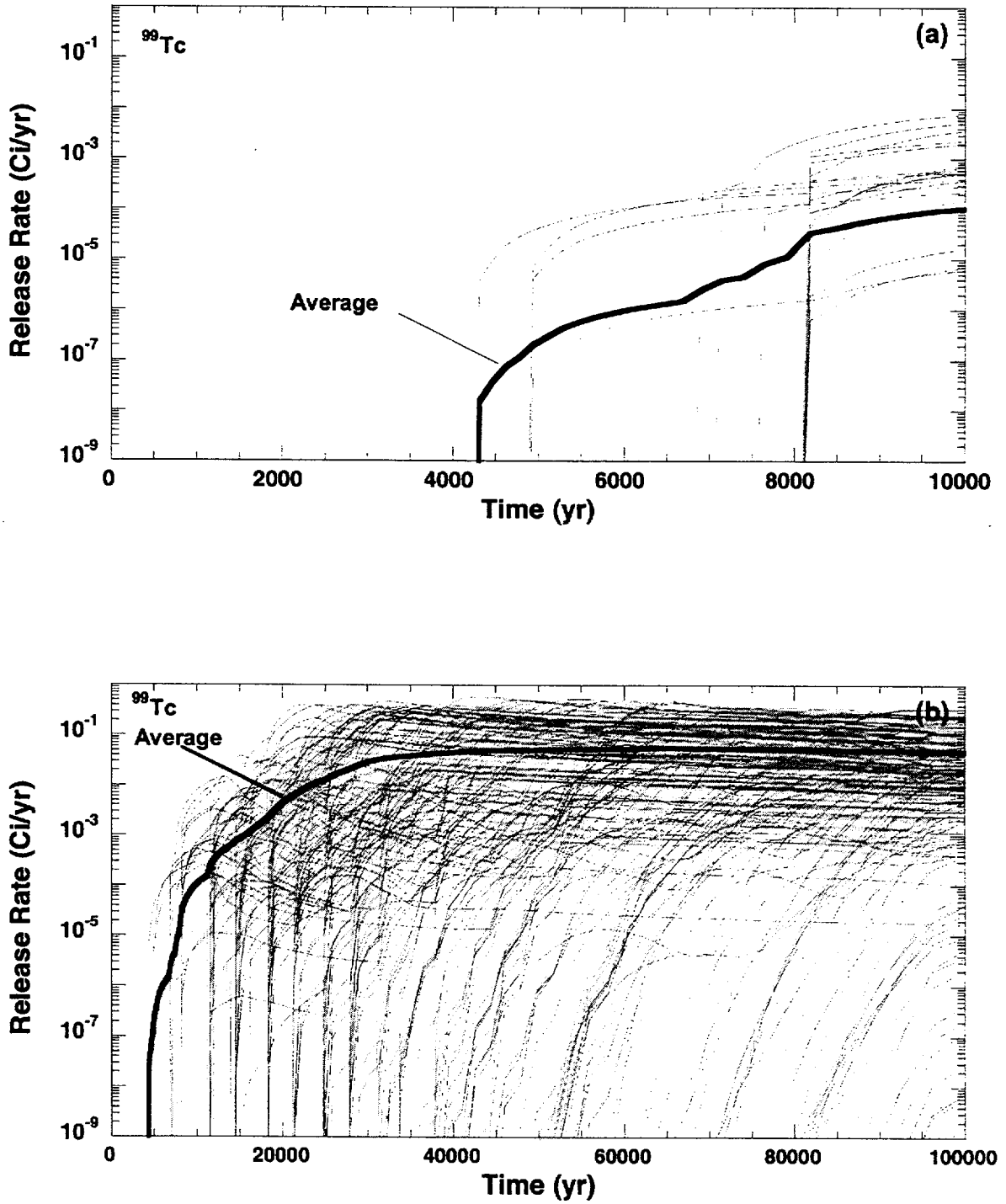

Figure 3-35. SZ release rates of ^{99}Tc over: (a) 10,000; and (b) 100,000 yr, including the average release rate, in subarea 1, for 250 realizations.

Table 3-12. Average, maximum, and minimum SZ groundwater travel times, by subarea and average, for all subareas, from 250 realizations

	SZ Travel Time (yr)		
Subarea	**Minimum**	**Maximum**	**Average**
1	4730	7240	5990
2	4730	7240	5980
3	2130	3330	2730
4	2130	3320	2720
5	2180	3380	2720
6	2180	3380	2780
7	2180	3370	2770
Average (all subareas)	2890	4460	3680

maximum SZ GWTTs for the repository and for each subarea. The average for each subarea is obtained using equal weighting of GWTTs from each realization. Similarly, the repository average for all subareas is the mean of subarea averages.

The variability in the SZ travel times is approximately the same order of magnitude as for the UZ. The repository averaged SZ GWTTs range from about 2700 to 6000 yr; for the UZ, GWTTs vary from 200 to 1200 yr. A CCDF of the SZ GWTTs for all 250 realizations is presented in Figure 3-36. For comparison, a CCDF of the UZ travel times can be found in Figure 3-33.

3.4 COMPARISON OF DOSES FROM MEAN VALUE DATA SET AND MULTIPLE-REALIZATION CASES

To illustrate the difference between results from a mean value data set and results from multiple realizations, the peak expected dose is computed as a function of time from the multiple realizations. The peak dose from the mean-value data set is 2×10^{-5} mSv/yr (0.002 mrem/yr), whereas the peak expected dose from the multiple-realization case is 3×10^{-5} mSv/yr (0.003 mrem/yr) for the 10,000-yr TPI. For the 100,000-yr TPI, the peak dose from the mean value data set is 3×10^{-3} mSv/yr (0.3 mrem/yr) compared with 4×10^{-2} mSv/yr (4 mrem/yr) peak expected dose for the multiple-realization case. For comparison purposes, the primary nuclides contributing to peak dose are presented in Table 3-13.

The major contributors to the peak dose from table 3-13 in the mean value data set for 10,000 yr are ^{129}I and ^{36}Cl; for the multiple-realization case, they are ^{237}Np, ^{129}I, ^{99}Tc, and ^{234}U. For the 100,000-yr TPI, the major contributors to the peak dose in the mean value data set are ^{99}Tc, ^{129}I, and ^{79}Se, compared with ^{237}Np, ^{234}U, and ^{99}Tc, for the multiple-realization case. Thus, some radionuclides that are major contributors to peak dose could not be accounted for by the use of the mean value data set. This clearly indicates the inadequacy of the analysis using the mean value data set. However, as indicated before, the mean value data set provides a convenient means for observing deterministic trends in the intermediate outputs.

The variability in dose within realizations is shown in Figure 3-20, for 10,000 and 100,000 yr, together with the average dose. The minimum and maximum peak doses vary over 5 orders of magnitude,

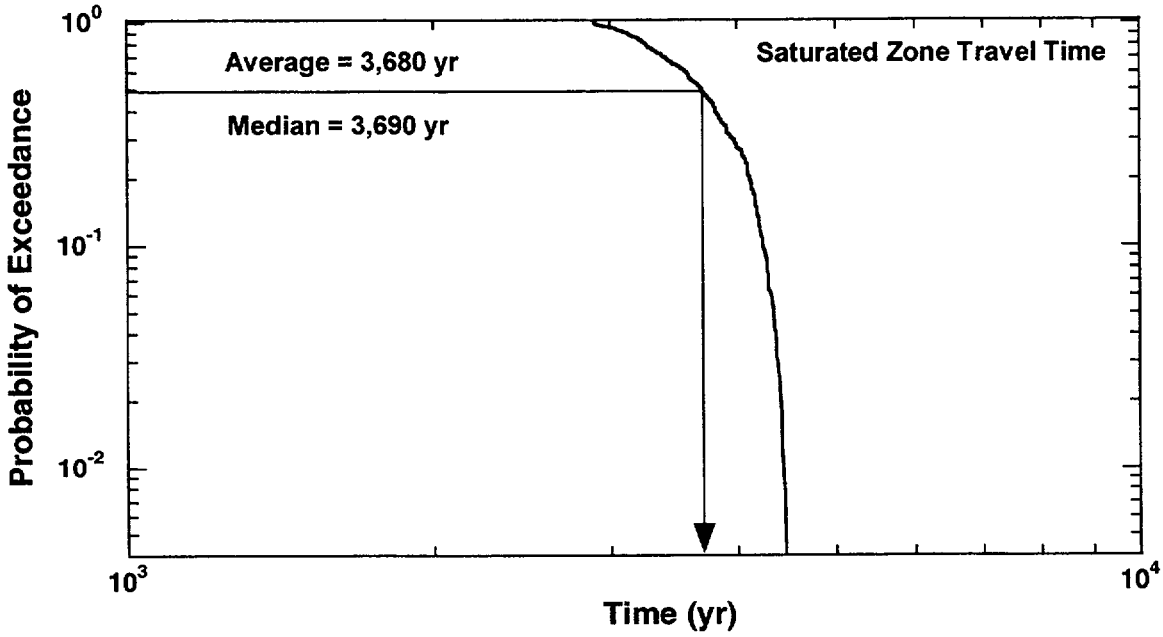

Figure 3-36. CCDF of UZ GWTTs, for 250 realizations.

Table 3-13. Primary radionuclides contributing to peak expected dose

	10,000 yr		100,000 yr	
Radionuclide	**Mean Value Data Set**	**Multiple-Realization Data Set**	**Mean Value Data Set**	**Multiple-Realization Data Set**
^{237}Np	0	0.389	0	0.924
^{129}I	0.95	0.349	0.38	0.015
^{99}Tc	0.0002	0.138	0.59	0.022
^{234}U	0	0.1	0	0.035
^{36}Cl	0.05	0.014	0.004	0
^{79}Se	0	0.010	0.03	0

from about 4×10^{-9} to 0.003 mSv/yr (4×10^{-7} to 0.3 mrem/yr), for 10,000 yr, and 2×10^{-6} to 0.5 mSv/yr (2×10^{-4} to 50 mrem/yr), for 100,000 yr. The doses occurring before 10,000 yr are from initially defective and seismic failures of WPs. From 11,000 to 46,000 yr, corrosion failures occur and contribute to increased dose. At about 85,000 yr, a slight increase in dose is observed, attributable to the arrival of ^{237}Np, and switching from DCFs, associated with the pluvial climate, to a present-day climate.

Figure 3-37 shows the variation in peak dose and the arrival time of the peak dose at the pumping well, for ^{99}Tc and ^{237}Np. For more than one-half the realizations, the ^{99}Tc peak dose does not arrive until after 90,000 yr, whereas the ^{237}Np peak dose does not occur for most realizations until the end of the 100,000-yr TPI. The difference in results arises because ^{99}Tc retardation factors are less than those for ^{237}Np. Although the peak dose is not captured in all realizations, a maximum simulation time of 100,000 yr is long enough to evaluate the peak dose for the 10,000-yr TPI and a significant time period thereafter.

The groundwater dose expressed as a percent of total dose for the radionuclides ^{245}Cm, ^{241}Am, ^{237}Np, ^{239}Pu, ^{234}U, ^{230}Th, ^{129}I, ^{99}Tc, ^{14}C, ^{79}Se, and ^{36}Cl is illustrated in Figure 3-38, for all 250 realizations. The radionuclides ^{237}Np, ^{234}U, ^{230}Th, ^{129}I, ^{99}Tc, ^{79}Se, and ^{36}Cl contribute at least 1 percent to the groundwater dose for any single realization. The radionuclides with the greatest consistency in contributing to peak dose in all realizations are ^{237}Np, followed by ^{129}I and ^{99}Tc. The results plotted in Figure 3-39, of the expected dose for each nuclide, show similar behavior over the 10,000- and 100,000-yr TPI, as does Figure 3-38, with the same nuclides having the largest contribution to the groundwater dose.

The volume of well water pumped, which is used as the dilution volume for the 20-km receptor group location, is assigned a uniform distribution ranging from 6.2×10^6 to 1.8×10^7 m^3/yr (2.2×10^7 to 6.3×10^8 ft^3/yr. Figure 3-40 illustrates the relationship between the peak groundwater dose to the receptor in 100,000 yr and the dilution volume for 250 realizations. The scatterplot reveals a slight trend of decreasing peak groundwater dose with dilution volume. The mass release rates from the SZ are converted into a groundwater dose by dividing the mass release rate by the dilution volume and multiplying by the DCF. Consequently, higher dilution volumes should be associated with lower groundwater dose.

3.5 ALTERNATIVE CONCEPTUAL MODELS

This section compares repository performance, as measured by dose, for the mean value data set, with doses computed from mean values for alternative conceptual models described in Section 2.3. The alternative models include different conceptualizations for fuel dissolution, fuel wetting, and transport. Only the general trends in the groundwater dose of the alternative models relative to the basecase are described in this section. Discussion of the sensitivity of TPA output to a conceptual model, using multiple realizations, is provided in Section 4.4.

Sensitivity of repository performance to the basecase model abstractions was evaluated by performing TPA simulations using alternative conceptual models. Conceptual models can either be activated with flags in the TPA input file, or a conceptual model may be evaluated by modifying TPA input parameters. Both approaches are used in this section to specify a conceptual model and to analyze the influences of the conceptual model on groundwater dose. Conceptual models activated with flags in the TPA input file include the four dissolution rate models, the bathtub and flowthrough models, bypassing invert transport, and the particle and grain surface-area models. Parameter values in the TPA input file are modified to evaluate conceptual models for focused flow, matrix diffusion, no retardation, and cladding protection.

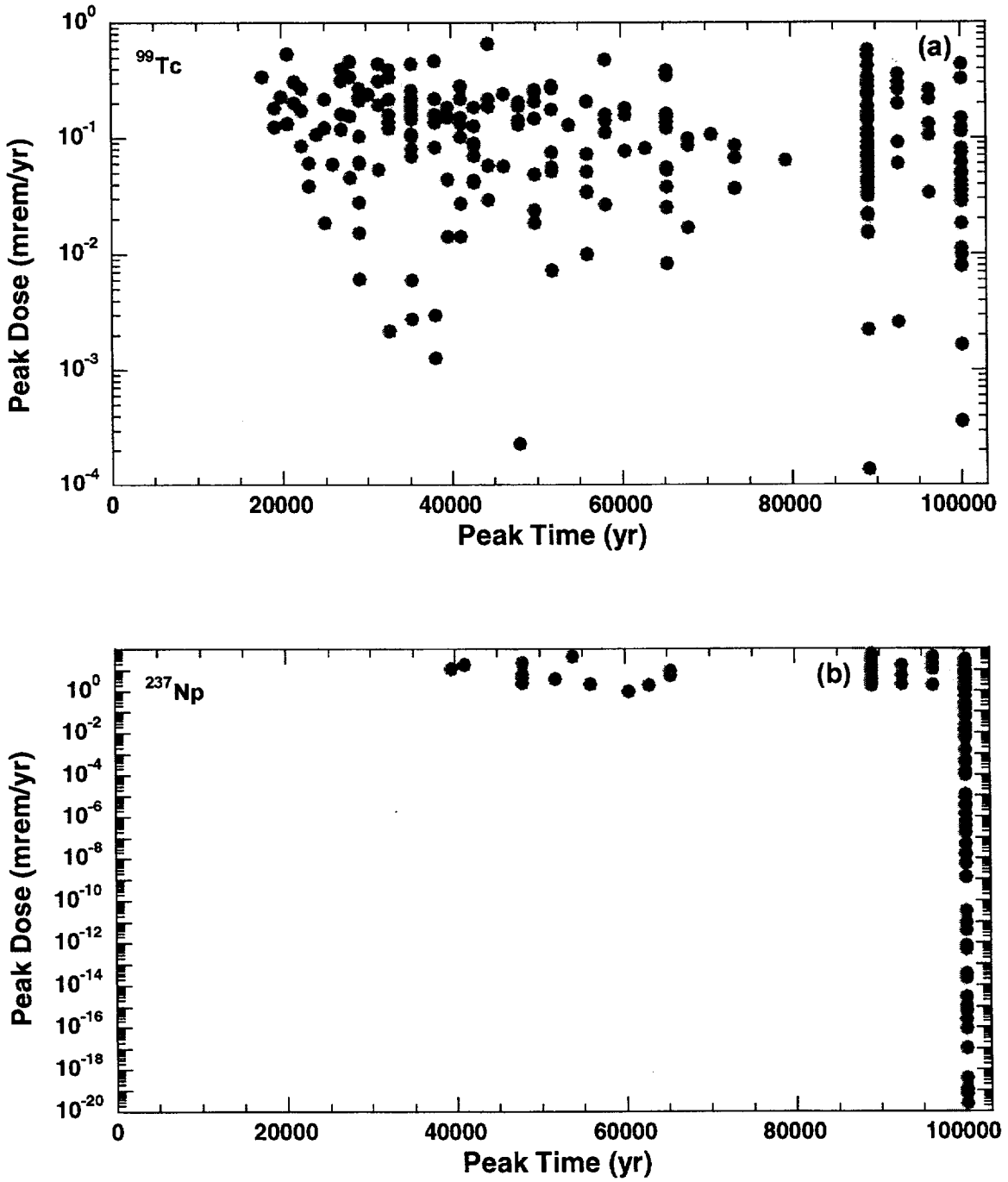

Figure 3-37. Peak groundwater dose of: (a) ^{99}Tc; and (b) ^{237}Np; and time of the peak dose, for 250 realizations.

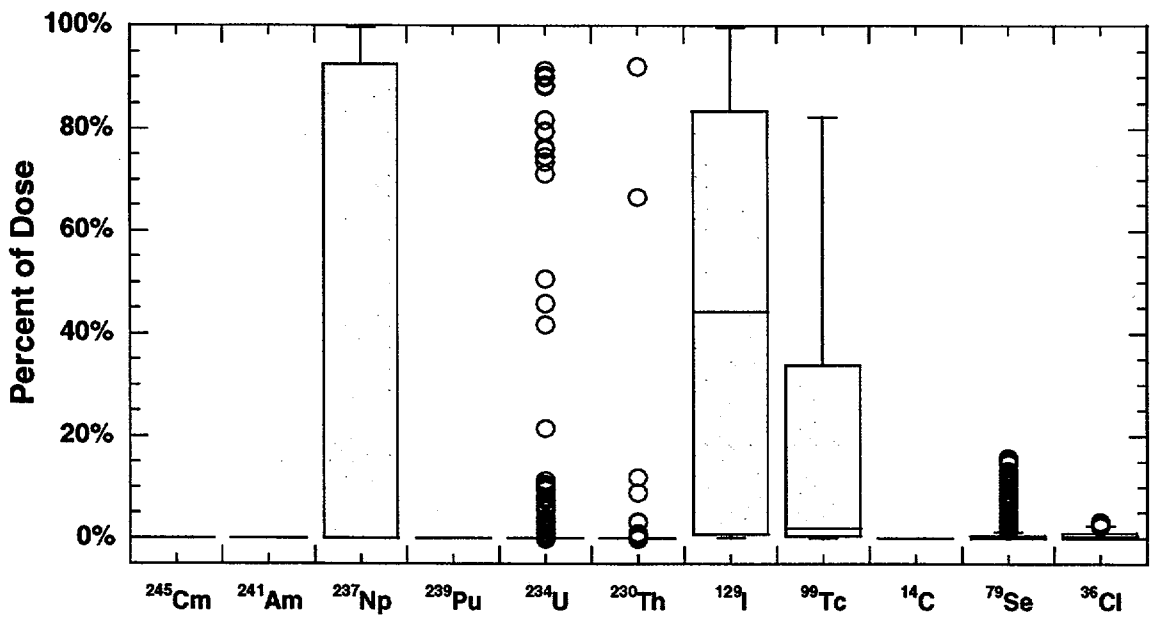

Figure 3-38. Percent each radionuclide contributes to the peak groundwater dose, for 250 realizations.

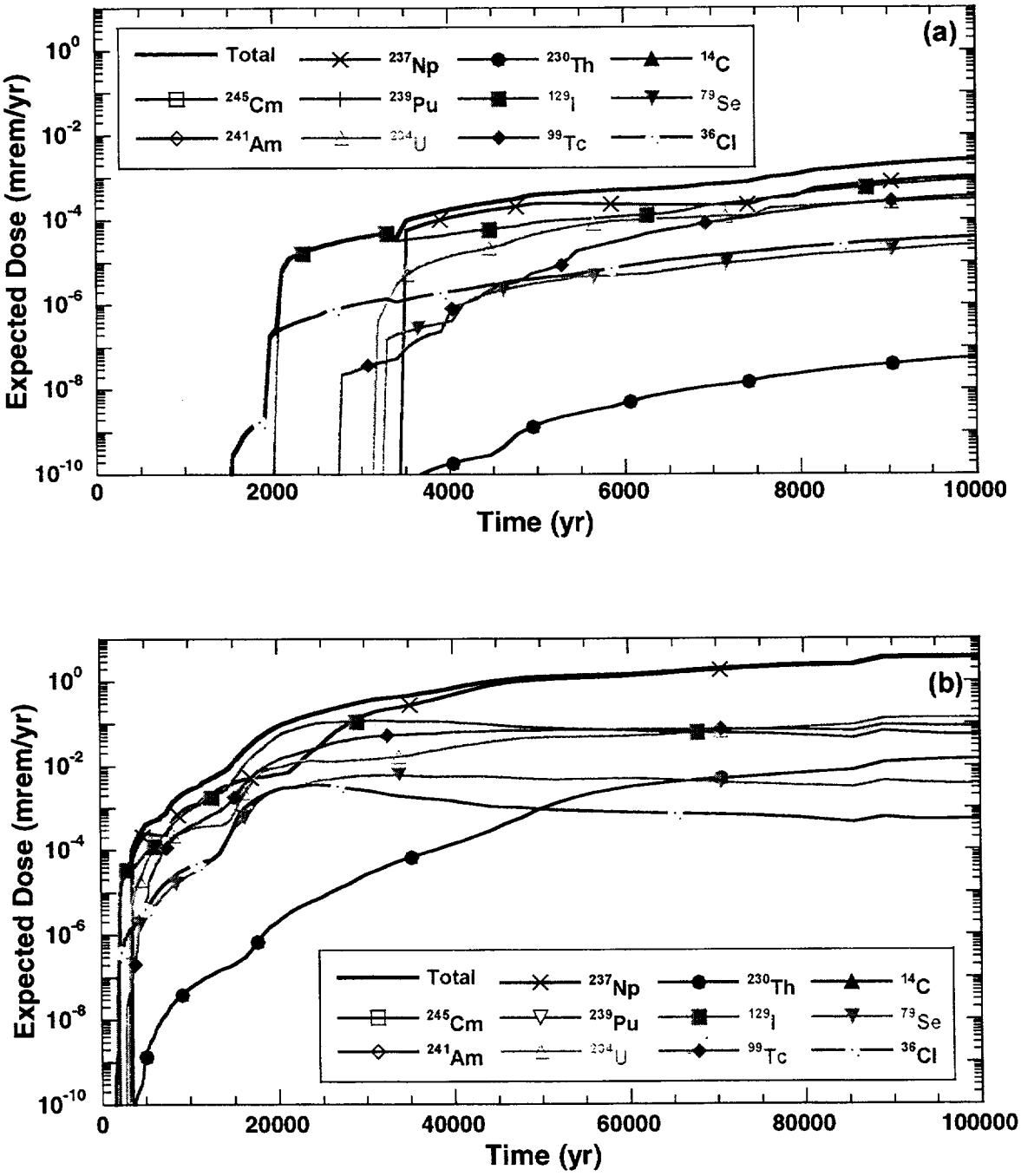

Figure 3-39. Average groundwater dose in: (a) 10,000, and (b) 100,000 yr, for each nuclide, including the total dose, for 250 realizations.

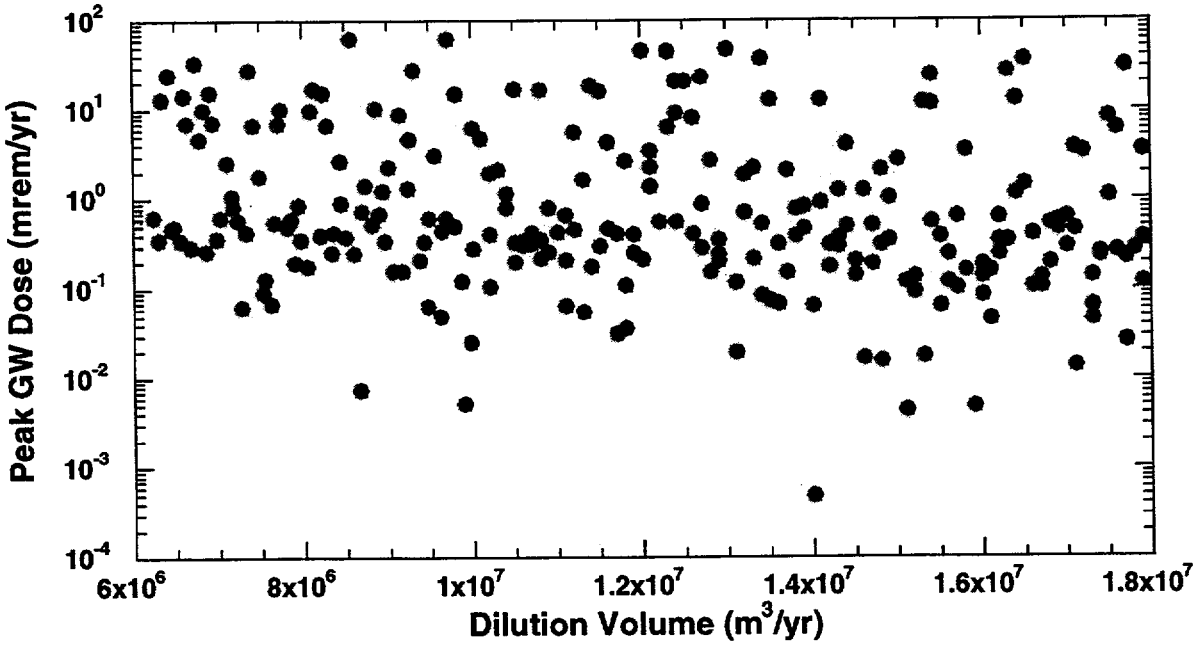

Figure 3-40. Peak groundwater dose and the volume of well water pumped, for 250 realizations. (The well water dilutes the plume of radionuclides traveling in the SZ.)

Figures 3-41 through 3-43 present groundwater dose in 10,000 and 100,000 yr for the basecase mean value data set, together with groundwater doses from the TPA alternative conceptual models. For the conceptual models evaluated using the mean value data set, repository performance spans almost 7 orders of magnitude for the 100,000-yr TPI and encompasses the basecase dose. The general trend in groundwater dose exhibited in Figures 3-41 through 3-43 indicates a wide range in the sensitivity of groundwater dose to the conceptual model. The alternative models with the most deviation from the basecase dose are the no retardation case, which is more than 2 orders of magnitude greater than the basecase, and the Schoepite and Clad-M1 cases, which are 3 to 4 orders of magnitude less than the basecase dose, through most of the 100,000-yr TPI. The following sections discuss the alternative conceptual models grouped by fuel dissolution, fuel wetting, and transport assumptions, and compare the groundwater dose with the basecase groundwater dose, computed with mean values. The TPA Version 3.2 code "User's Guide" (Mohanty and McCartin, 1998) presents a description of these models.

3.5.1 Fuel-Dissolution Models

Results from TPA simulations, using three different fuel-dissolution models, are evaluated by comparing the groundwater dose from each of the models with the basecase groundwater doses. The groundwater doses from the basecase, and from the fuel-dissolution, three-alternative conceptual models, are presented in Figure 3-41.

3.5.1.1 Fuel-Dissolution Model 1

The groundwater doses in Figure 3-41 (labeled as Model1) indicate an earlier release and higher dose through about 60,000 yrs. From 60,000 to 100,000 years, the basecase dose is greater than that calculated with fuel-dissolution model1. At the end of the 100,000-yr TPI, the dose from the first fuel-dissolution-rate model is more than two orders of magnitude less than the basecase dose (Model 2 used). Dissolution Model 1 is characterized by a higher release rate resulting from faster dissolution, compared with Model 2. But faster dissolution (congruent) results in faster source depletion from the WP for the dissolution-limited radionuclides. Consequently, the release rate for Model 1 becomes less than that for Model 2 at longer times. The dose for this conceptual model follows a sinusoidal pattern, after 20,000 yr, attributable to variations in the transport of nuclides to the receptor location not only by nuclide but by subarea. This effect is not evident in the basecase dose, and further studies are underway to explain this behavior.

3.5.1.2 Fuel-Dissolution Model 3 (Natural Analog)

The groundwater doses in Figure 3-41 (labeled as Natan), which are the same as the results from the schoepite dissolution model, show a slightly later release, with lower doses, throughout the 100,000-yr TPI, than the basecase dose, indicating a slower dissolution rate. Just as with the first fuel-dissolution-rate model, which exhibits a release rate that peaks and drops quickly, the dose for this conceptual model follows a sinusoidal pattern after 20,000 yr, attributable to differences in the transport of nuclides to the receptor location not only by nuclide, but by subarea. The variations in dose for this dissolution model are smaller compared with the first model, but greater, compared with Model 2. Further studies are under way to explain this behavior.

3.5.1.3 Fuel-Dissolution Model 4 (Schoepite Dissolution)

The groundwater doses in Figure 3-41 (labeled as Schoepite) indicate a slightly later release with lower doses throughout the 100,000-yr TPI. Just as with the first and natural analog fuel-dissolution-rate models, the dose for this conceptual model follows a similar sinusoidal pattern after 20,000 yr, attributable to differences in the transport of nuclides to the receptor location not only by nuclide, but by subarea. However, the variations in dose are similar for this dissolution model and the first model, although the groundwater dose at 100,000 yr is more than 3 orders of magnitude less than the basecase dose. Justification for the trend in the curve is similar to that of the natural analog model. Further studies are under way to explain the trend.

3.5.2 Fuel-Wetting Assumptions

The amount of water contacting a WP affects the EBS release rate and the time of the release. This section presents results that investigate the assumptions for fuel wetting with five alternative conceptual models. The groundwater doses computed using these models and the basecase results are provided in Figure 3-42.

3.5.2.1 Flowthrough Model with Fuel-Dissolution Model 2

The groundwater doses in Figure 3-42 (labeled as Flwthru-2) have an earlier release and higher dose than the basecase dose from the beginning of the simulation, through about 20,000 yr. An earlier dose is expected because in the flowthrough model, release from the WP occurs instantaneously (i.e., no time to fill WP). From about 20,000 to 40,000 yr, the basecase dose is greater than the dose computed with this conceptual model. Beyond 40,000 yr, the groundwater doses are almost equal. One of the reasons these two doses are almost equal is that at high flow rates into the WP, the flowthrough model behaves like the bathtub model once the bathtub is full.

3.5.2.2 Flowthrough Model with Fuel-Dissolution Model 1

Groundwater doses in Figure 3-42 (labeled as Flwthru-1) indicate an earlier release and higher dose from the beginning of the simulation through about 60,000 yr, while from about 60,000 to 100,000 yr, the basecase dose is greater than the dose computed with the flowthrough model. This behavior is consistent with the faster dissolution rate and source depletion associated with Model 1. At 100,000 yr, the basecase dose is about 3 orders of magnitude greater than the flowthrough model dose. The greatest difference between these plots is the behavior of the doses over time. The basecase dose exhibits a smoother behavior than the flowthrough model dose, which shows a sinusoidal pattern caused by the arrival of different nuclides and releases from different subareas at the receptor location.

3.5.2.3 Focused Flow

As presented in Figure 3-42, the groundwater doses (labeled as Focflow) computed using a focused flow of water onto the WP are greater than the basecase dose, before about 7000 yr, indicating an earlier release. The groundwater doses are approximately 1 order of magnitude less than the basecase dose, from about 7000 to 100,000 yr. These results are consistent with solubility limited releases associated with higher flows at earlier times and lower doses thereafter, attributable to fewer wet WPs.

3.5.2.4 Cladding Credit with Model 1

The groundwater doses in Figure 3-42 (labeled as Clad-M1) calculated for this conceptual model are less than the groundwater doses for the basecase, from about 5000 yr, to the end of the 100,000-yr TPI. Before 5000 yr, the dose with cladding protection is greater than the basecase dose. During the 5000–100,000-yr period, the general trends in the dose computed with cladding protection follow a sinusoidal pattern that is attributable to subarea and nuclide variability. The groundwater dose for this alternative conceptual model is about 6 orders of magnitude less than the basecase dose, at 100,000 yr.

3.5.2.5 Grain-Size Model with Fuel Dissolution Model 1

Groundwater doses in Figure 3-42 (labeled as Grain1) are characterized by an earlier release and higher dose than the basecase dose, from the beginning of the simulation through about 60,000 yr. The high dose results from a high dissolution rate, the result of a larger surface area associated with the grain-base model, in which grain size as opposed to the particle size is used for determining the surface area over which water contacts SF. From about 60,000 to 100,000 yr, the source becomes depleted and the basecase dose is greater than the dose computed using the grain-based surface area model. At the end of the 100,000-yr TPI, the dose is more than 3 orders of magnitude less than the basecase dose. The sinusoidal behavior of the dose is attributable to the arrival of different nuclides and releases from different subareas at the receptor location.

3.5.3 Transport Alternatives

The three alternative conceptual models that investigate assumptions of transport in the EBS, UZ, and SZ are assessed in this section. Figure 3-43 presents the groundwater doses for these conceptual models and the basecase dose.

3.5.3.1 No Retardation of Pu, Am, and Th

As presented in Figure 3-43, the groundwater doses (labeled as NoRet) calculated assuming no retardation in the UZ and SZ are greater than the basecase dose for the entire 100,000-yr TPI. Moreover, the general characteristics of the groundwater doses are consistent with the dose with no retardation, and approximately 2 orders of magnitude greater than the basecase dose.

3.5.3.2 No-Invert Model

Using the basecase mean value data set, flow through the invert is greater than the concrete permeability, and fracture flow does occur. Thus, the invert does not affect the radionuclide release rates from the EBS. Consequently, the basecase doses and the doses computed when bypassing the invert transport computations using the TPA input file flag are the same.

3.5.3.3 Matrix Diffusion

The groundwater doses presented in Figure 3-43 (labeled Matdif) with matrix diffusion are less than the basecase doses, from the beginning of the simulation time to about 25,000 yr, because of the retention of radionuclides in the matrix lateral to the fracture transport path. From approximately 25,000 to 60,000 yr, the dose exhibits a sinusoidal behavior that appears to be attributable to subarea variations in the arrival time

of nuclides, at the receptor location, that are not present in the basecase groundwater dose. Further investigation is underway to explain this behavior. After 60,000 yr, the groundwater dose computed with matrix diffusion increases, and at 100,000 yr, is almost 1 order of magnitude greater than the basecase groundwater dose. The increase in dose is caused by the increase in the release rate presumably resulting from the reversal in the diffusion (matrix to fracture). The increasing doses from the matrix diffusion case are nonintuitive, and may be caused by the way the NEFTRAN flow legs are specified in the basecase and alternative models. For the basecase model, the saturated flow pathway is specified as a "composite" flow leg, for which a single equivalent medium represents several hydrogeologic media in series. NEFTRAN does not allow this feature when the matrix diffusion option is stipulated. Although average travel times are the same for both models, the treatment of dispersion is different.

3.6 DISRUPTIVE EVENTS

The TPA results from faulting and igneous activity are presented in this section for single and multiple realizations. The groundwater doses for the disruptive events and the ground-surface doses from igneous activity are compared with doses computed using the basecase data set.

3.6.1 Single-Realization Analysis of Disruptive Events

To determine the number of WPs ruptured by seismically induced rockfalls, which is part of the basecase, the time evolution of seismicity that includes the number, time, and magnitude of seismic events is obtained using the seismic hazard curve presented in Figure 3-44. The vertical extent of rockfall associated with different categories of seismic events (Figure 3-45), and the joint spacing information (Figure 3-46) for computing the rockfall area, are used in determining the rockfall volume. The rockfall volume is then used in computing impact stress which, when inducing a plastic strain on the WP at the contact of impact exceeding 2 percent, will fail the WP. Other associated information is presented in Table 3-14 and Figure 3-47.

To determine the number of WPs failed by a faulting disruptive event, the TPA code uses the time of the faulting event and the fault length and width information summarized in Table 3-15. Faults modeled in the TPA code are hidden faults (i.e., either unknown and unmapped faults or underestimated faults), and thus the TPA calculations recognize that the WPs will be emplaced with an appropriate setback distance from known faults. The conditional probability for a faulting event is 1.69×10^{-4}/yr (Mohanty and McCartin, 1998).

Igneous activity contributes to WP failure for both extrusive and intrusive events. As modeled, extrusive events result in the direct release of radionuclides to the ground surface, whereas intrusive events contribute to groundwater releases. The igneous event occurs between 100- and 10,000-yr postclosure, with a recurrent probability of 10^{-7}/yr. The parameters corresponding to the determination of the timing of future igneous events, subsurface areas affected by a volcanic event, and the number of WPs affected by intrusions extending laterally from the volcanic conduit, are presented in Table 3-16.

After the volcanic event penetrates the repository and exhumes SF, areal density from deposition of ash and radionuclides is computed at the compliance point. Input parameters, such as eruption height, wind velocity, and parameters that determine the transport and deposition of radionuclides in ash, are presented in Table 3-16. The radionuclides modeled for extrusive releases, in addition to those evaluated for groundwater transport, are listed in Table 3-17 with corresponding initial inventories and half-lives.

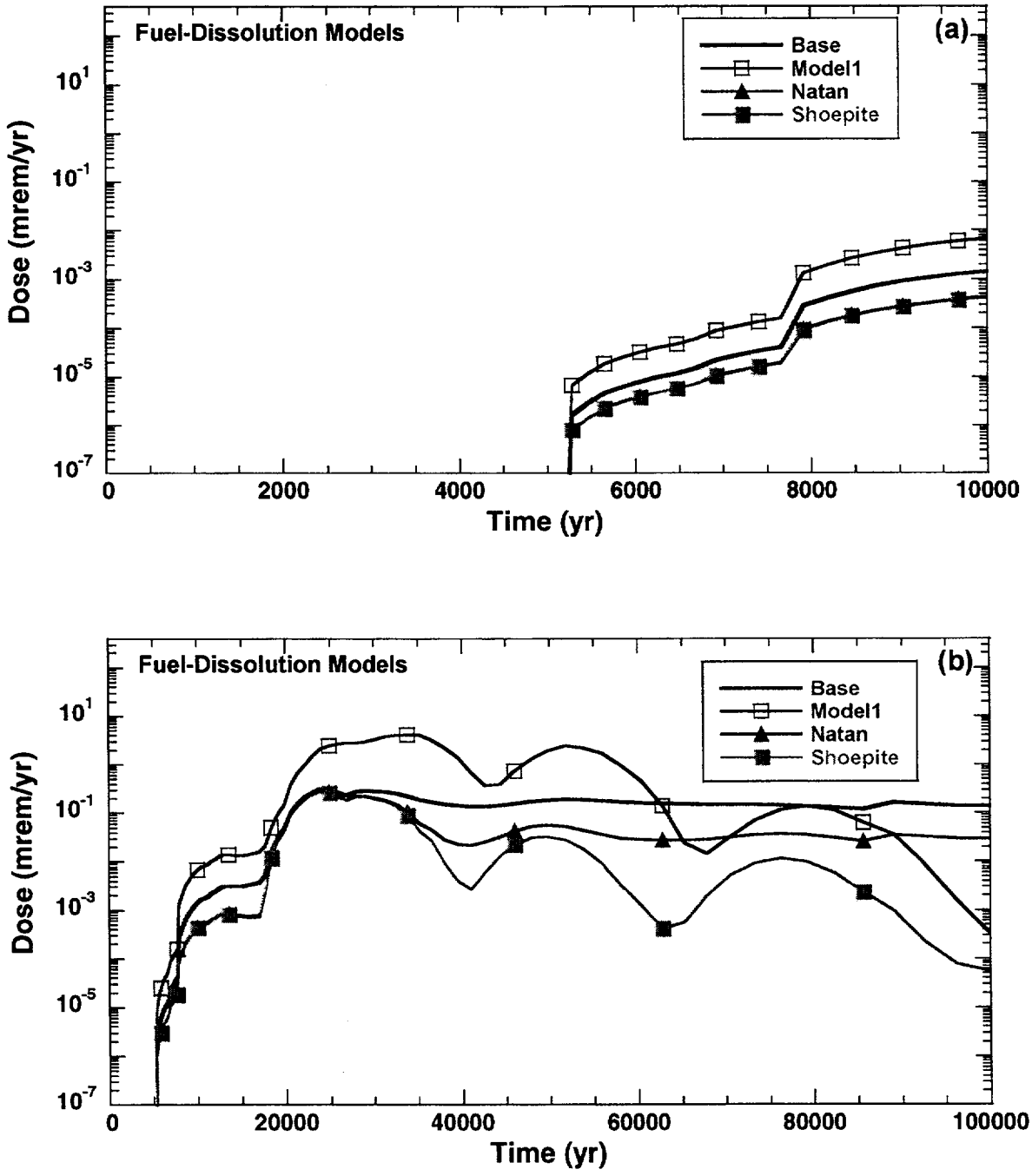

Figure 3-41. Groundwater dose from the basecase and the fuel-dissolution alternative conceptual models for: (a) 10,000, and (b) 100,000 yr, using the mean value data set.

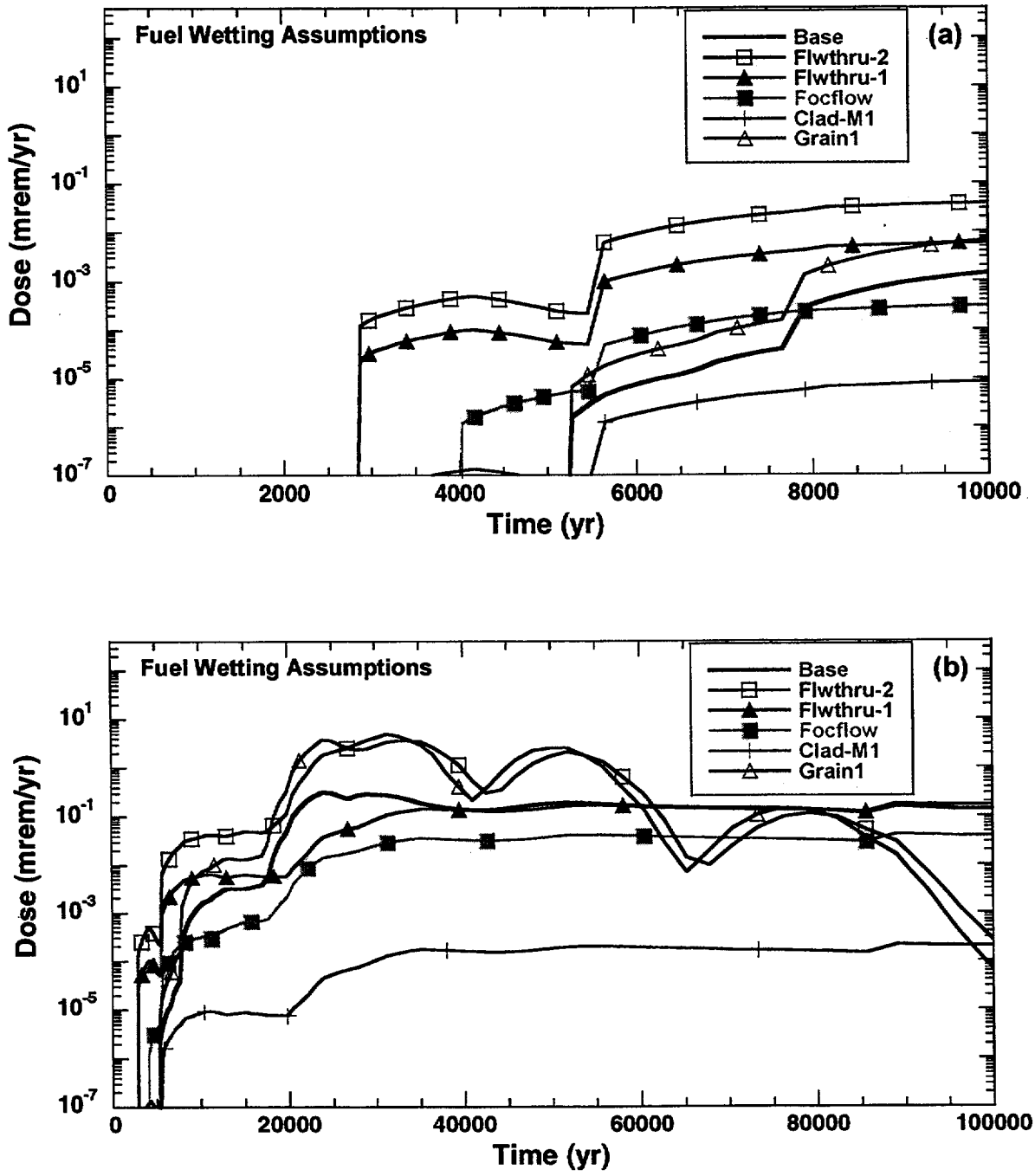

Figure 3-42. Groundwater dose from the basecase and the fuel-wetting alternative conceptual models, for: (a) 10,000; and (b) 100,000 yr, using the mean value data set.

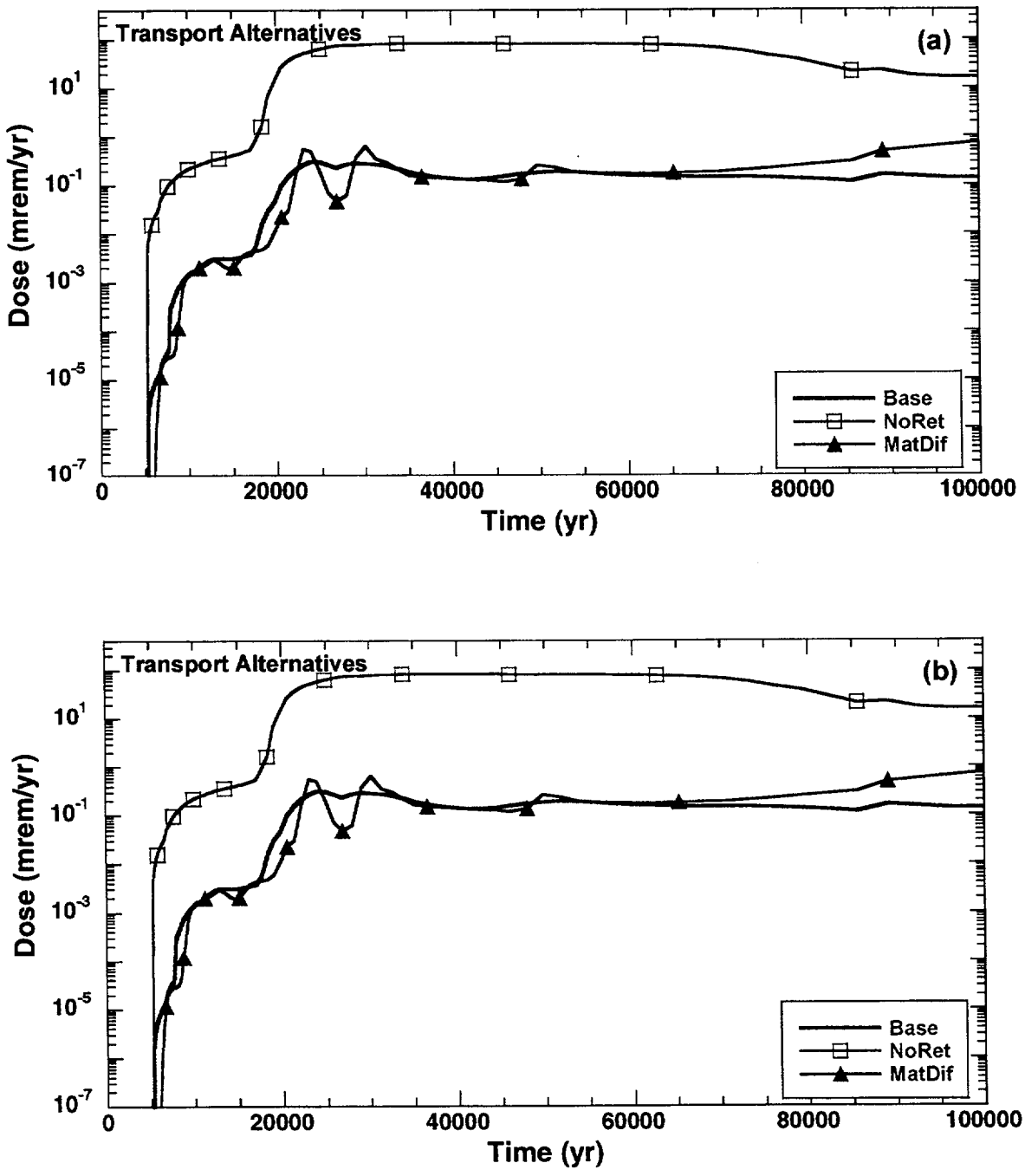

Figure 3-43. Groundwater dose from the basecase and the transport alternative conceptual models for: (a) 10,000; and (b) 100,000 yr, using the mean value data set.

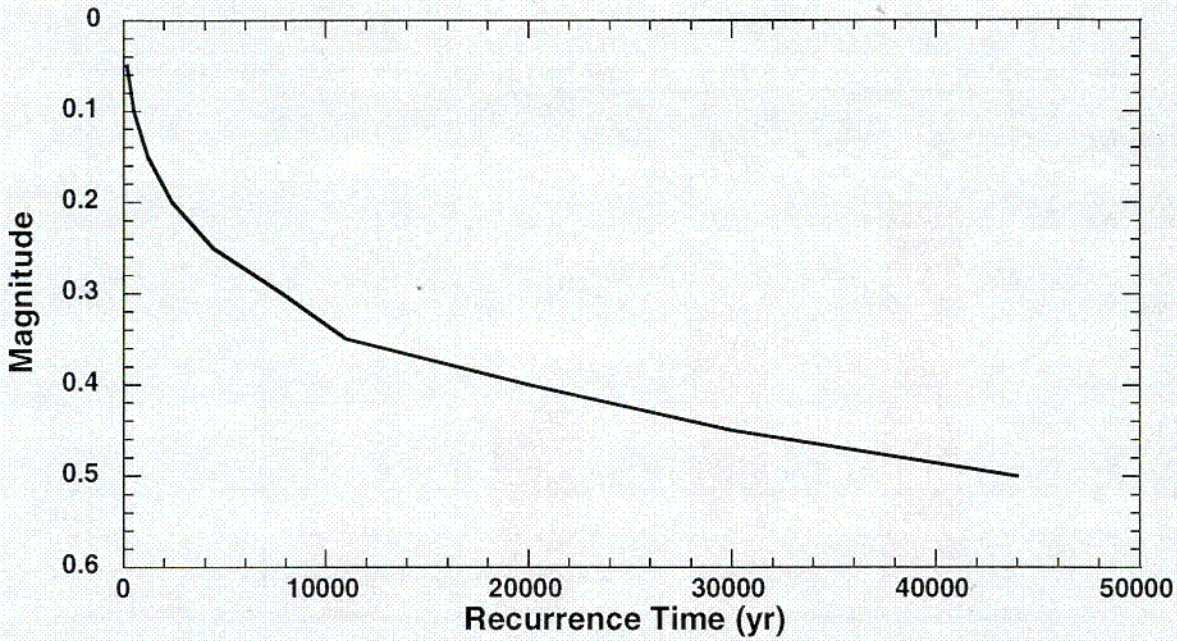

Figure 3-44. Seismic hazard curve comprises ground accelerations and recurrence times used to determine the time of seismic events.

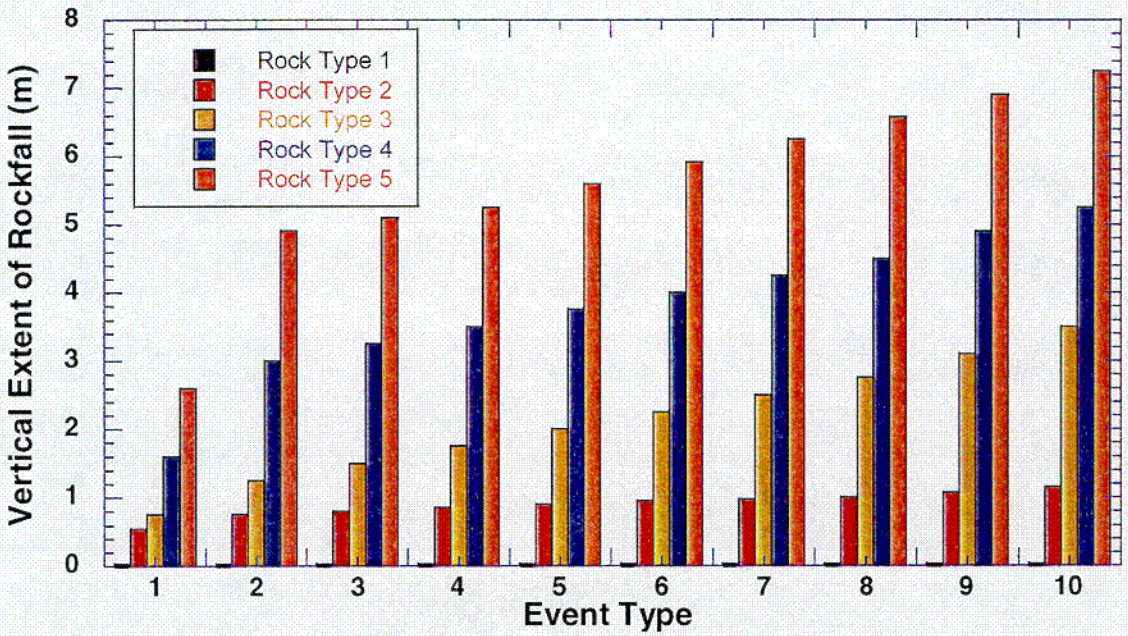

Figure 3-45. Vertical extent of rockfall associated with the 5 rock types and 10 seismic events defined by the seismic hazard curve.

C06

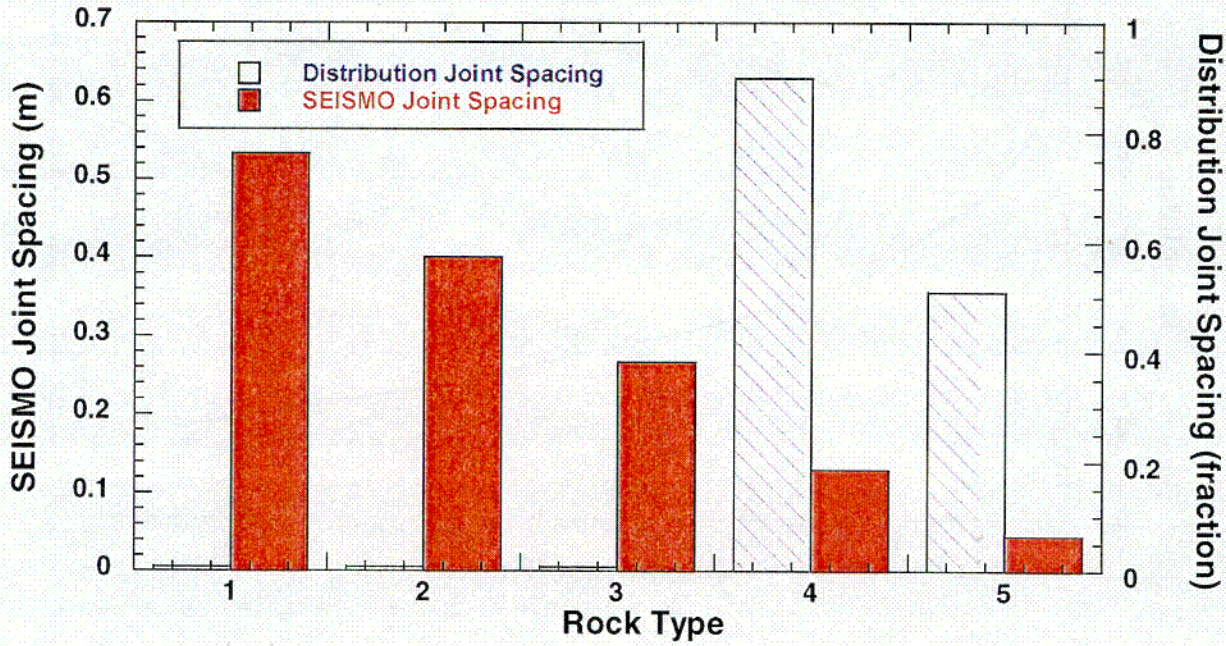

Figure 3-46. Joint spacing of the 5 rock types and 10 seismic events.

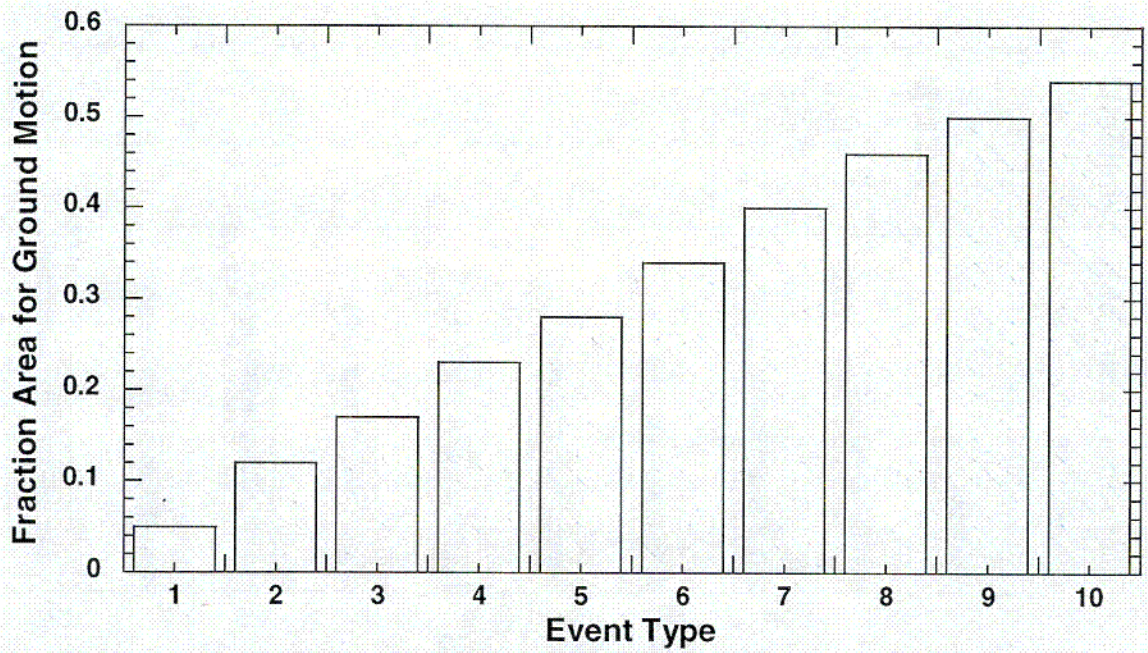

Figure 3-47. Fraction of the area with ground motion for each of the 10 seismic events defined by the seismic hazard curve.

C07

Table 3-14. Parameters used in determining seismic failure of WPs

Parameter	Mean Value	Distribution
WP stiffness for SEISMO	1.21×10^{10} Pa m	—
WP modulus of elasticity for SEISMO	2.07×10^{11} Pa	—
Rock modulus of elasticity for SEISMO	3.45×10^{10} Pa	Normal; 2.76×10^{10}, 4.14×10^{10}
WP Poisson ratio for SEISMO	2.00×10^{-1}	—
Rock Poisson ratio for SEISMO	2.00×10^{-1}	Normal; 0.15, 0.25
Rock falling distance for SEISMO	2.00 m	—
WP falling distance for SEISMO	3.00×10^{-1} m	—
WP number of support pair for SEISMO	2.00	—
WP support stiffness for SEISMO	5.50×10^{9} Pa m	—
WP ultimate strength	4.50×10^{8} N/m^2	—
Grain density for Topopah Spring – welded for SEISMO	2.55 g/cm^3	—
WP yield point	2.00×10^{-3}	—
WP plastic elongation	2.00×10^{-2}	—

Table 3-15. Faulting disruptive event parameters

Parameter	Mean Value	Distribution
Time of next faulting event in region of interest	4.89×10^{3} yr	Finite exponential; 100.0, 10000.0, 2.0×10^{-5}
Threshold displacement for fault disruption of waste package	2.00×10^{-1} m	User distribution; 4 values: 0.1, 0.2, 0.3, 0.4
X coordinate of faulting event in region of interest	5.48×10^{5} m	Uniform; 547400.0, 548600.0
Y coordinate of faulting event in region of interest	4.08×10^{6} m	Uniform; 4076200.0, 4079040.0
Probability for NW orientation of faults	5.00×10^{-2}	—
Random number to determine fault orientation	5.00×10^{-1}	Uniform; 0.0, 1.0
NW fault strike orientation measured from North — clockwise	−32.5°	—
NE fault strike orientation measured from North — clockwise	10°	—
NW fault trace length	4.00×10^{3} m	—
NE fault trace length	4.00×10^{3} m	—
NW fault zone width	2.16×10^{1} m	Beta; 0.5, 275.0, 1.25, 15.0
NE fault zone width	2.85×10^{1} m	Beta; 0.5, 365.0, 1.25, 15.0
NW amount of largest credible displacement	1.34×10^{-1} m	—
NE amount of largest credible displacement	1.34×10^{-1} m	—
NW cumulative displacement rate	5.00×10^{-5} mm/yr	—
NE cumulative displacement rate	5.00×10^{-5} mm/yr	—

Table 3-16. Igneous activity parameters

Parameter	Mean Value	Distribution
Time of next volcanic event in region of interest	5.05×10^{3} yr	Finite exponential; 100.0, 10000.0, 1.0×10^{-7}
X location in region of interest	5.48×10^{5} m	—
Y location in region of interest	4.08×10^{6} m	—
Random number to determine if extrusive or intrusive volcanic event	5.00×10^{-1}	Uniform; 0.0, 1.0
Fraction of time volcanic event is extrusive	9.99×10^{-1}	—
Angle of volcanic dike measured from north—clockwise	7.50°	Uniform; 0.0, 15.0
Length of volcanic dike	6.50×10^{3} m	Uniform; 2000.0, 11000.0
Width of volcanic dike	5.50 m	Uniform; 1.0, 10.0
Diameter of volcanic cone	5.13×10^{1} m	Uniform; 24.6, 77.9
Density of air at standard pressure	1.29×10^{-3} g/cm^3	—
Viscosity of air at standard pressure	1.80×10^{-4} g/cm-s	—
Constant relating fall time to eddy diffusivity	4.00×10^{2} cm^2/sec$^{5/2}$	—
Maximum particle diameter for particle transport	1.00×10^{1} cm	—
Minimum fuel particulate size	1.00×10^{-4} cm	—
Mode fuel particulate size	1.00×10^{-3} cm	—
Maximum fuel particulate size	1.00×10^{-2} cm	—
Minimum ash density for variation with size	1.20 g/cm^3	—
Maximum ash density for variation with size	2.00 g/cm^3	—
Minimum ash log-diameter for density variation	−2.00	—
Maximum ash log-diameter for density variation	−1.00	—
Particle shape parameter	5.00×10^{-1}	—
Incorporation ratio	3.00×10^{-1}	—
Wind direction	−90°	—
Wind speed	1.20×10^{3} cm/sec	Exponential; 8.3×10^{-4}
Volcanic event duration	6.66×10^{5} sec	Log-uniform; 6.13×10^{4}, 7.24×10^{6}
Volcanic event power	3.02×10^{10} W	Log-uniform; 2.57×10^{9}, 3.55×10^{11}
Volcanic column constant beta	1.00×10^{1}	—
Ash mean particle log-diameter	1.00×10^{-1} cm	Log triangular; 0.01, 0.1, 1.0
Ash particle size distribution standard deviation	1.00	—
Relative rate of blanket removal	1.00×10^{-3} /yr	—
Fraction of precipitation lost to evapotranspiration	6.80×10^{-1}	—
Fraction of irrigation lost to evapotranspiration	5.00×10^{-1}	—
Annual precipitation	8.50×10^{-2} m/yr	—
Annual irrigation	1.52 m/yr	—
Fraction of year soil is saturated from precipitation	5.40×10^{-3}	—
Fraction of year soil is saturated from irrigation	2.00×10^{-1}	—

Table 3-16. Igneous activity parameters (cont'd)

Parameter	Mean Value	Distribution
Ash bulk density	1.40 g/cm^3	—
Ash volumetric moisture fraction at saturation	4.00×10^{-1}	—
Depth of the rooting zone	1.50×10^{-1} m	—

Table 3-17. Initial inventory and half-life of *additional* radionuclides considered for ground-surface release, but not for groundwater release

Radionuclide	Inventory at 10 yr from Reactor (Ci/WP)	Half-life (yr)
^{227}Ac	5.07×10^{-5}	2.18×10^{1}
^{108m}Ag	1.17×10^{-1}	1.27×10^{2}
^{242m}Am	7.31×10^{1}	1.52×10^{2}
^{243}Am	1.50×10^{2}	7.38×10^{3}
^{243}Cm	1.49×10^{2}	2.85×10^{1}
^{244}Cm	1.12×10^{4}	1.81×10^{1}
^{246}Cm	2.50×10^{-1}	4.73×10^{3}
^{135}Cs	3.43	2.30×10^{6}
^{137}Cs	7.46×10^{5}	3.00×10^{1}
^{93}Mo	9.86×10^{-2}	3.50×10^{3}
^{94}Nb	4.92	2.03×10^{4}
^{59}Ni	2.40×10^{1}	8.00×10^{4}
^{63}Ni	2.98×10^{3}	9.20×10^{1}
^{231}Pa	1.90×10^{-4}	3.28×10^{4}
^{210}Pb	4.61×10^{-7}	2.23×10^{1}
^{107}Pd	1.02	6.50×10^{6}
^{240}Pu	4.96×10^{3}	6.54×10^{3}
^{241}Pu	7.26×10^{5}	1.44×10^{1}
^{242}Pu	1.56×10^{1}	3.87×10^{5}
^{238}Pu	2.06×10^{4}	8.77×10^{1}
^{226}Ra	3.58×10^{-6}	1.60×10^{3}
^{151}Sm	3.10×10^{3}	9.00×10^{1}
^{126}Sn	6.99	1.00×10^{5}
^{121m}Sn	7.78	5.00×10^{1}
^{90}Sr	5.18×10^{5}	2.91×10^{1}
^{229}Th	1.36×10^{-6}	7.34×10^{3}
^{232}U	2.42×10^{-1}	7.20×10^{1}
^{233}U	2.34×10^{-4}	1.59×10^{5}
^{235}U	1.65×10^{-1}	7.04×10^{8}
^{236}U	2.34	2.34×10^{7}
^{238}U	3.11	4.47×10^{9}
^{93}Zr	1.81×10^{1}	1.53×10^{6}

Parameters associated with surface erosion of radionuclides from the ash blanket deposited after an extrusive igneous event are presented in Table 3-18. For the ground-surface pathway, the areal densities calculated for each radionuclide, computed with the ASHPLUME (Jarzemba et al., 1997) ash transport model, are used in determining the dose TEDEs, by using the DCFs presented in Table 3-19.

3.6.2 Multiple-Realization Analysis of Disruptive Events

The variability in the average dose arising from faulting events and igneous activity for the multiple-realization simulations is presented in this section. The dose history for faulting events for the 100,000-yr TPI without probability weighting is presented in Figure 3-48(a). The average groundwater dose from the faulting events is approximately 20 percent greater than the dose without a faulting event at 10,000 yr. However, after 10,000 yr, the releases from WPs failed by corrosion dominate the dose; the groundwater dose with faulting and the basecase in the 100,000-yr TPI are not distinguishable.

The probability-weighted expected dose from igneous activity is presented in Figure 3-48(b) together with the groundwater dose computed using the basecase data set. In the 10,000-yr TPI, the probability-weighted dose from igneous activity is about 2 to 4 orders of magnitude greater than the basecase groundwater dose. The next section presents the methodology used to determine the risk arising from faulting and igneous disruptive events.

3.7 CALCULATION OF RISK

Risk is defined in this section as the probability-weighted dose. Doses are calculated from three scenario classes: (i) basecase with seismicity; (ii) faulting; and (iii) igneous activity. The probability of the three scenario classes is assumed to sum to unity. This implies that other scenario classes are either too improbable, or have consequences too small, to affect the overall risk materially.

The average risk to a receptor can be computed by summing contributions to dose from each Monte Carlo simulation, weighted by the scenario probability and the conditional probability of each realization within the scenario. The methodology for computing conditional risk (i.e., assuming that the scenario has a probability of one) from scenarios other than extrusive igneous activity is presented in Section 3.7.1. The methodology used to determine the conditional risk from scenarios with extrusive igneous activity is described in Section 3.7.2. The methodology for combining the conditional risks to an overall risk is presented in Section 3.7.3.

3.7.1 Scenarios Other Than Extrusive Igneous Activity

The risk or effective dose equivalent is the product of the consequence (i.e., dose) and the probability that the dose has occurred. Estimates of dose are uncertain because the models and their input parameters are uncertain, as are the times of occurrence of the disruptive events such as faulting and intrusive igneous activity. Monte Carlo analysis is used to account for the uncertainty in parameters and events. The Monte Carlo analysis propagates the uncertainty in model inputs through the conceptual models. A Monte Carlo simulation evaluates a model repeatedly, using input values that have been randomly selected from the probability distributions for the input variables. The output of the Monte Carlo analysis is a set of results such as dose versus time, for each of the randomly chosen input sets of values. Generally, each Monte Carlo output result has equal probability. Thus, each dose curve from the Monte Carlo analysis has a probability of occurrence equal to $1/N$, where N is the number of Monte Carlo samples. The analysis in this section does

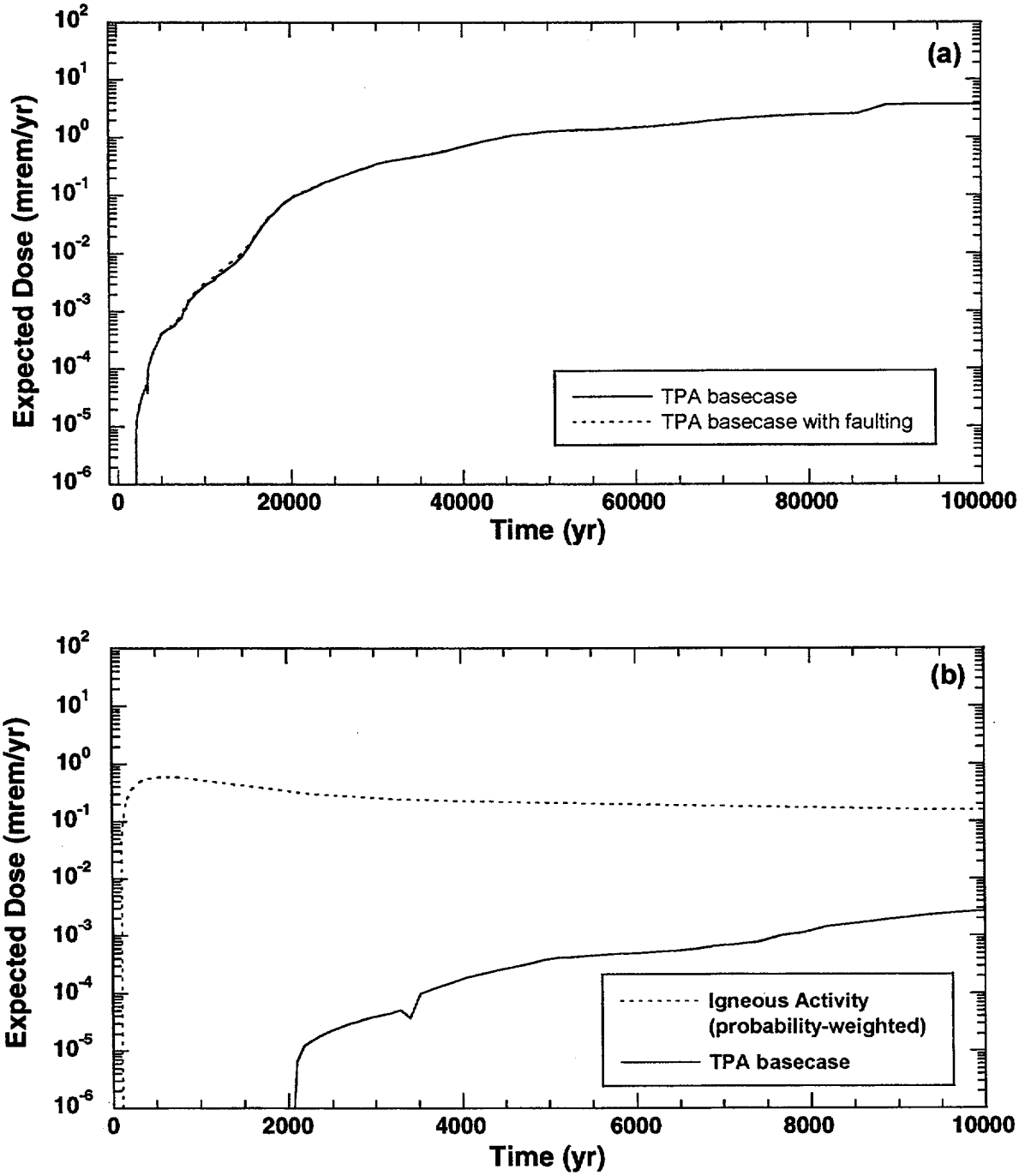

Figure 3-48. Groundwater dose in 10,000 and 100,000 yr with and without: (a) faulting, and (b) igneous activity, in 10,000 yr, for 250 realizations. (Only the ground-surface dose for releases caused by extrusive igneous activity in (b) is probability-weighted. The basecase and faulting doses are not probability-weighted.)

Table 3-18. Parameters used in computing ash and radionuclide removal from the ground surface

Element	K_d in Volcanic Ash (cm^3/g)	Solubility in Volcanic Ash (mol/L)
Ac	4.50×10^{2}	1.00×10^{-6}
Am	1.90×10^{3}	1.00×10^{-6}
C	5.00	1.00
Cs	2.80×10^{2}	1.00
Cl	0.00	1.00
Cm	4.00×10^{3}	1.00×10^{-6}
I	1.00	1.00
Pb	2.70×10^{2}	3.20×10^{-7}
Mo	1.00×10^{1}	1.00
Np	5.00	1.00×10^{-4}
Ni	4.00×10^{2}	2.00×10^{-3}
Nb	1.60×10^{2}	1.00×10^{-8}
Pd	5.50×10^{1}	9.50×10^{-4}
Pu	5.50×10^{2}	5.00×10^{-6}
Pa	5.50×10^{2}	3.20×10^{-8}
Ra	5.00×10^{2}	1.00×10^{-7}
Sm	2.45×10^{2}	5.00×10^{-6}
Se	1.50×10^{2}	1.00
Au	5.50×10^{1}	1.00
Sr	1.50×10^{1}	1.30×10^{-4}
Tc	1.00×10^{-1}	1.00
Th	3.20×10^{3}	3.20×10^{-9}
Sb	1.30×10^{2}	5.00×10^{-8}
U	3.50×10^{1}	4.50×10^{-5}
Zr	6.00×10^{2}	3.20×10^{-10}

Other parameters

Parameter	Mean Value	Distribution
Distance cutoff for dose conversion duality in DCAGS module	2.00×10^{1} km	—
Airborne mass load for igneous activity dose calculation	1.00×10^{-3} g/m3	Log-uniform; 1.0×10^{-4}, 1.0×10^{-2}
Occupancy factor for igneous activity dose calculation	2.40×10^{-1}	—
Depth of resuspendable layer	3.00×10^{-1} cm	—

Table 3-19. Biosphere dose conversion factors of all 43 nuclides for ground surface at the 20-km receptor location

	Nonpluvial and Pluvial Dose Conversion Factor (DCF)			
Radionuclide	**Direct Exposure (rem/yr)/(Ci/m²)**	**Inhalation (rem/yr)/(Ci/m³)**	**Ingestion of Animal Products (rem/yr)/(Ci/m²)**	**Ingestion of Crops (rem/yr)/(Ci/m²)**
^{227}Ac	3.80	7.02×10^{13}	2.13×10^{2}	4.73×10^{4}
^{108m}Ag	6.20×10^{4}	2.97×10^{9}	3.70	2.40×10^{2}
^{241}Am	6.70×10^{2}	4.66×10^{12}	1.50×10^{1}	9.80×10^{3}
^{242m}Am	7.30×10^{1}	4.46×10^{12}	1.41×10^{1}	9.53×10^{3}
^{243}Am	1.30×10^{3}	4.62×10^{12}	1.50×10^{1}	9.81×10^{3}
^{14}C	3.90×10^{-1}	2.19×10^{7}	0.00	1.70×10^{-1}
^{36}Cl	1.70×10^{1}	2.30×10^{8}	1.70×10^{4}	3.90×10^{4}
^{243}Cm	3.10×10^{3}	3.22×10^{12}	2.80×10^{1}	6.80×10^{3}
^{244}Cm	2.20×10^{1}	2.60×10^{12}	2.30×10^{1}	5.40×10^{3}
^{245}Cm	2.10×10^{3}	4.77×10^{12}	4.20×10^{1}	1.00×10^{4}
^{246}Cm	1.90×10^{1}	4.73×10^{12}	4.20×10^{1}	1.00×10^{4}
^{135}Cs	8.30×10^{-1}	4.77×10^{7}	1.00×10^{2}	5.50×10^{1}
^{137}Cs	1.30×10^{4}	3.35×10^{8}	6.90×10^{2}	3.80×10^{2}
^{129}I	6.20×10^{2}	1.82×10^{9}	2.20×10^{3}	1.60×10^{3}
^{93}Mo	1.30×10^{2}	2.99×10^{8}	1.10×10^{1}	1.90×10^{2}
^{94}Nb	3.70×10^{4}	4.35×10^{9}	2.70×10^{-3}	4.40×10^{1}
^{59}Ni	0.00	2.83×10^{7}	4.30	1.90
^{63}Ni	0.00	6.60×10^{7}	1.20×10^{1}	5.20
^{237}Np	7.30×10^{2}	5.67×10^{12}	6.50×10^{2}	2.50×10^{4}
^{231}Pa	9.80×10^{2}	1.35×10^{13}	3.80×10^{1}	3.30×10^{4}
^{210}Pb	6.20×10^{1}	1.42×10^{11}	1.09×10^{3}	1.96×10^{4}
^{107}Pd	0.00	1.34×10^{8}	1.70	4.70
^{238}Pu	8.30	4.11×10^{12}	4.43	8.60×10^{3}
^{239}Pu	8.80	4.50×10^{12}	4.90	9.50×10^{3}
^{240}Pu	2.00×10^{1}	4.50×10^{12}	4.90	9.50×10^{3}
^{241}Pu	1.30×10^{-1}	8.65×10^{10}	9.51×10^{-2}	1.84×10^{2}
^{242}Pu	1.70×10^{1}	4.31×10^{12}	4.70	9.00×10^{3}
^{226}Ra	1.60×10^{2}	9.00×10^{10}	1.20×10^{3}	3.60×10^{3}
^{79}Se	5.10×10^{-1}	1.03×10^{8}	3.60×10^{1}	6.20×10^{1}
^{151}Sm	1.20×10^{-1}	3.14×10^{8}	1.70×10^{-1}	1.70
^{121m}Sn	1.20×10^{2}	1.21×10^{8}	1.90×10^{1}	1.88×10^{1}
^{126}Sn	1.30×10^{3}	1.05×10^{9}	1.69×10^{2}	1.68×10^{2}
^{90}Sr	6.70	1.36×10^{10}	2.49×10^{3}	6.92×10^{3}
^{99}Tc	1.90	8.73×10^{7}	1.10×10^{2}	2.30×10^{3}
^{229}Th	2.10×10^{3}	2.25×10^{13}	8.53×10^{1}	1.02×10^{4}
^{230}Th	1.80×10^{1}	3.42×10^{12}	1.80	1.50×10^{3}
^{232}U	2.50×10^{1}	6.91×10^{12}	3.82×10^{2}	4.54×10^{3}
^{233}U	1.80×10^{1}	1.42×10^{12}	8.50×10^{1}	9.90×10^{2}
^{234}U	1.80×10^{1}	1.39×10^{12}	8.30×10^{1}	9.80×10^{2}
^{235}U	3.60×10^{3}	1.29×10^{12}	7.82×10^{1}	9.14×10^{2}
^{236}U	1.60×10^{1}	1.32×10^{12}	7.90×10^{1}	9.20×10^{2}
^{238}U	1.30×10^{1}	1.24×10^{12}	7.53×10^{1}	9.02×10^{2}
^{93}Zr	0.00	3.38×10^{9}	1.86×10^{-3}	4.75

not explicitly include conceptual model uncertainty, other than that captured by changes in the input parameters. Alternative conceptual models are covered in Sections 2.3 and 3.5.

The expected dose-versus-time relationship for scenario *j* (e.g., intrusive volcanic scenario) can be developed by summing, over all realizations, the probability-weighted contributions from the family of dose relationships produced by the *N* Monte Carlo samples. The mathematical representation of this calculation is:

$$\overline{D}_j(t) = \sum_{i=1}^{N} p_i C_{i,j}(t) \tag{3-1}$$

where

$\overline{D}_j(t)$ — average annual dose to the receptor individual as a function of time for the *j*th scenario;

$C_{i,j}$ — dose as a function of time for the *i*th realization of the *j*th scenario;

p_i — probability assigned to the dose curve for the *i*th realization. For Monte Carlo sampling, $p_i = (1/N)$; and

N — number of model simulations that compose the family of dose curves (i.e., *N* Monte Carlo samples of the model inputs are used to generate *N* model outputs in the form of dose curves).

The index indicates that the event can occur at any time between [0,t].

3.7.2 Extrusive Igneous-Activity Scenario

For the igneous-activity scenario, dose consequences are largest for events that occur soon after repository closure, while the relatively short-lived but high-activity radionuclides such as ^{241}Am are still present in significant quantities. Radionuclides can reach the affected population in short times (hours to days), but persist in the environment and also cause lower levels of exposure long after the event (hundreds to thousands of years). The time of occurrence of the event is extremely important to the dose consequences, and is, therefore, included in the probabilistic analysis as one of the sampled parameters. The fact that there are short-term, relatively high consequences and long-term, lower consequences from igneous events complicates the probabilistic analysis by requiring a large number of Monte Carlo samples to resolve the overall expected dose on both the short- and long-term time scales. To get a reasonably converged mean value, hundreds of realizations must be performed at each potential occurrence time, which may be impractical with the present models run in the usual Monte Carlo fashion.

Because the expected dose-versus-time curve is anticipated to be smooth, a much more efficient convolution approach to generating the curve is to develop the expected dose for igneous events at a few, discrete event times and then use linear interpolation between the discrete event times. The procedure for developing the expected dose curve involves the following steps:

- Conduct Event-Time-Specific Probabilistic Analyses
  Specific occurrences of igneous activity are selected for the evaluation rather than randomly selecting occurrence times in a Monte Carlo approach. A separate probabilistic analysis, based on the parameter uncertainty, is conducted for each specific occurrence time. In the present model, the event times were 100; 500; and 1000 to 10,000 yr, in 1000-yr steps.

- Generate Conditional Expected Dose Curves for Specific Event Times
  Each of the separate probabilistic analyses described previously is used to develop a separate conditional expected dose curve for the specified occurrence times, using Eq. (3-1).

- Generate Probability-Weighted Dose Curve for Specific Event Times
  The probability-weighted dose $\overline{D}_n$ for the specific event times, is generated by multiplying the conditional dose curves by the probability in a given year that an igneous event occurred (annual probability can be used provided it is constant over time). Figure 3-49 presents the series of probability-weighted dose curves calculated in this analysis.

- Generate an Overall Expected Dose Curve

  The expected dose at any given time t is the sum of conditional expected dose $\overline{\Re}$; overall, the expected dose curve from igneous activity occurring over the TPI is determined by cumulating probability-weighted dose over time, using the probability-weighted dose curves at the 12 specified event times. Equation (3-2) describes how the expected annual dose to the receptor individual is estimated in this approach:

$$\overline{\Re}(t) = \sum_{n=1}^{E} (\Delta t)_n \overline{D}_n(t) \tag{3-2}$$

where

$\overline{\Re}(t)$ — expected annual dose to the receptor individual as a function of time;

$\overline{D}_n(t)$ — probability-weighted mean dose as a function of time for specific event time n;

$(\Delta t)_n$ — increment of time associated with event time n (if events are evaluated on a per year basis, this would be 1yr); and

E — number of specific event times used to represent variation in event uncertainty (interpolation between events can be used to generate dose curves for each year).

The probability-weighted dose curve calculated with this more efficient approach is presented in Figure 3-50. As expected, the consequences of an igneous event are highest at early times. The probability weighted dose curve goes through a maximum at around 500 yr. This results from the accumulation of dose from potential earlier events.

3.7.3 Combining Conditional Risks into an Overall Risk

The overall risk, $\overline{D}(t)$, is calculated by summing the scenario mean doses weighted by the scenario probability P_j . The mathematical representation of this calculation is:

$$\overline{D}_j(t) = \sum_{j=1}^{M} \overline{D}_j(t) P_j$$

where

$\overline{D}_j(t)$ — dose rate from scenario j, averaged over the Monte Carlo realizations;
M — number of scenario classes; and
P_j — annual probability of scenario j.

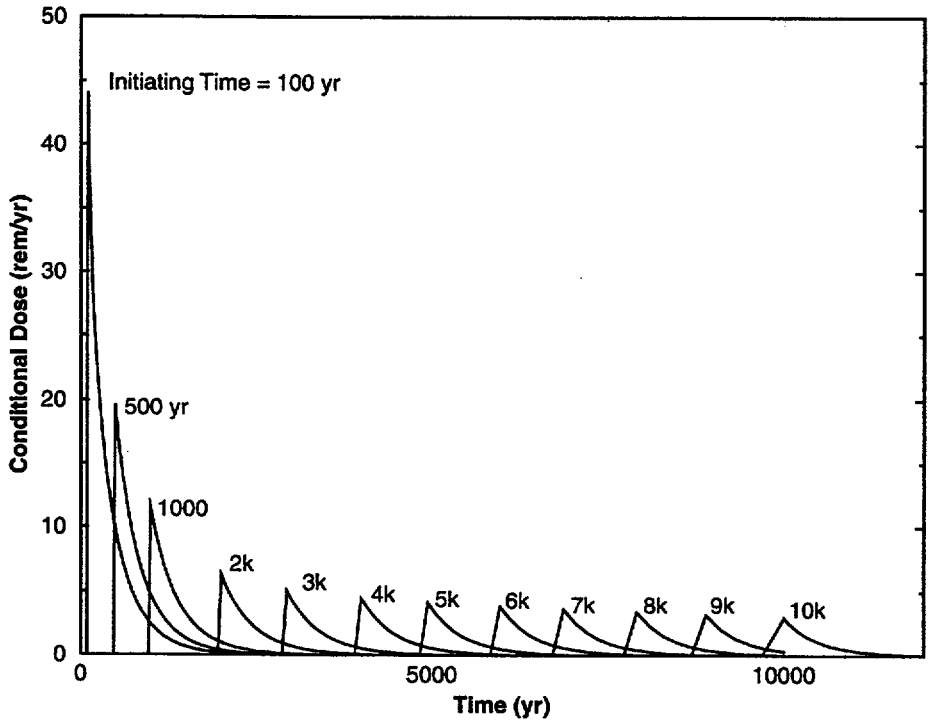

Figure 3-49. Mean dose arising from extrusive igneous-activity shown with various times for the volcanic event in 400 realizations.

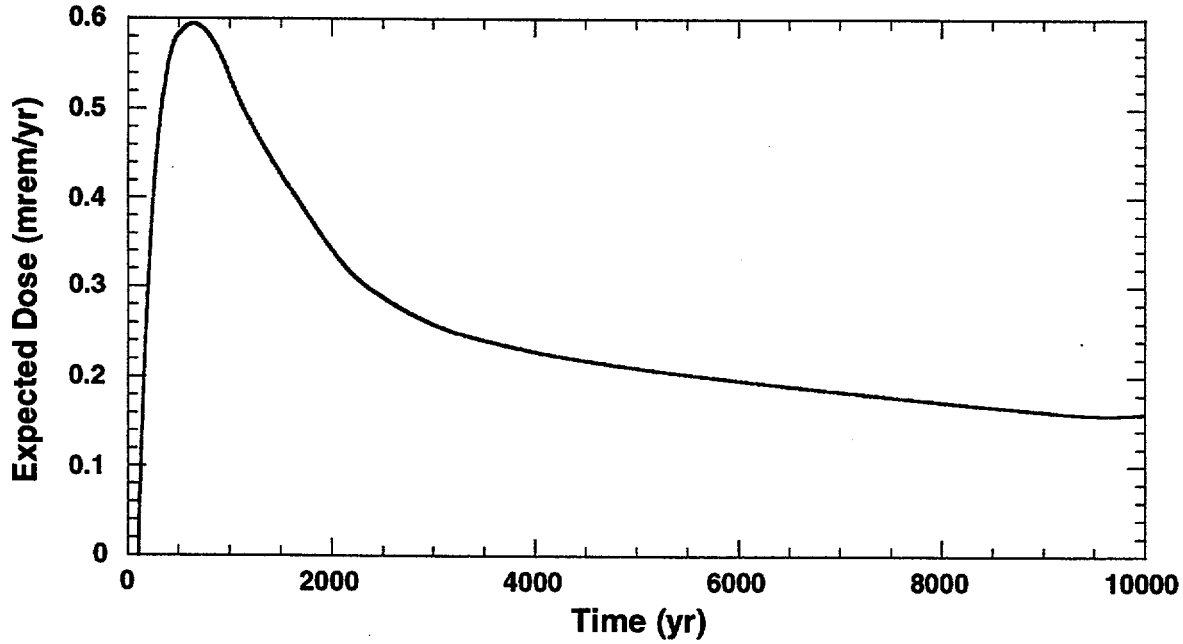

Figure 3-50. Contribution of extrusive igneous-activity to the total dose, weighted by an annual probability for the volcanic event of 10^{-7}.